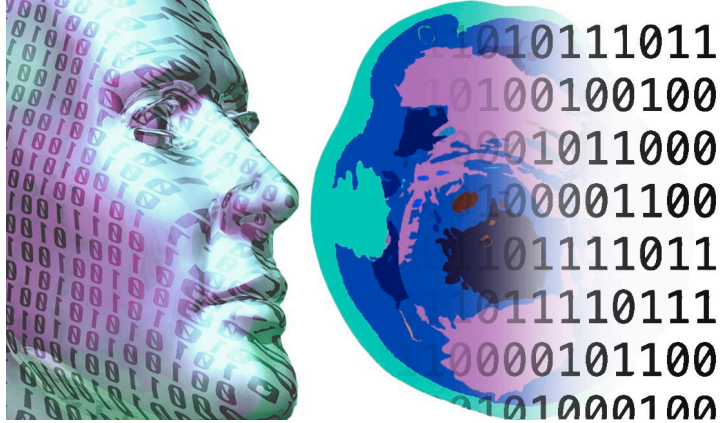

Characterizing and Inferring Neuronal Connectivity and Dynamics with Deep Geometry and Topology

Smita Krishnaswamy
Department of Computer Science, School of Medicine
Program for Applied Math
Program for Computational Biology & Bioinformatics
Wu Tsai Institute, Center for Neurocomputation and Machine Intelligence
Yale Institute for Foundations of Data Science

Building a neural parts list

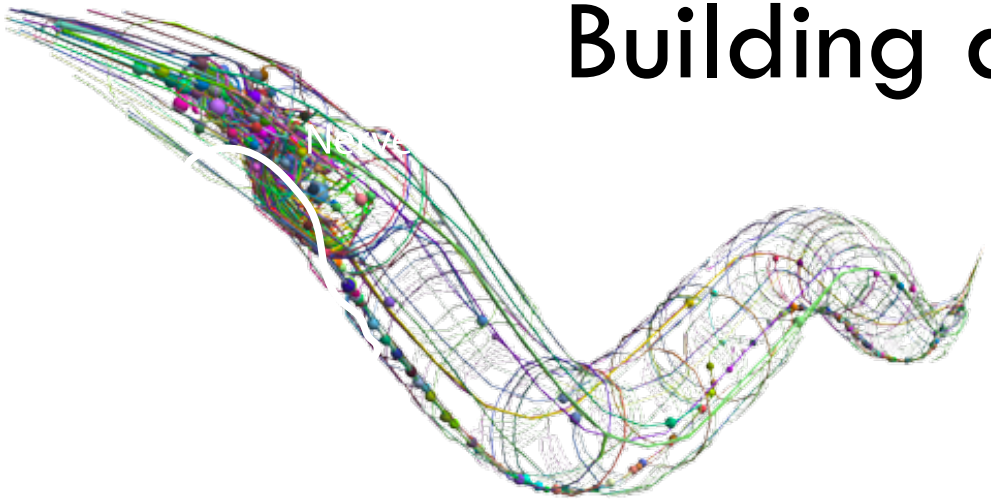

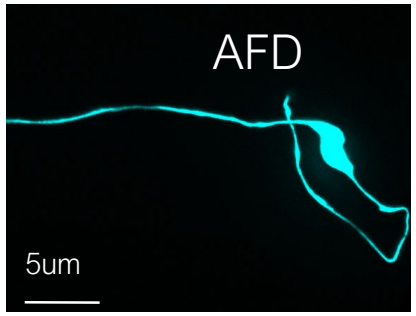

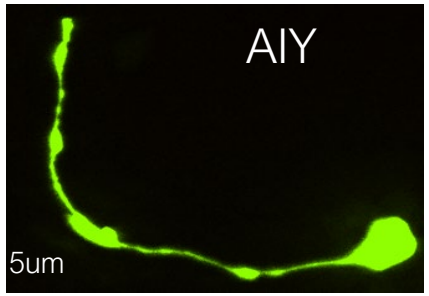

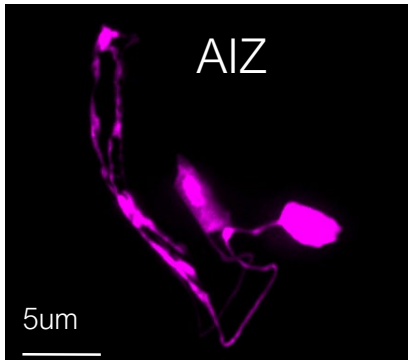

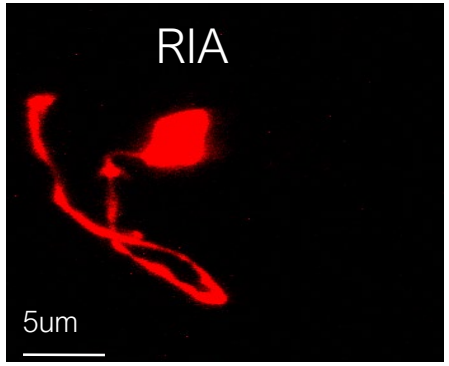

- 181 neurons
- Identities
- Morphologies
- Connections

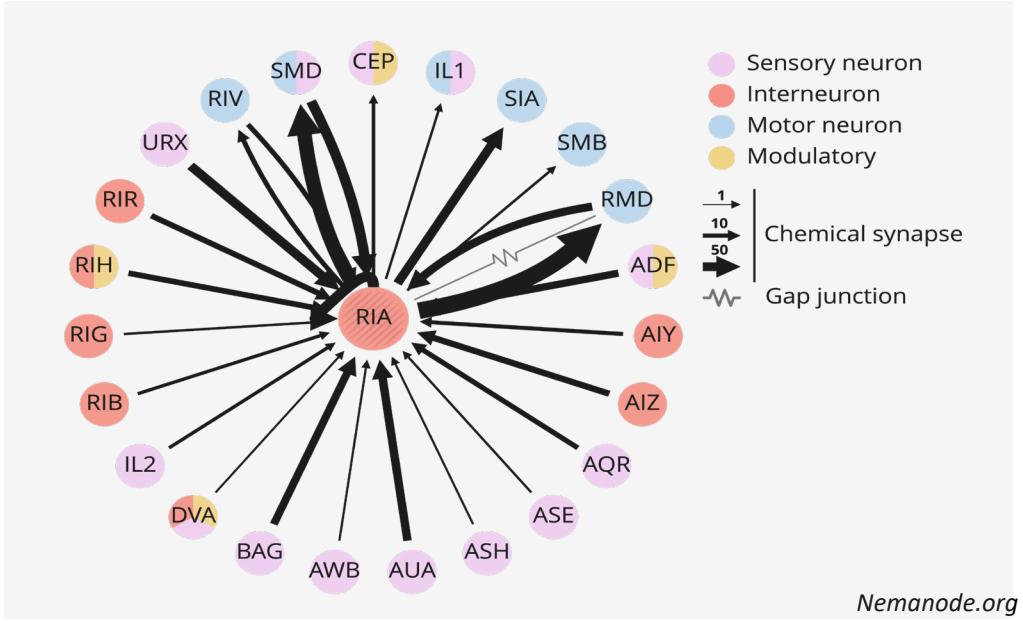

Structure at a variety of scales

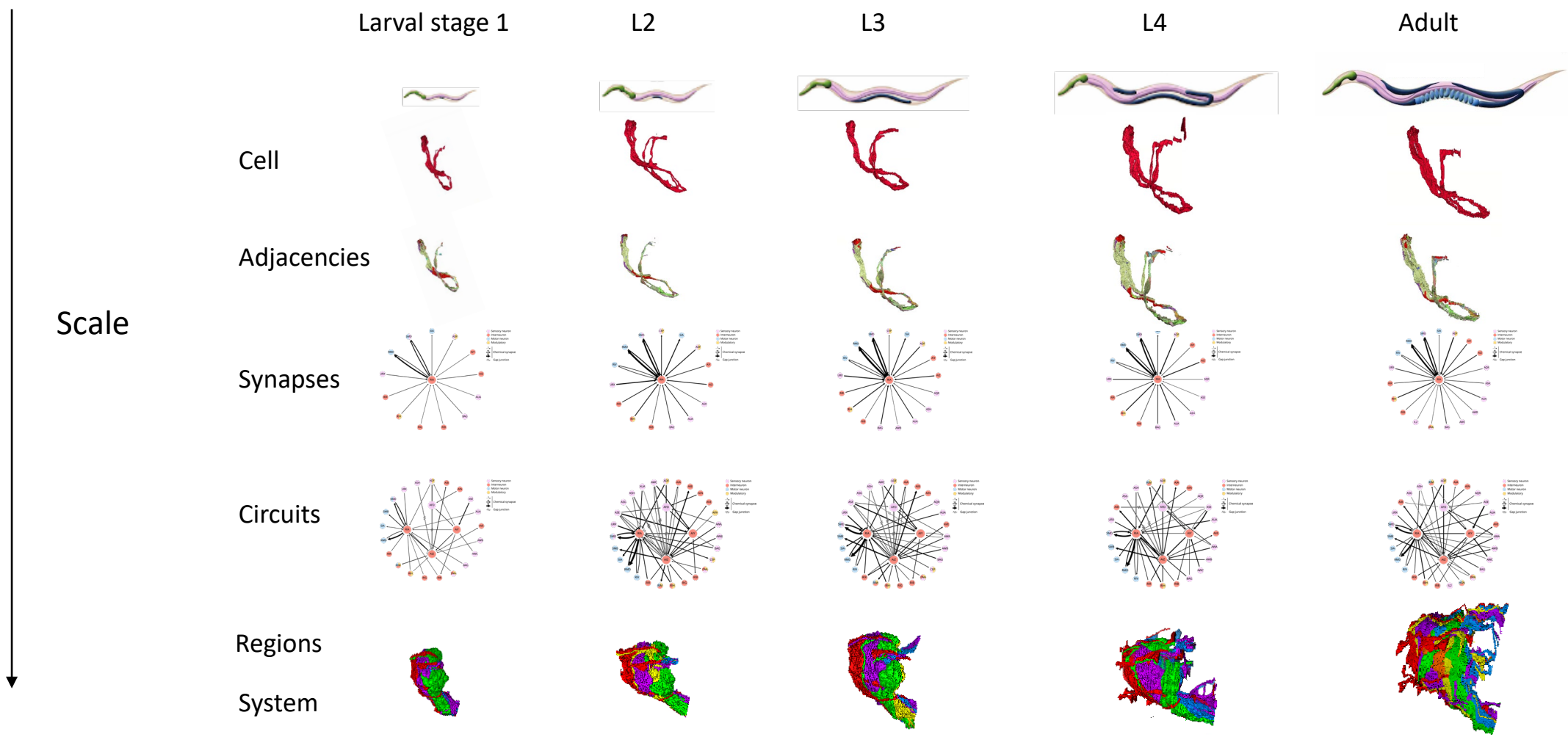

Challenges

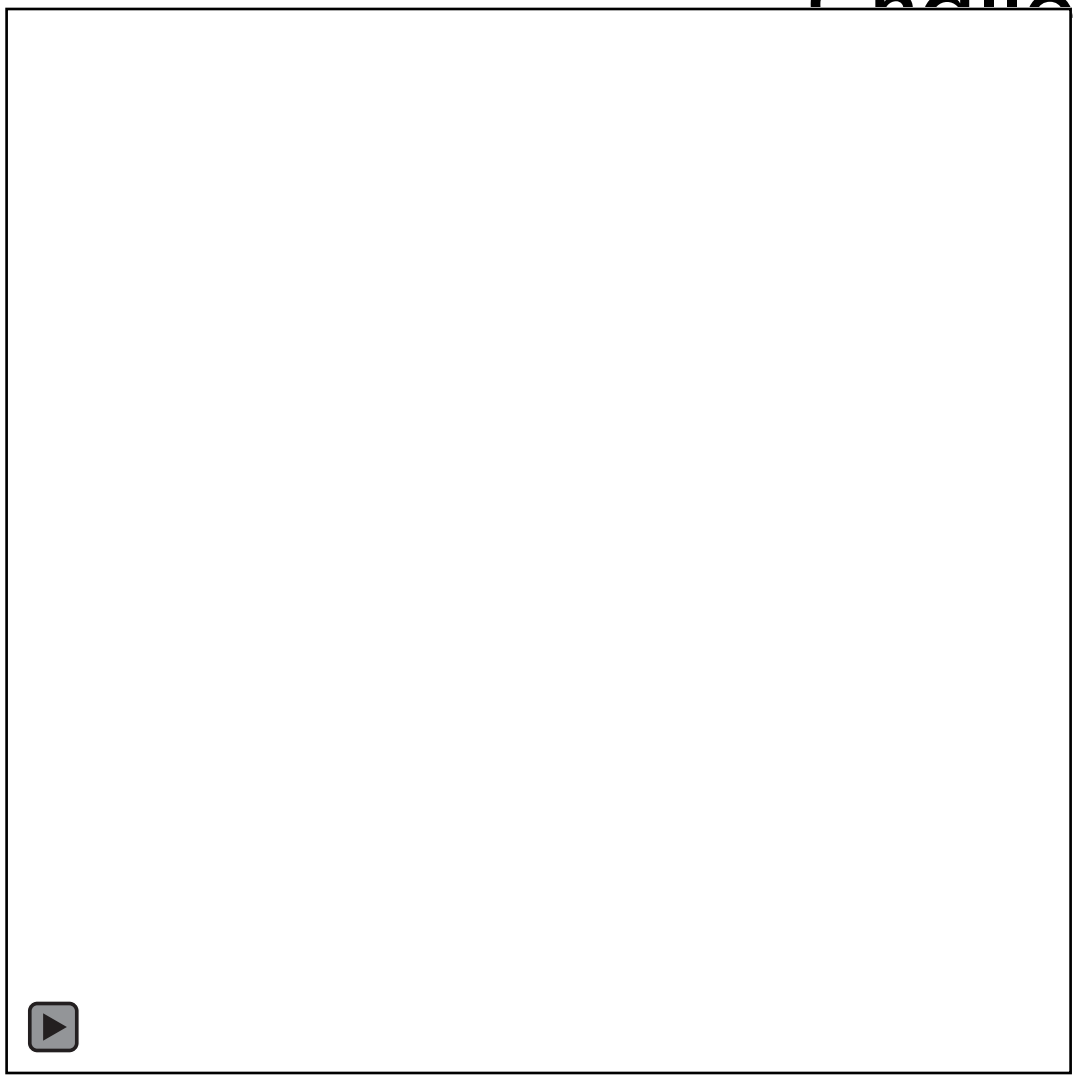

How do we go from high dimensional neural activations to neural insights?

Several challenges to overcome related to the noisy and distributed representations found in the brain.

Similar challenges in cellular data (scRNA) analysis

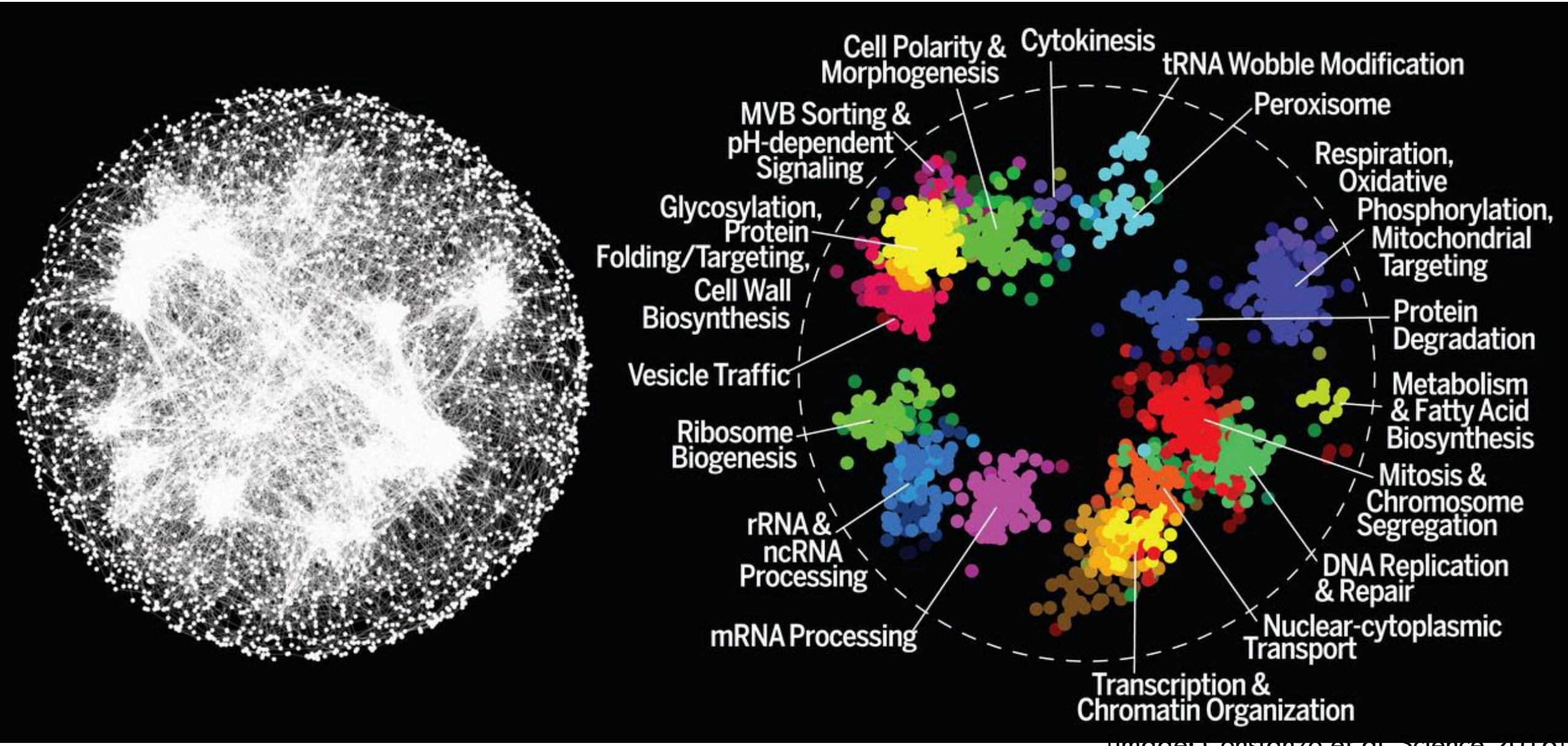

[Image: Constanzo et al. Science 2016]

Analysis Tasks

Denoising

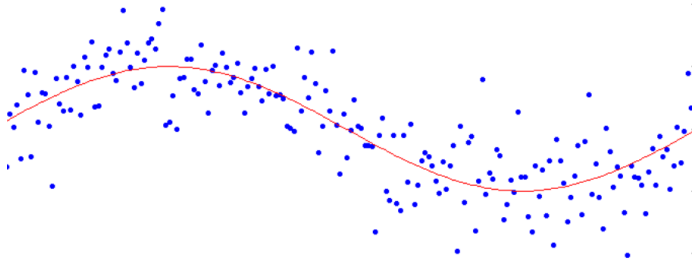

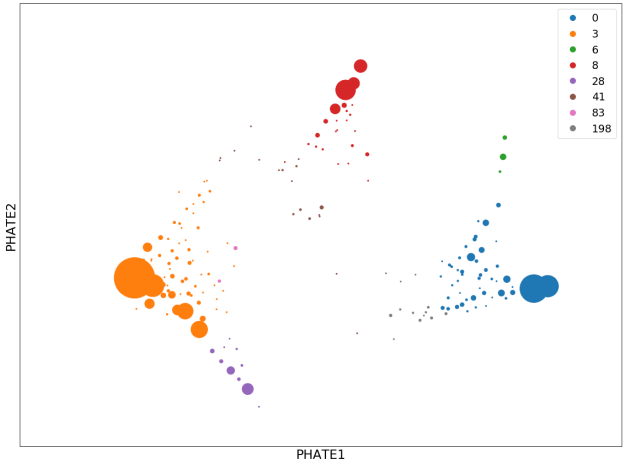

Distilling state space, visualization

Regulatory/Generative Network Inference

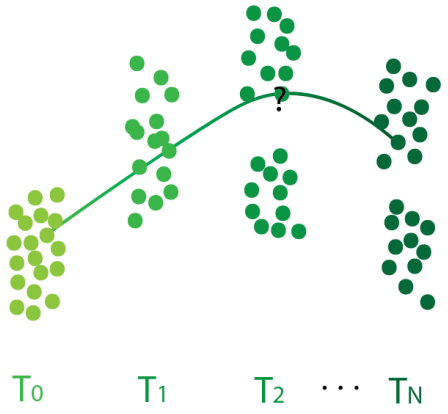

Dynamics from static snapshots

Data Geometry + Topology+ Deep Learning

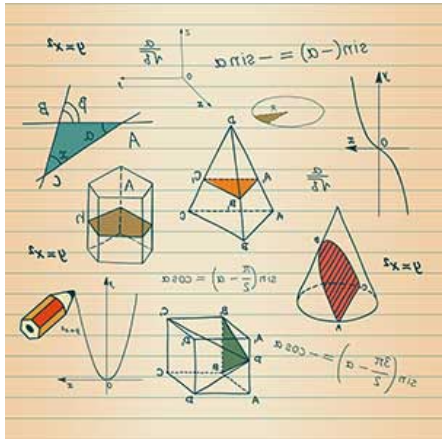

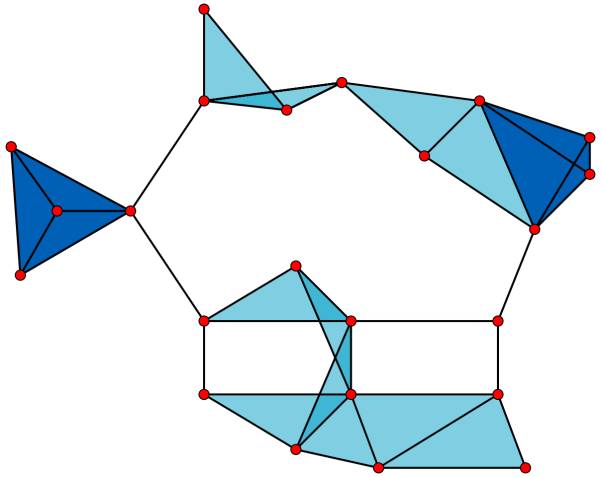

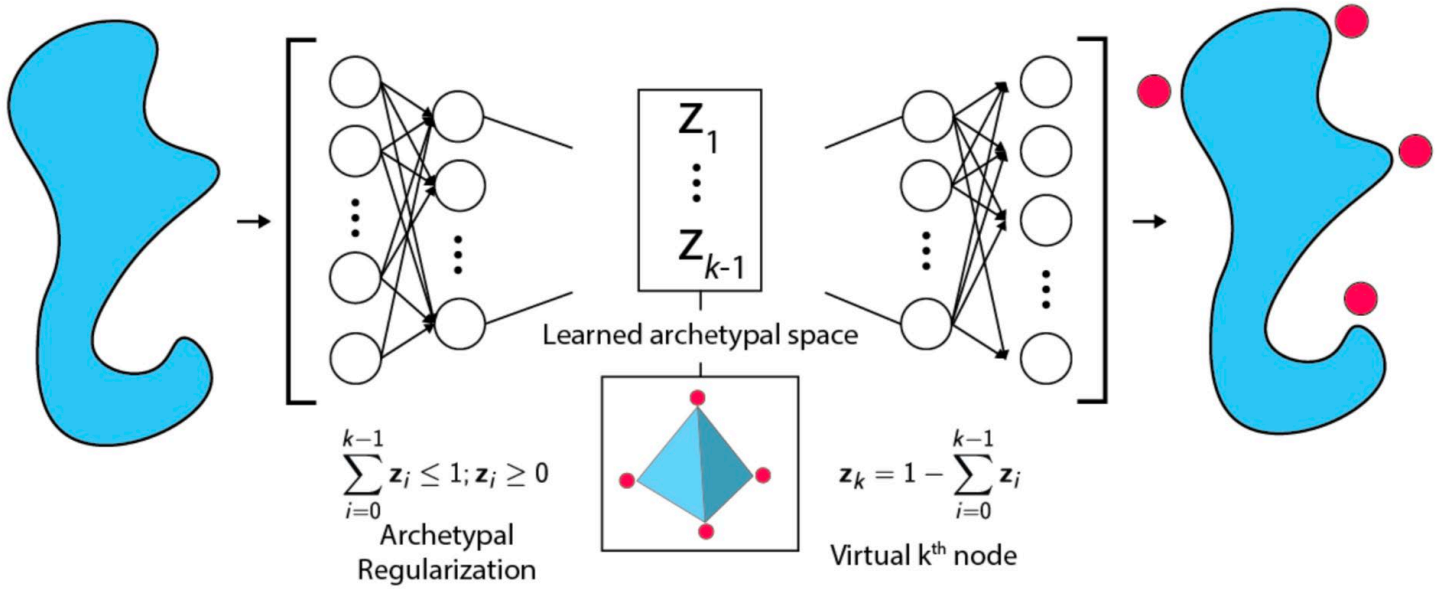

Diffusion Topology

(Huguet et al SIMODS 2023,
Brugnone N, Gonoposkiy A., IEEE Big Data 2019
Moyle et al. Nature 2021, Kuchroo et al. Nat Comm 2023)

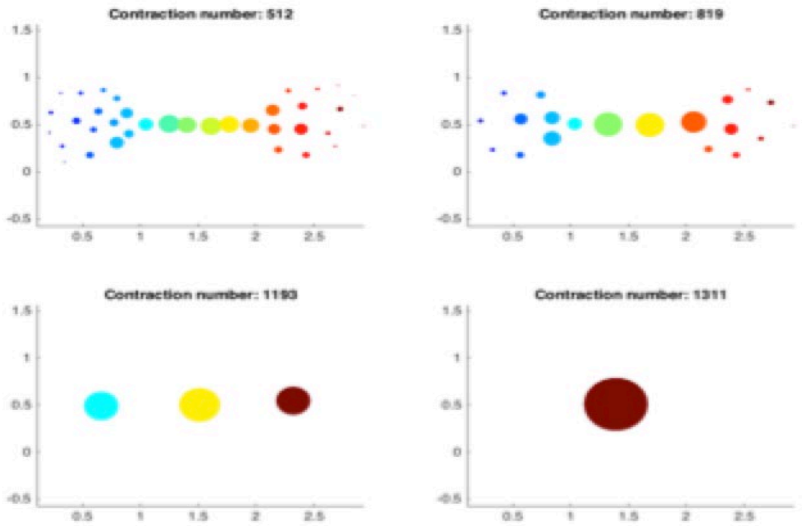

Main idea: allow natural groupings of datapoints to appear at all levels of granularity

Guillaume Huguet
Alex Tong
Nate Brugnone
Manik Kuchroo
Guy Wolf
Matt Hirn

High degree of complexity

Multi-level Organization

Characterization of D-dimensional Holes

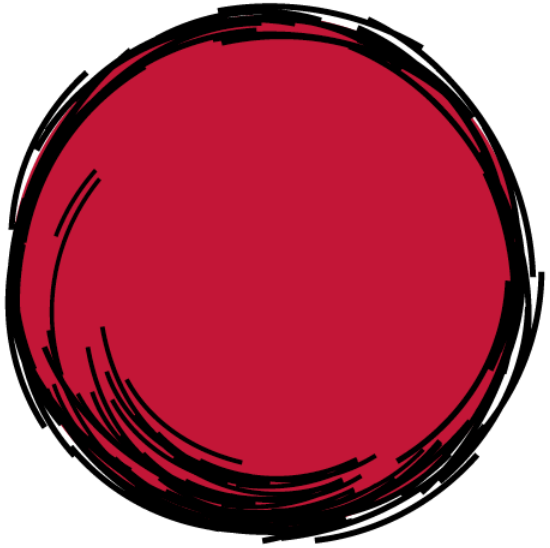

$\beta_0 = 1, \beta_1 = 0, \beta_2 = 1$

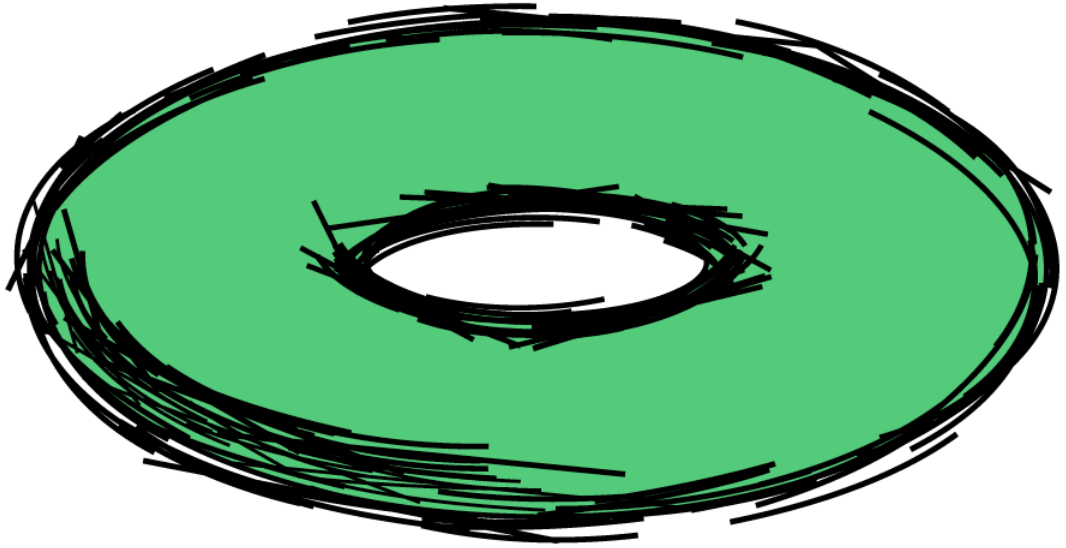

$\beta_0 = 1, \beta_1 = 2, \beta_2 = 1$

Computational Homology

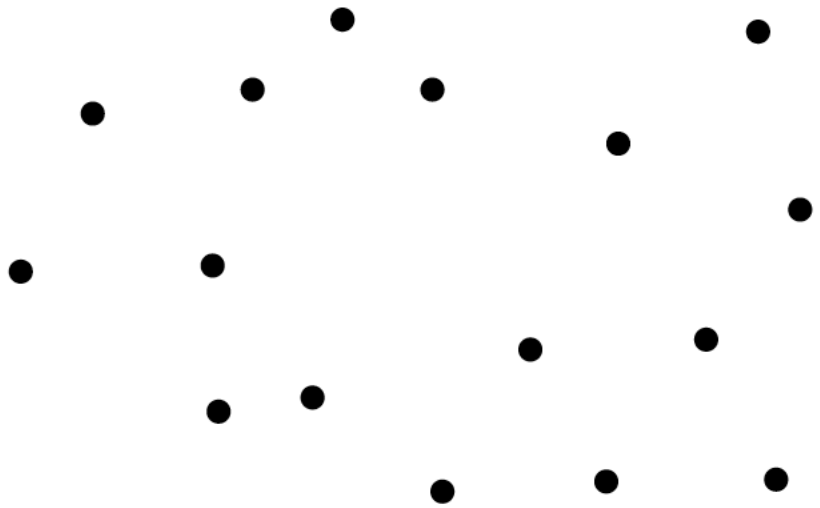

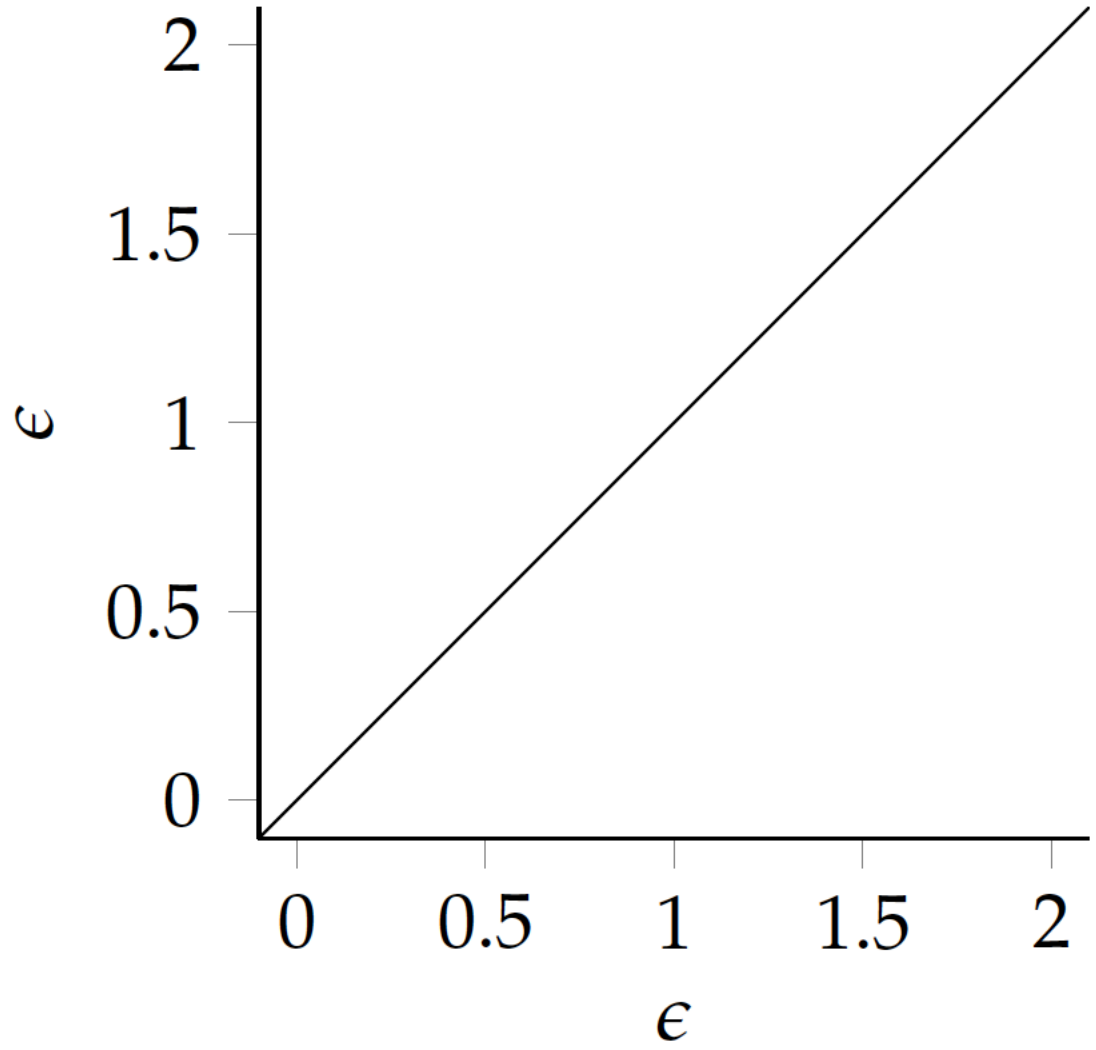

Computational Homology

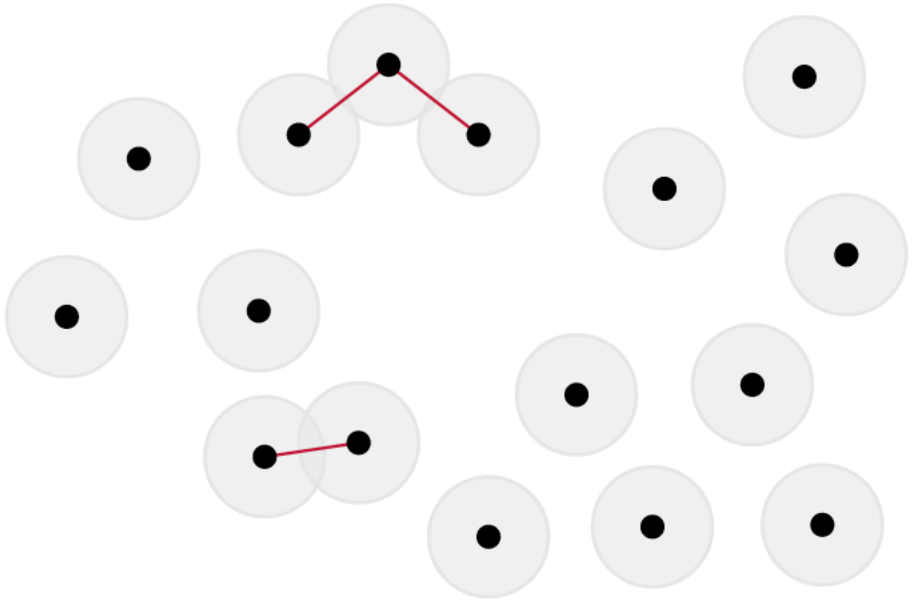

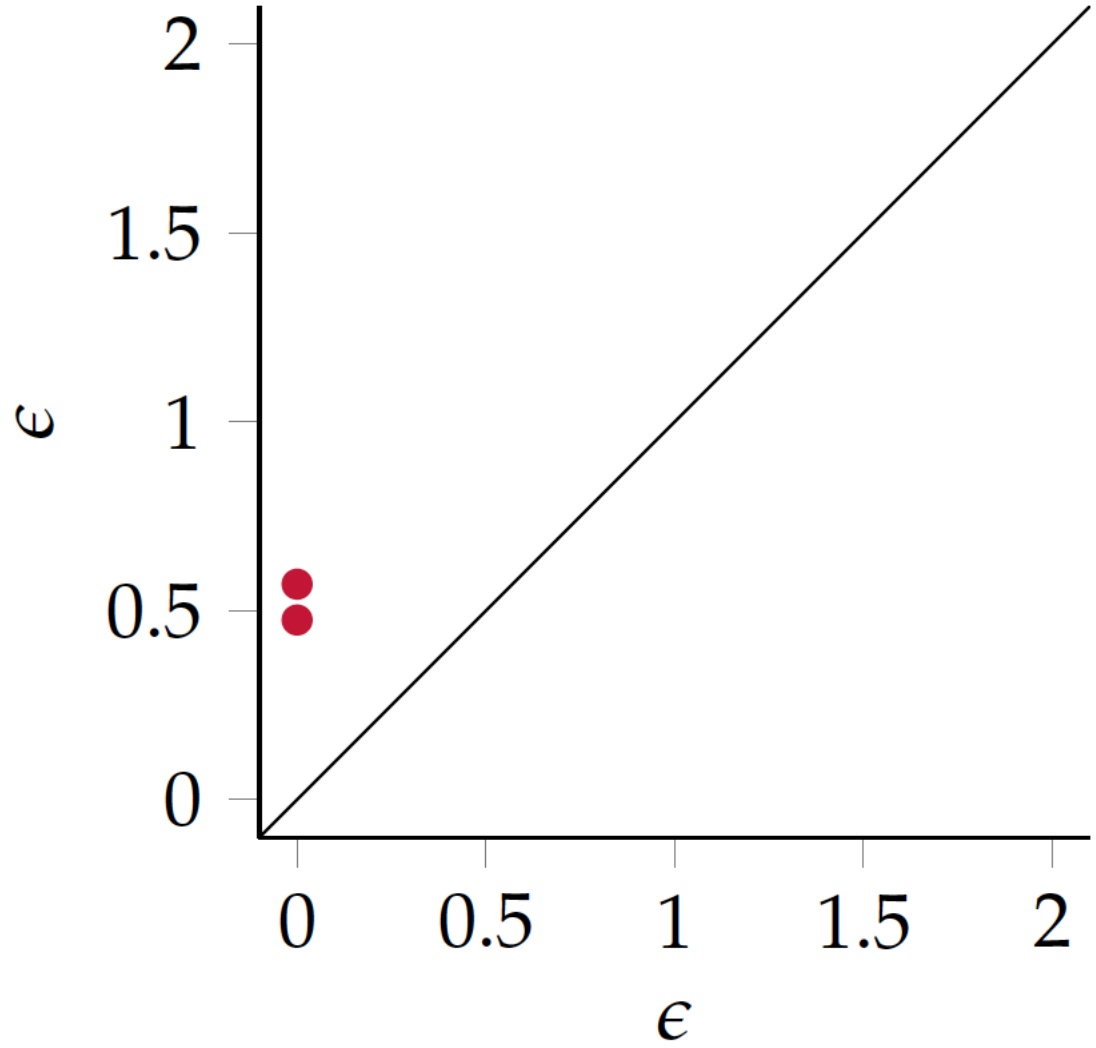

Computational Homology

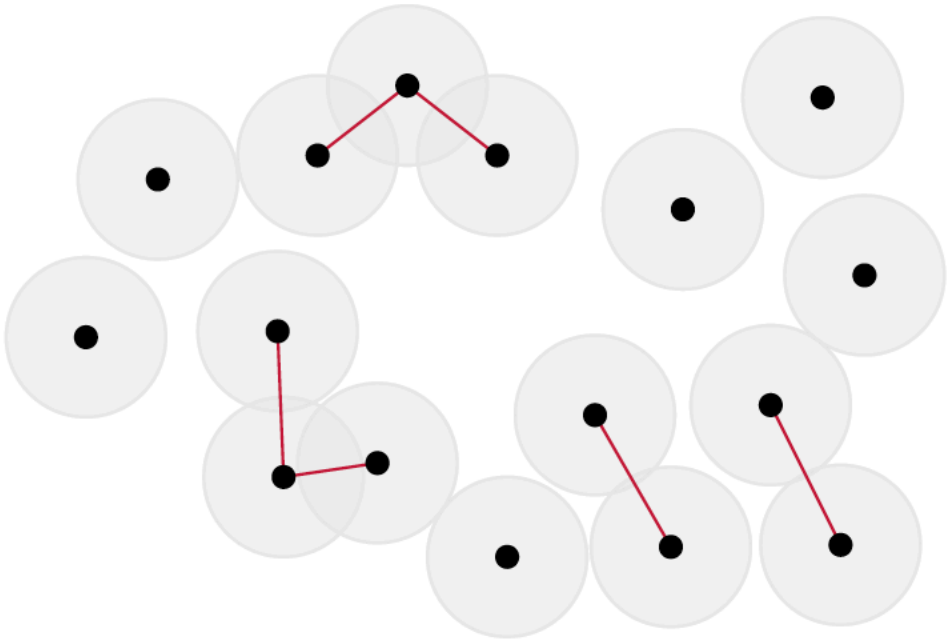

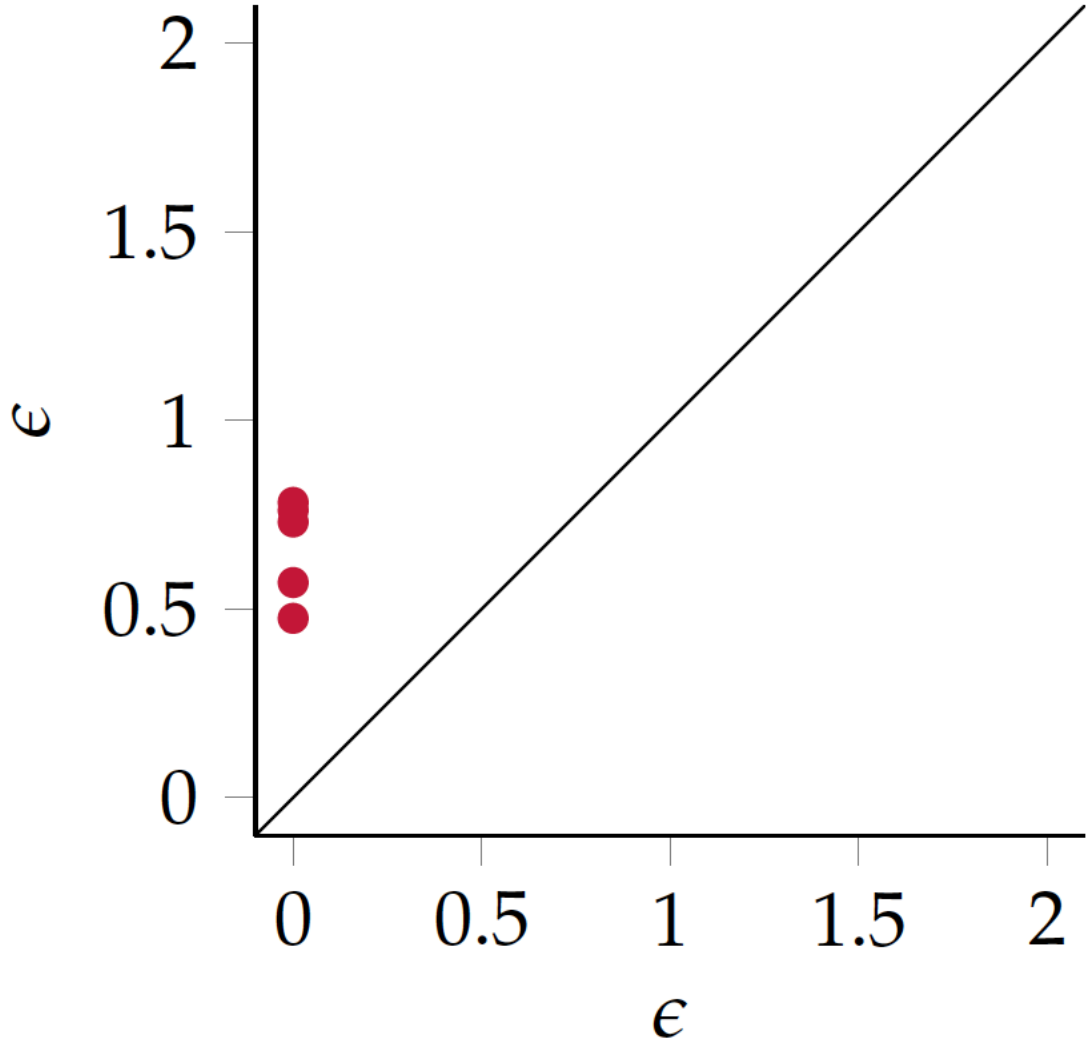

Computational Homology

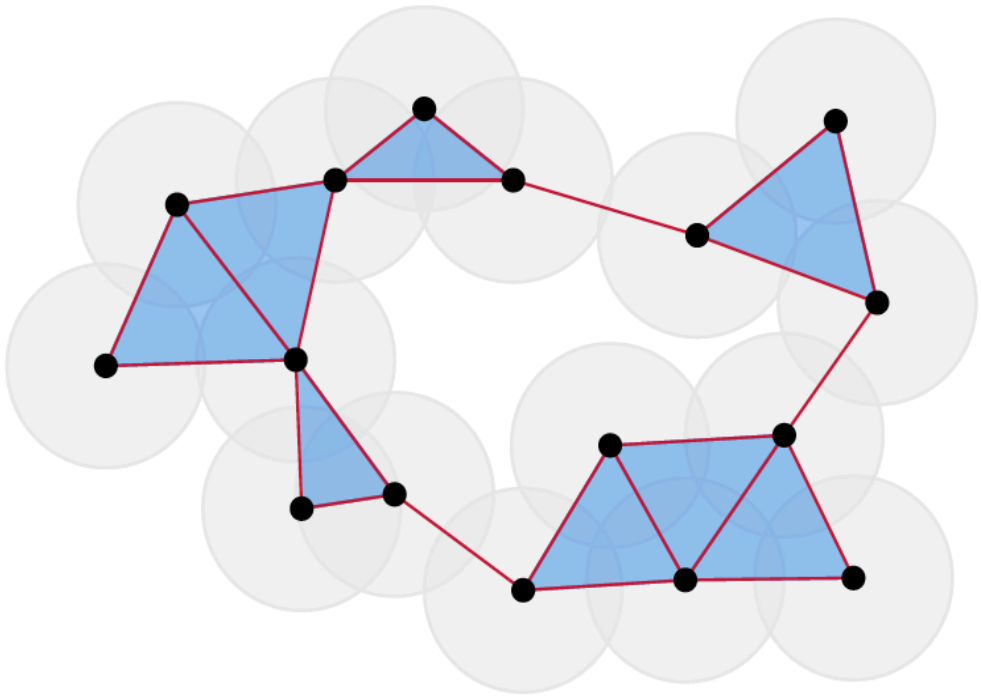

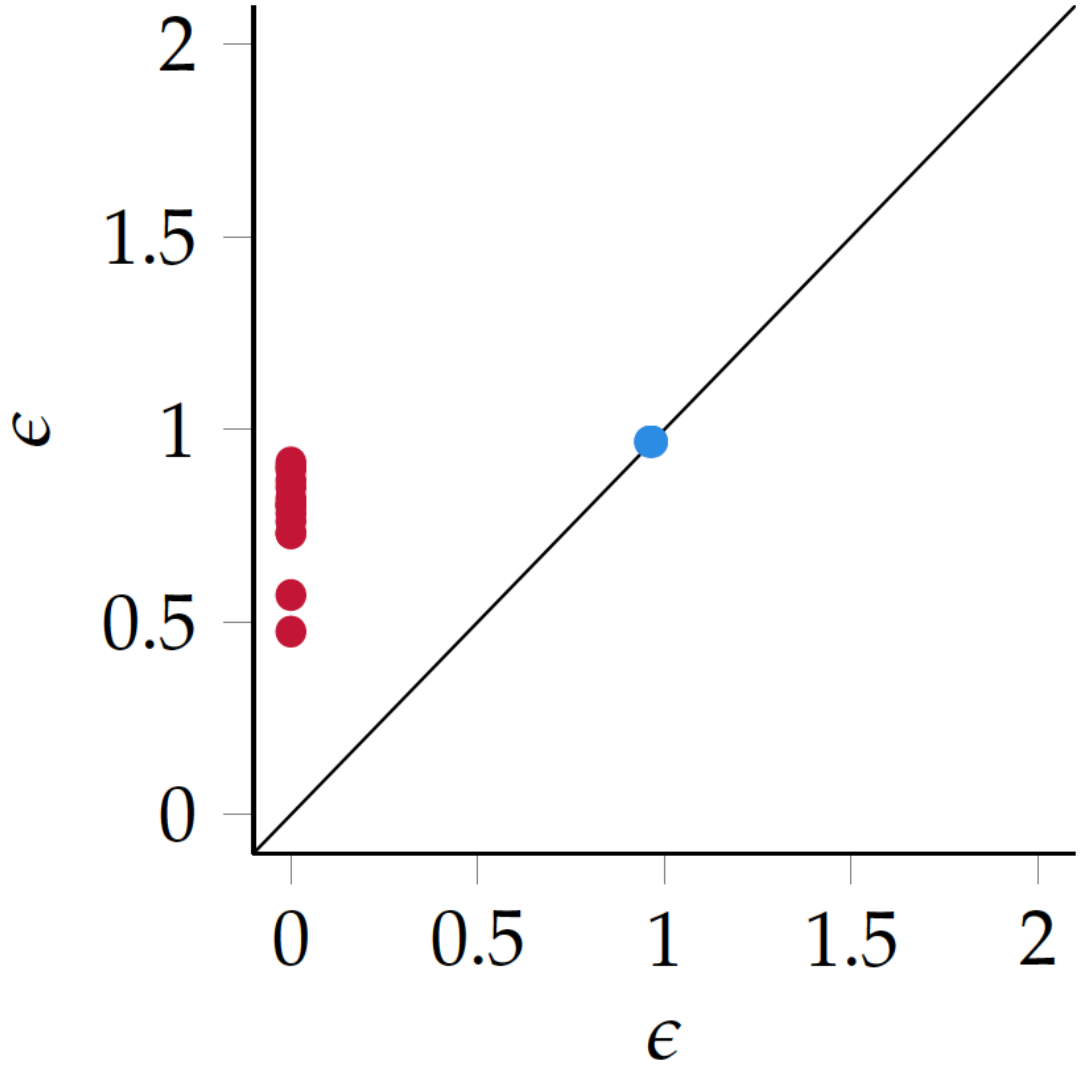

Computational Homology

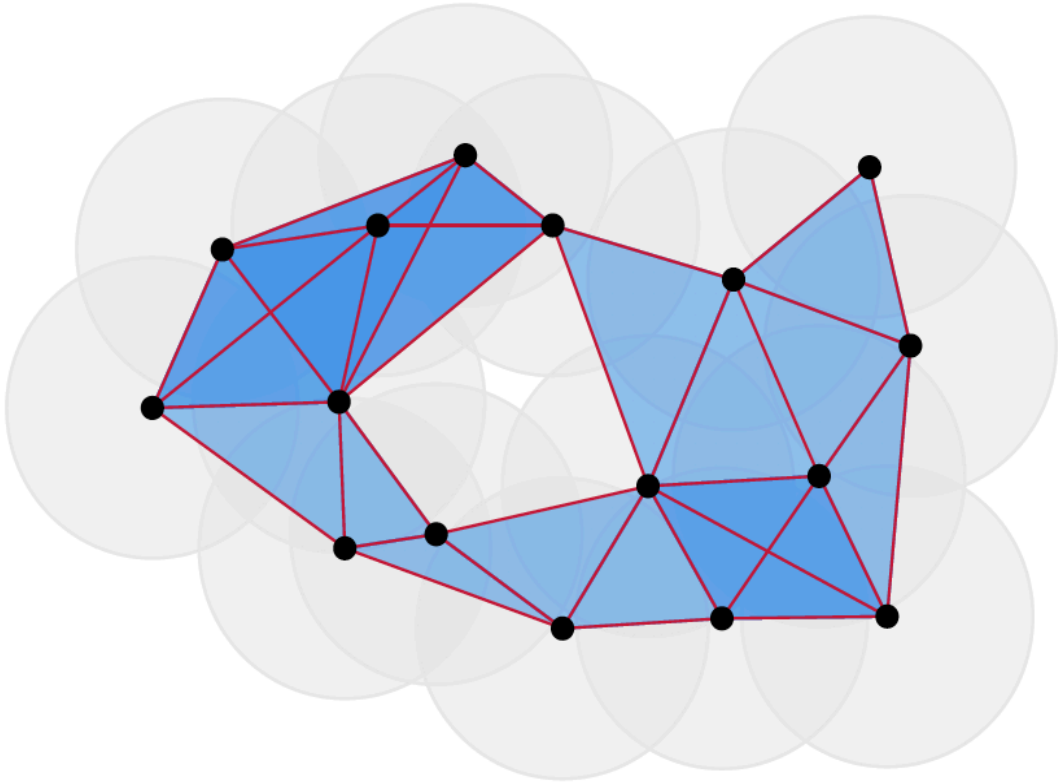

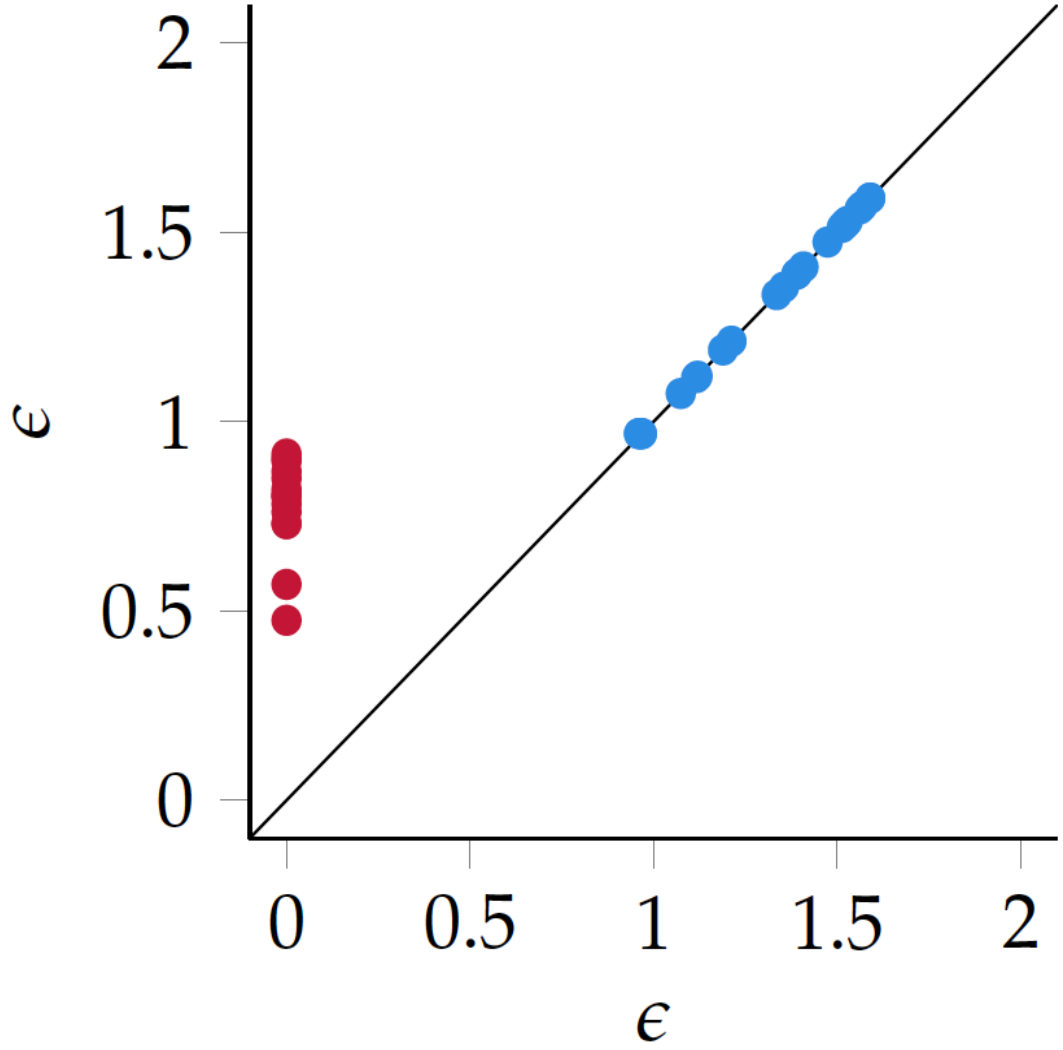

Computational Homology

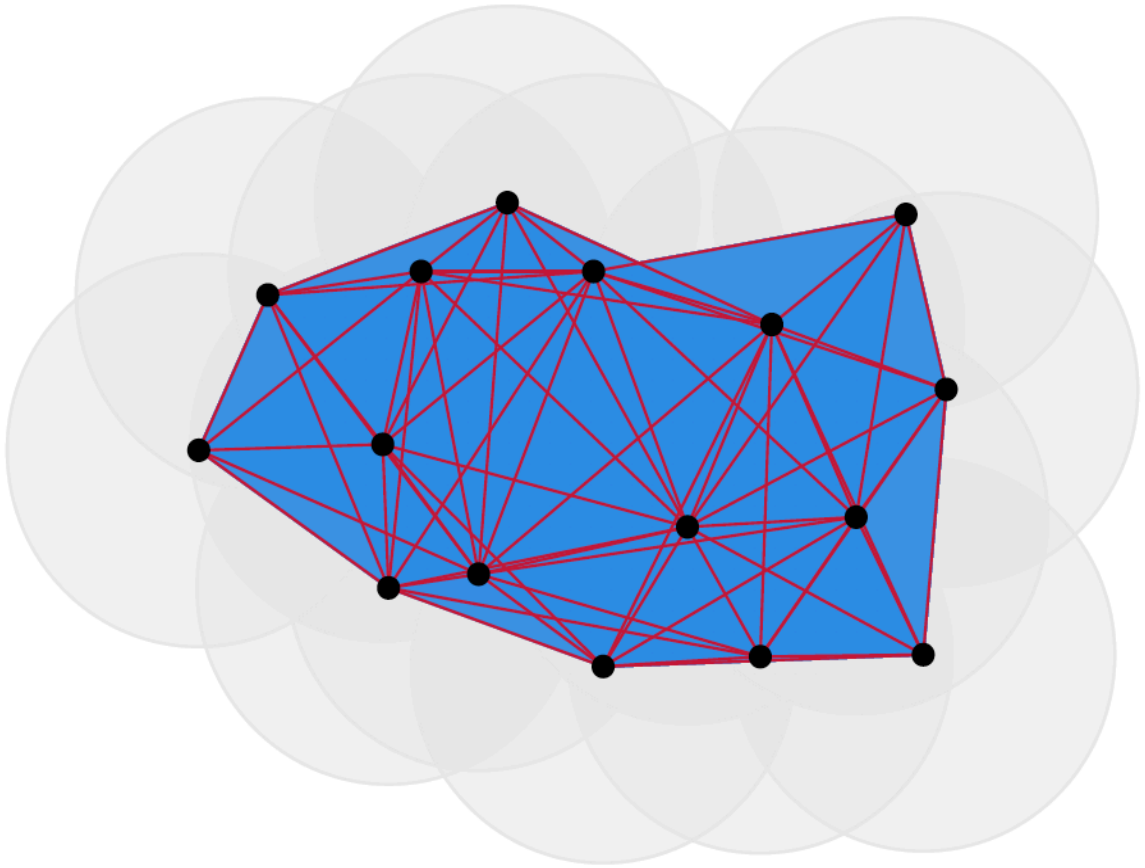

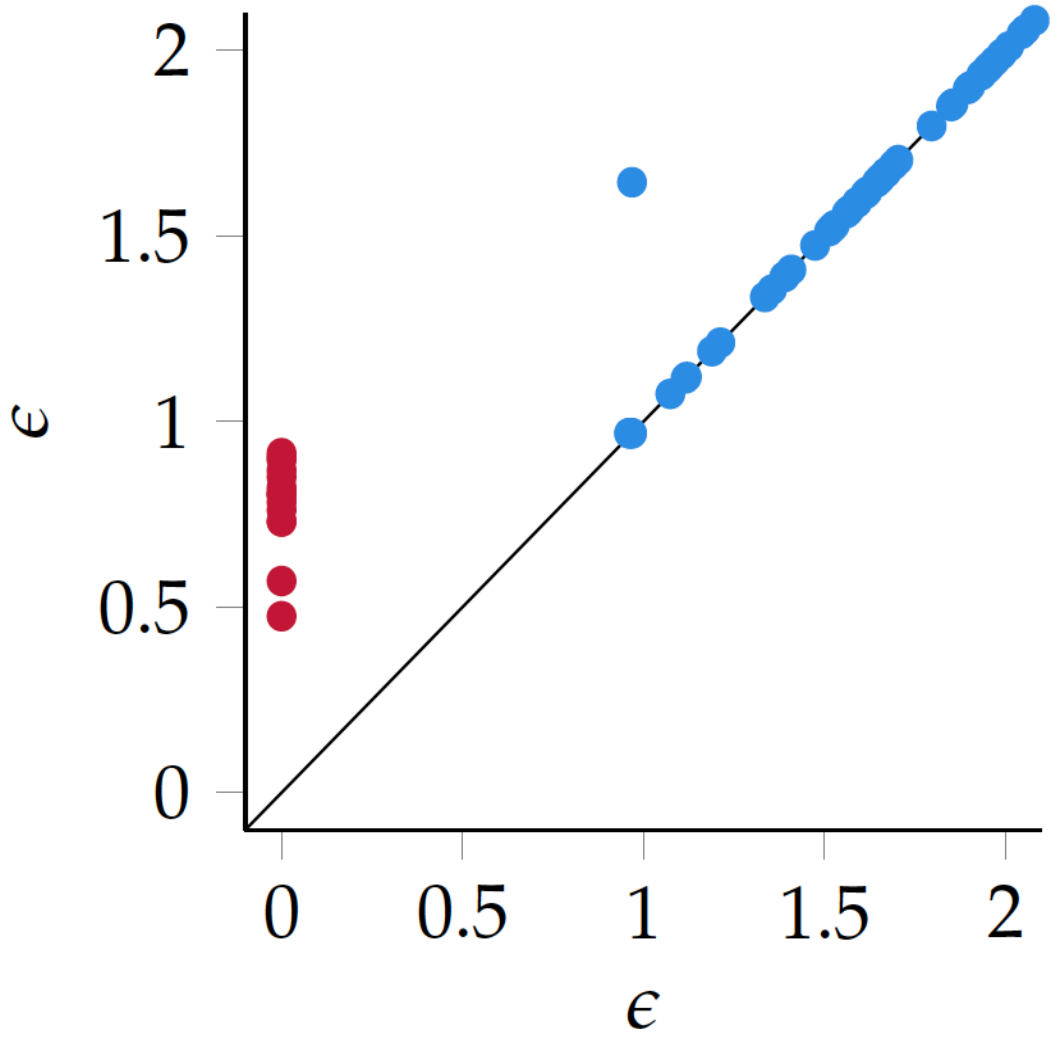

Problem: Noisy Connections

- Inference form noisy images/measurements
- Potentially inaccurate segmentations
- Solution
  - ==>Use redundancy and lower dimensionality in the graph spectrum to address this

Scientific data: often sampled from a manifold

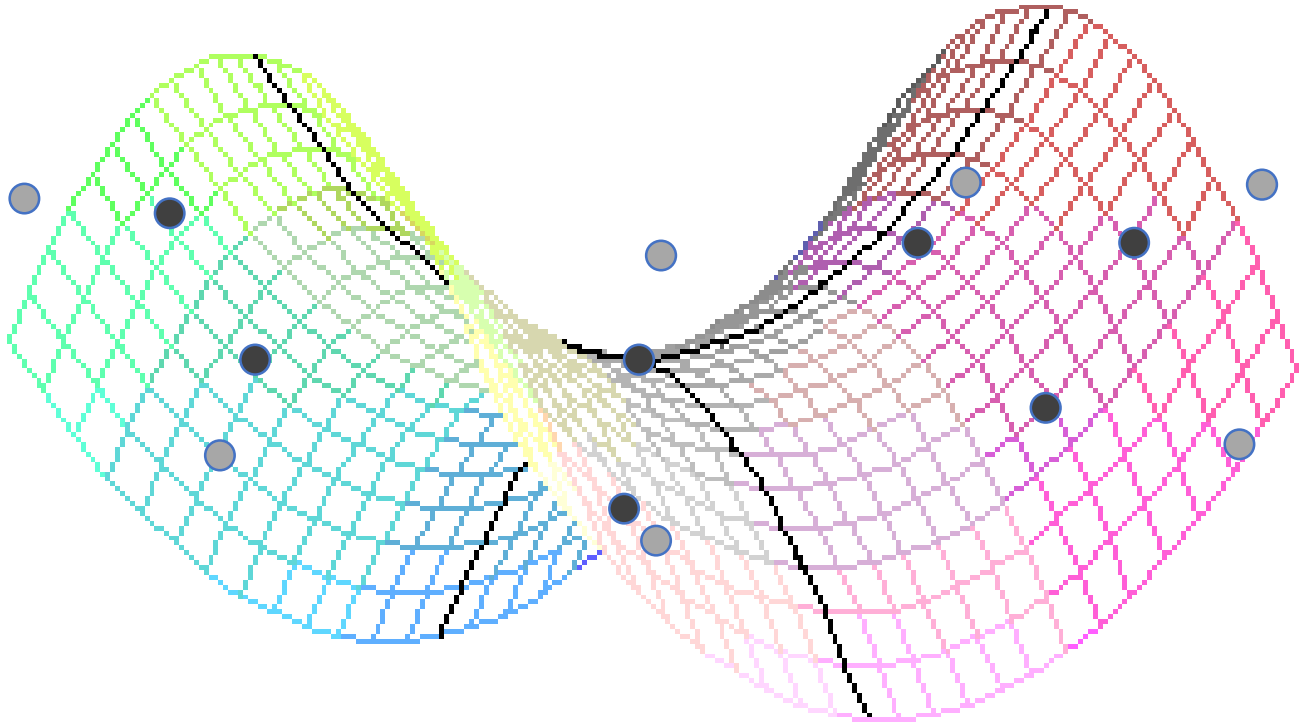

(with noise)

Why is a good assumption for scientific data?

Uncorrelated features

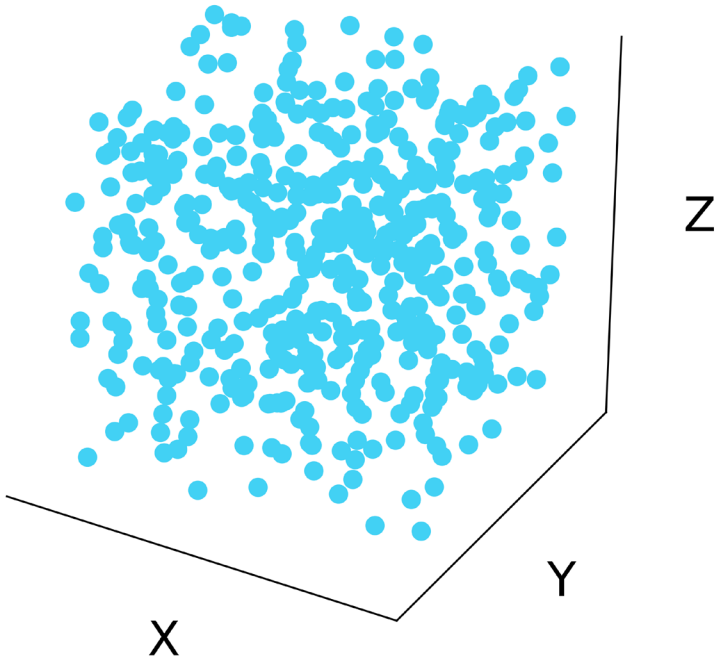

Mutually informative features

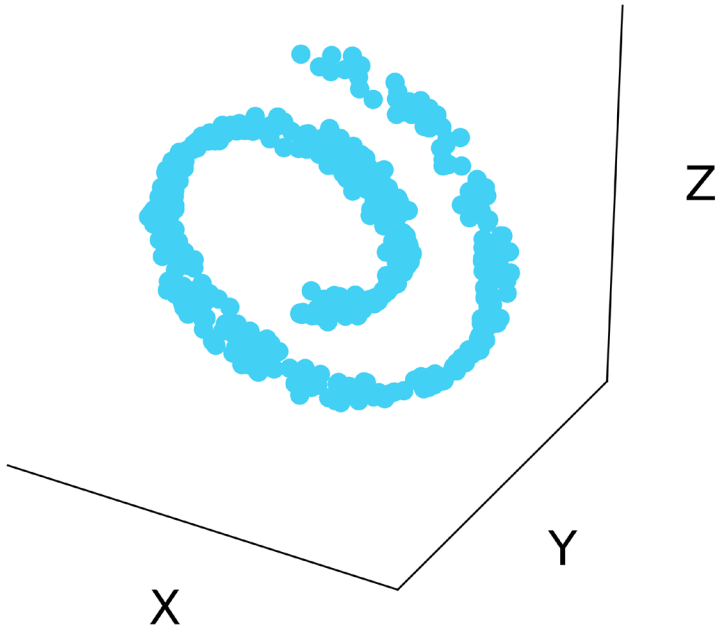

Bridging from Graphs to Manifolds

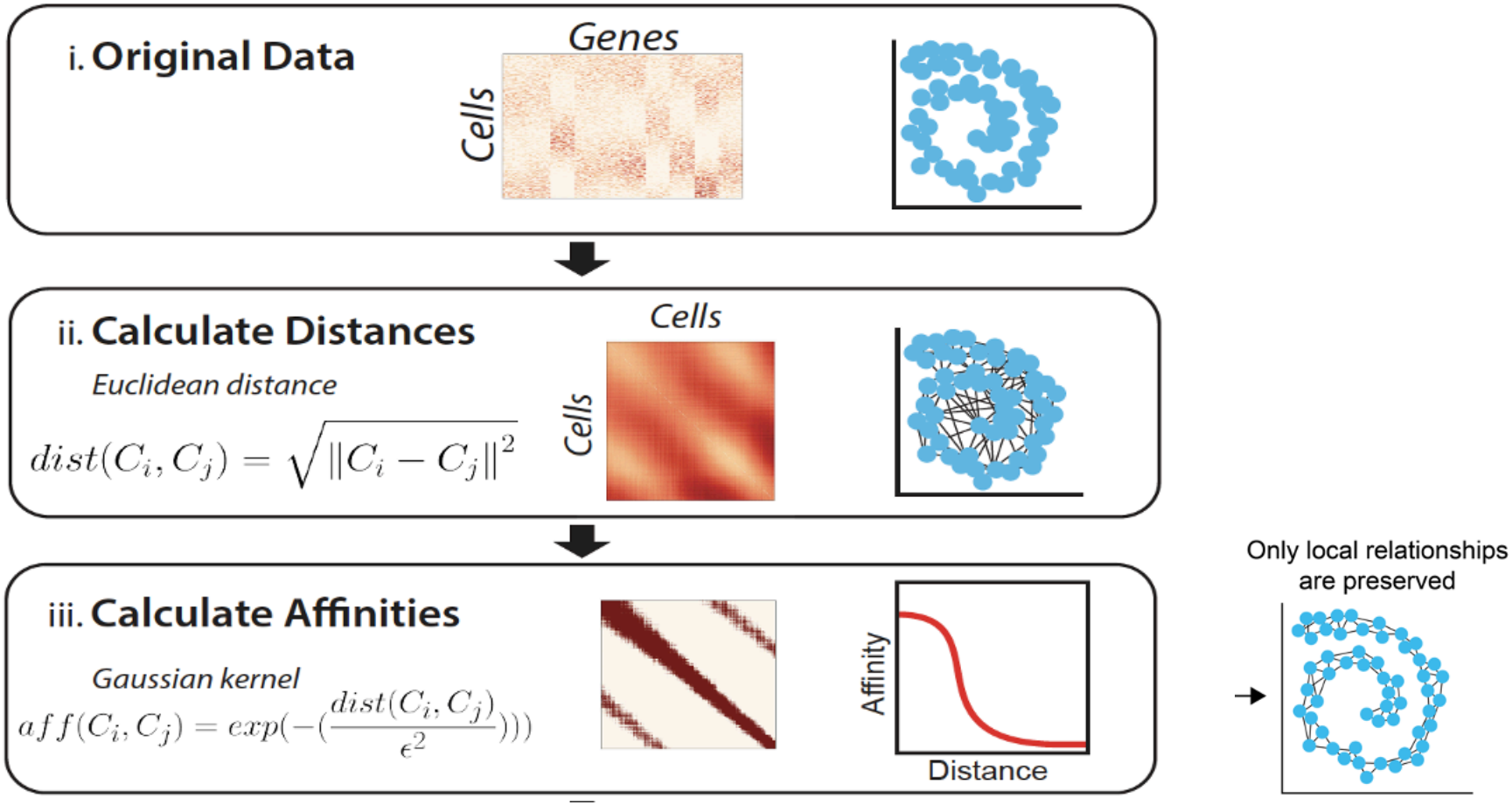

Data Diffusion Operator

Markov Matrix

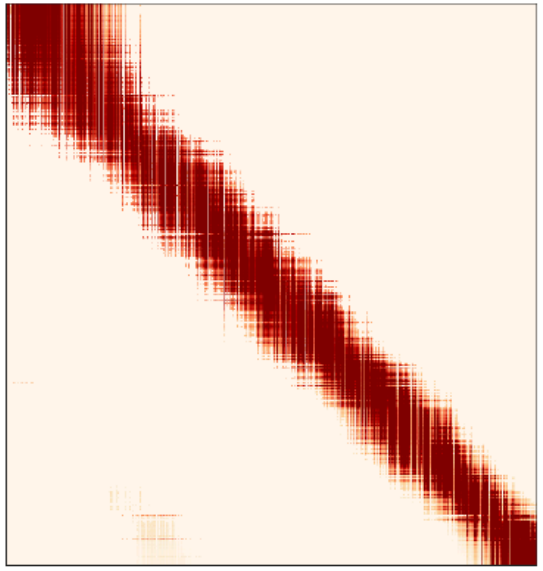

t

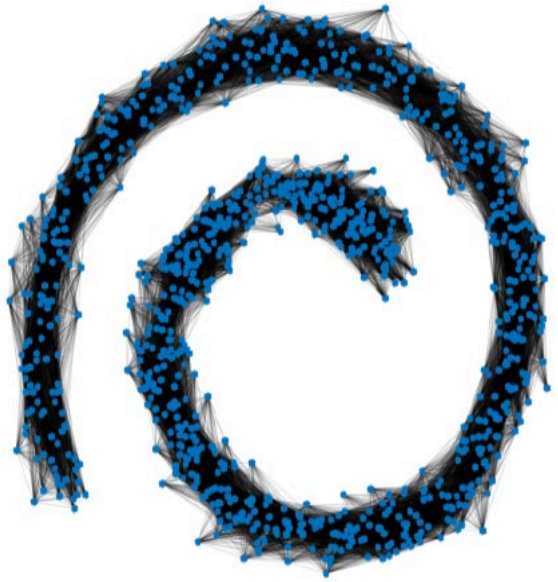

$$P(x_i, x_j) = \frac{A(x_i, x_j)}{\sum_j A(x_i, x_j)}$$

Diffusion Operator

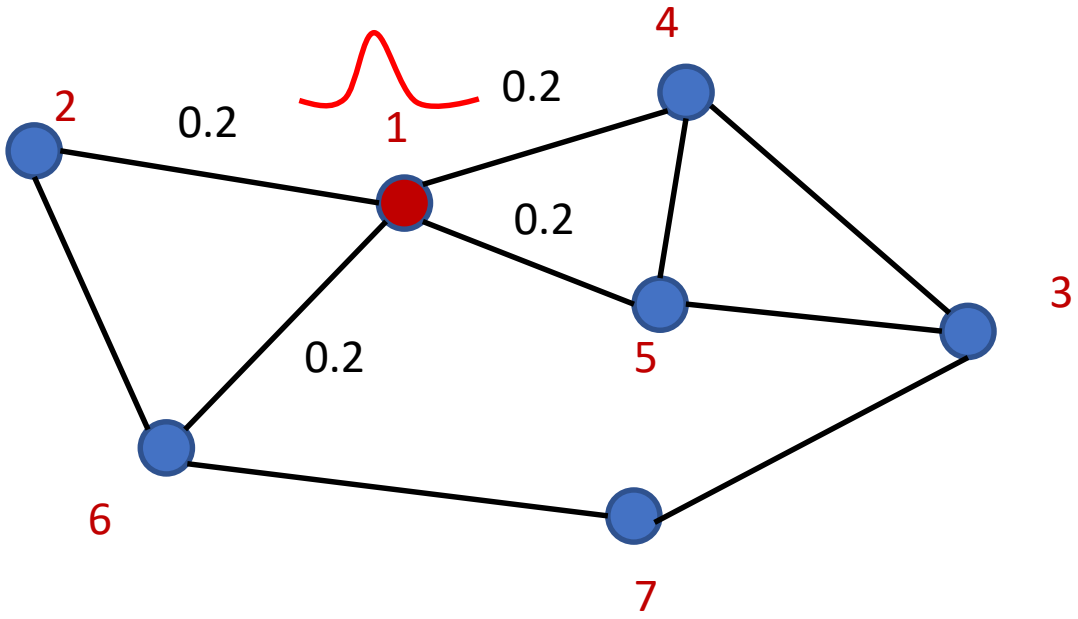

.2	.2	0	.2	.2	.2	0
.333	.333	0	0	0	.333	0
0	0	.25	.25	.25	0	.25
.25	0	.25	.25	.25	0	0
.25	0	.25	.25	.25	0	0
.25	.25	0	0	0	.25	.25
0	0	.333	0	0	.333	.333

$$P = D^{-1}A$$

Diffusion Maps—Manifold Embedding

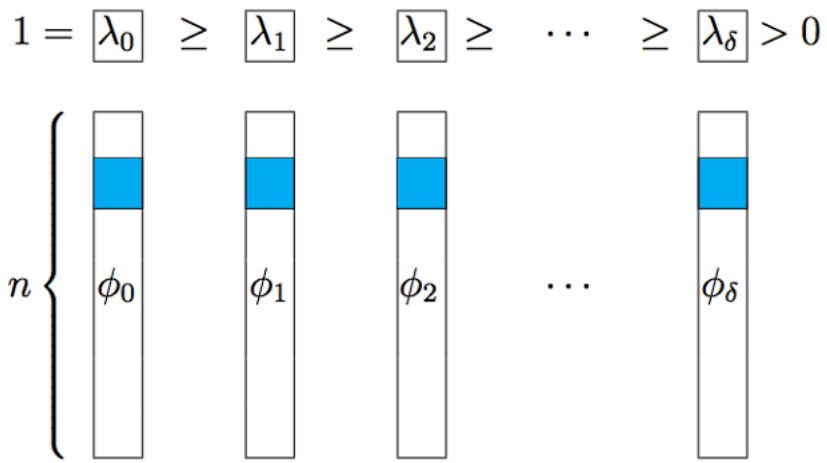

[Coifman, Lafon 2006]

Thrm [Coifman et al.] *The diffusion map* $\Phi_t(x_i) = [\lambda_1^t \phi_1(x_i), \ldots \lambda_N^t \phi_N(x_i)]^T$ *embeds data into a Euclidean space Where the Euclidean distance is equal to the diffusion distance* D_m.

$$D_m^2(x,y) = ||P^t(x,.) - P^t(y,.)||_2 = ||\ \Phi_t(x) - \Phi_t(y)||^2$$

Spectral clustering

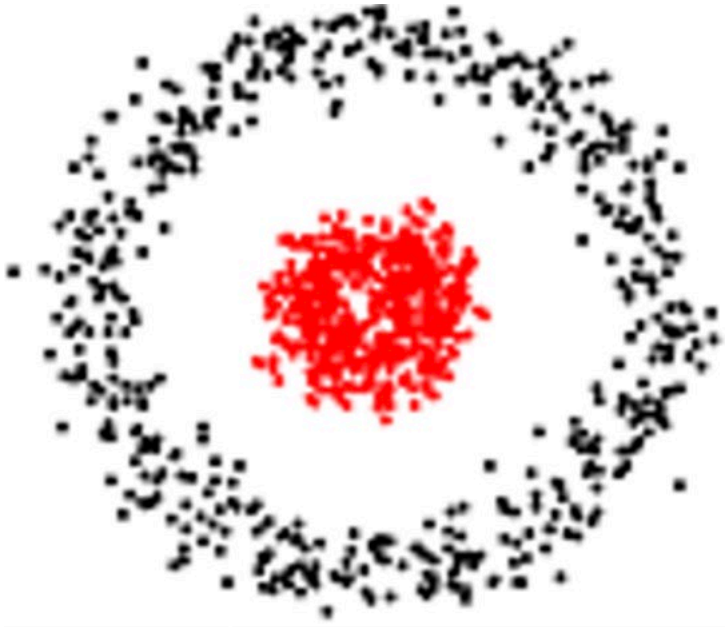

K-means graph spectra

K-means on a raw data

Diffusion Filtration

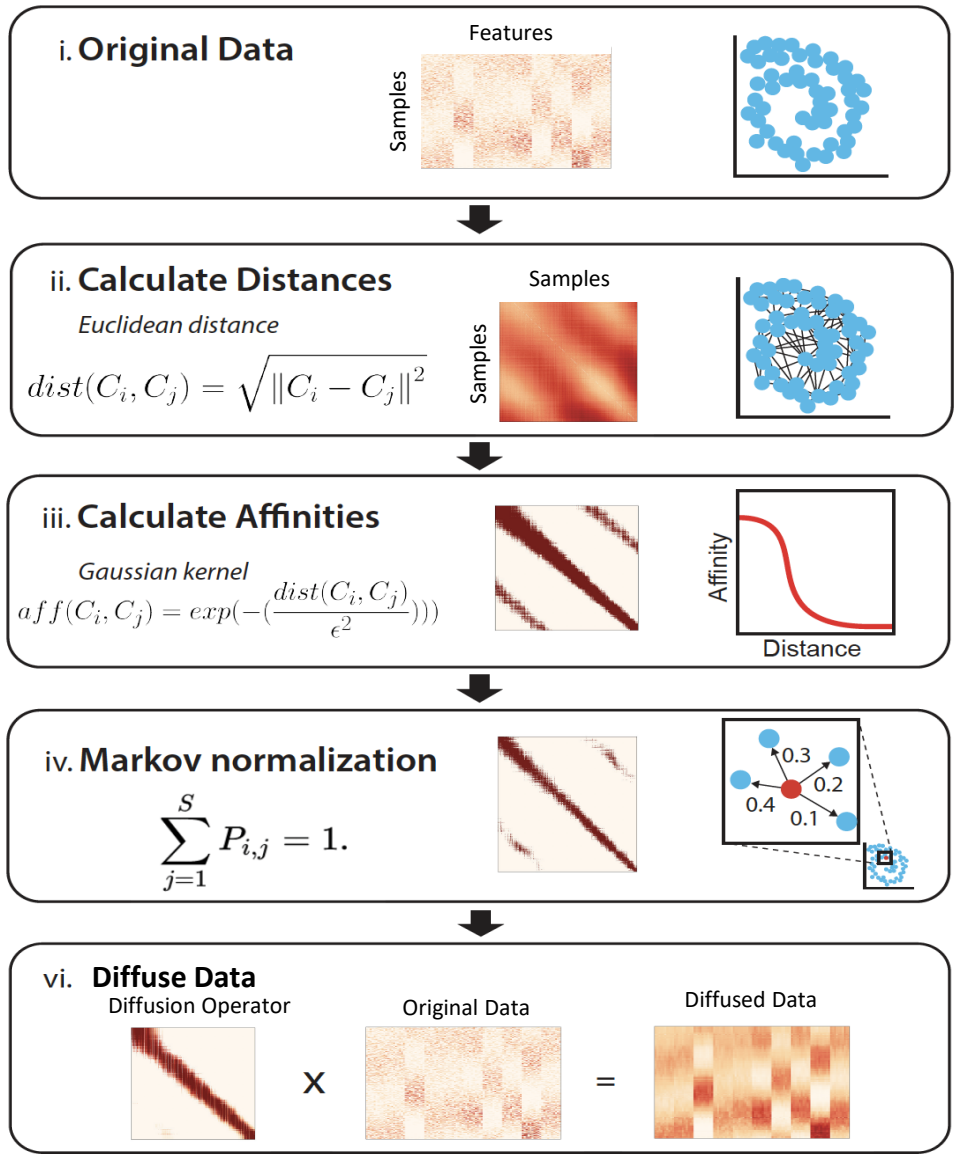

Huguet 2023, Brugnone et al. 2019

Creating a graph of the points

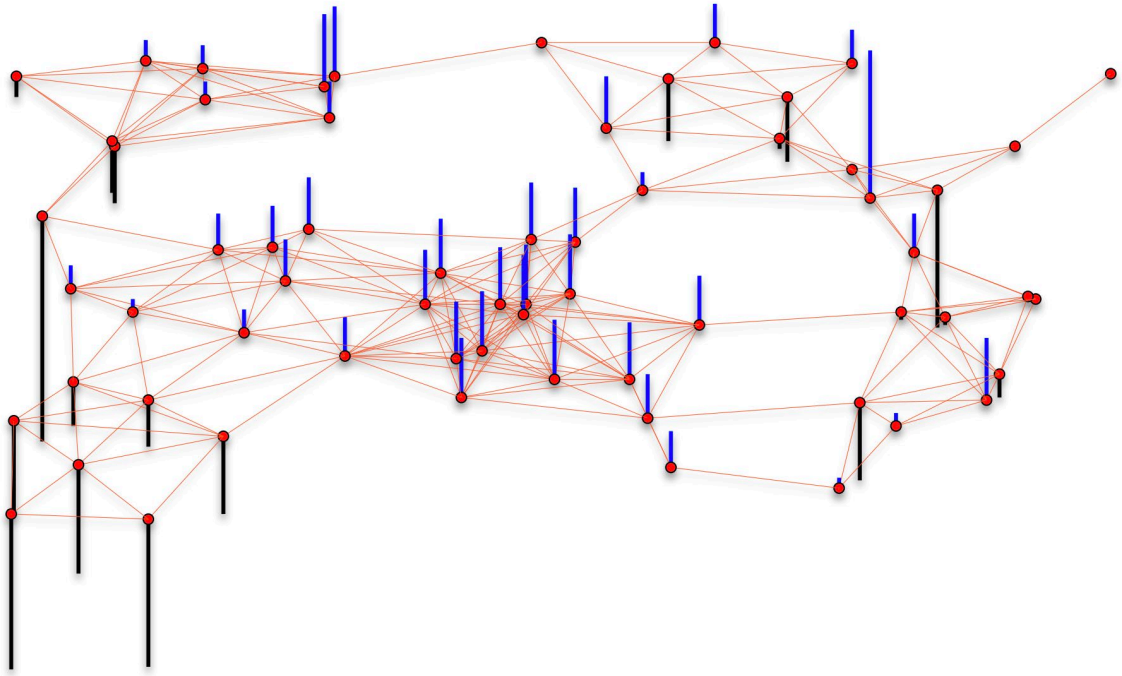

Features/coordinates are vertex features

Graph Fourier Transform

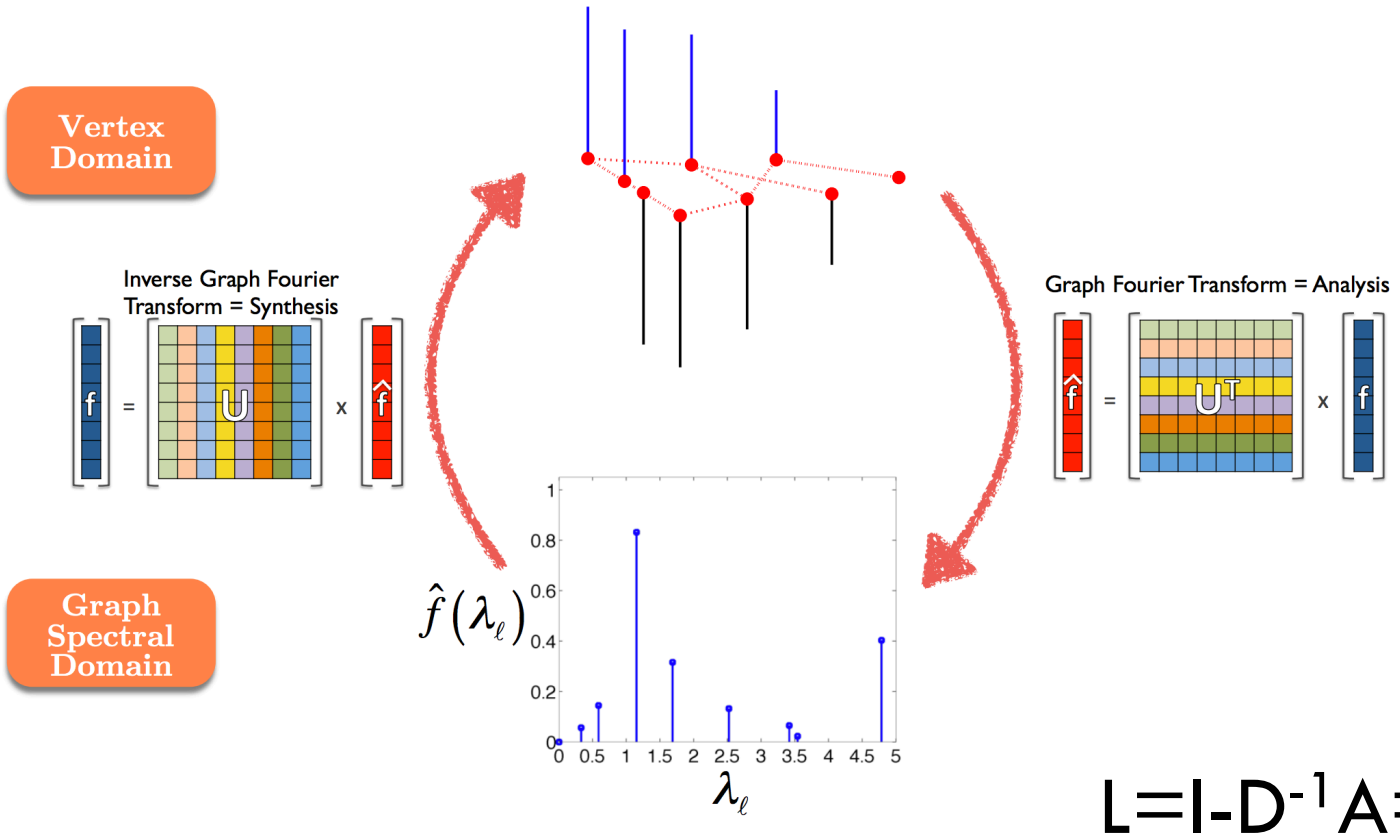

$L=I-D^{-1}A=I-P$

(Shuman et al. 2013)

Diffusion performs low pass filter

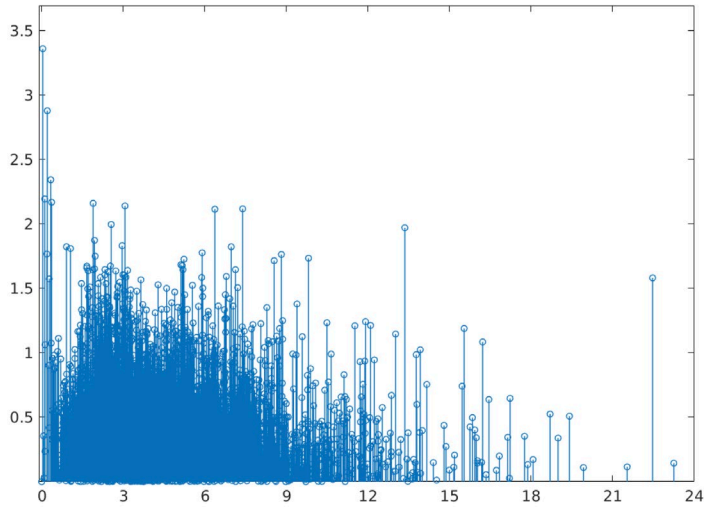

No Smoothing

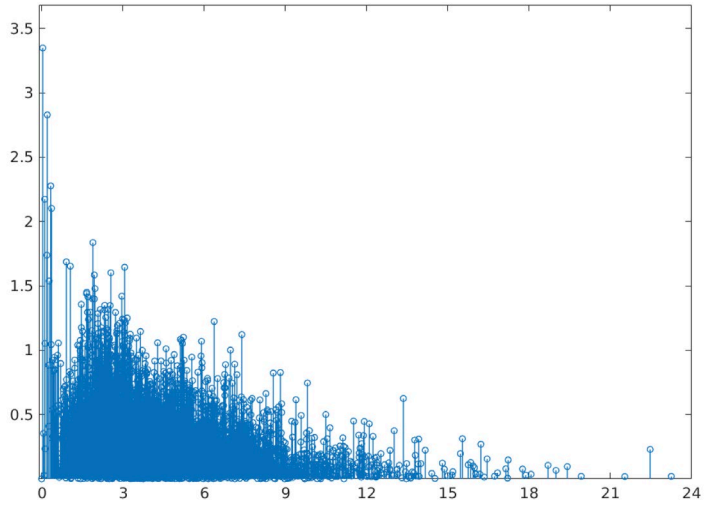

T=2

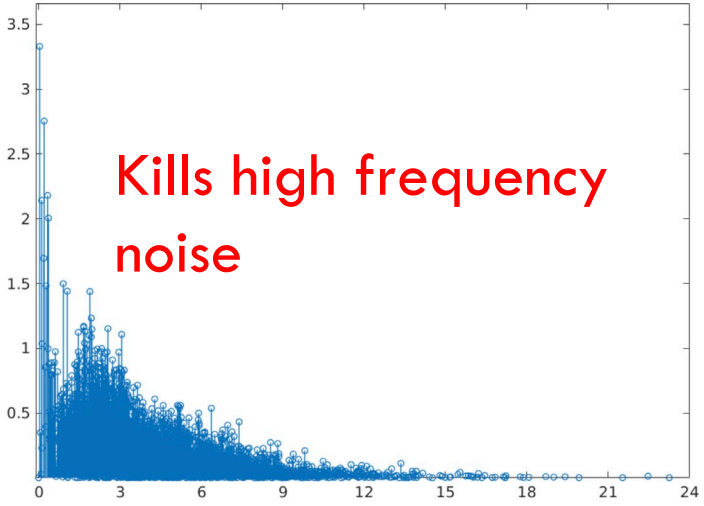

Kills high frequency noise

T=5

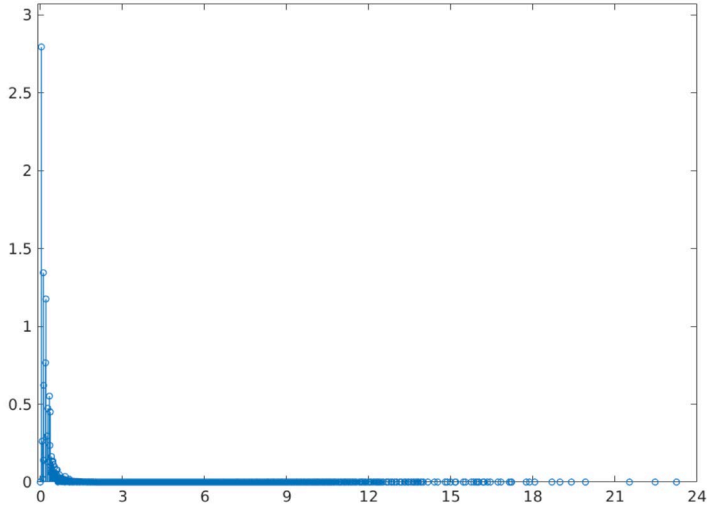

T=100

Smoothing in the spatial domain

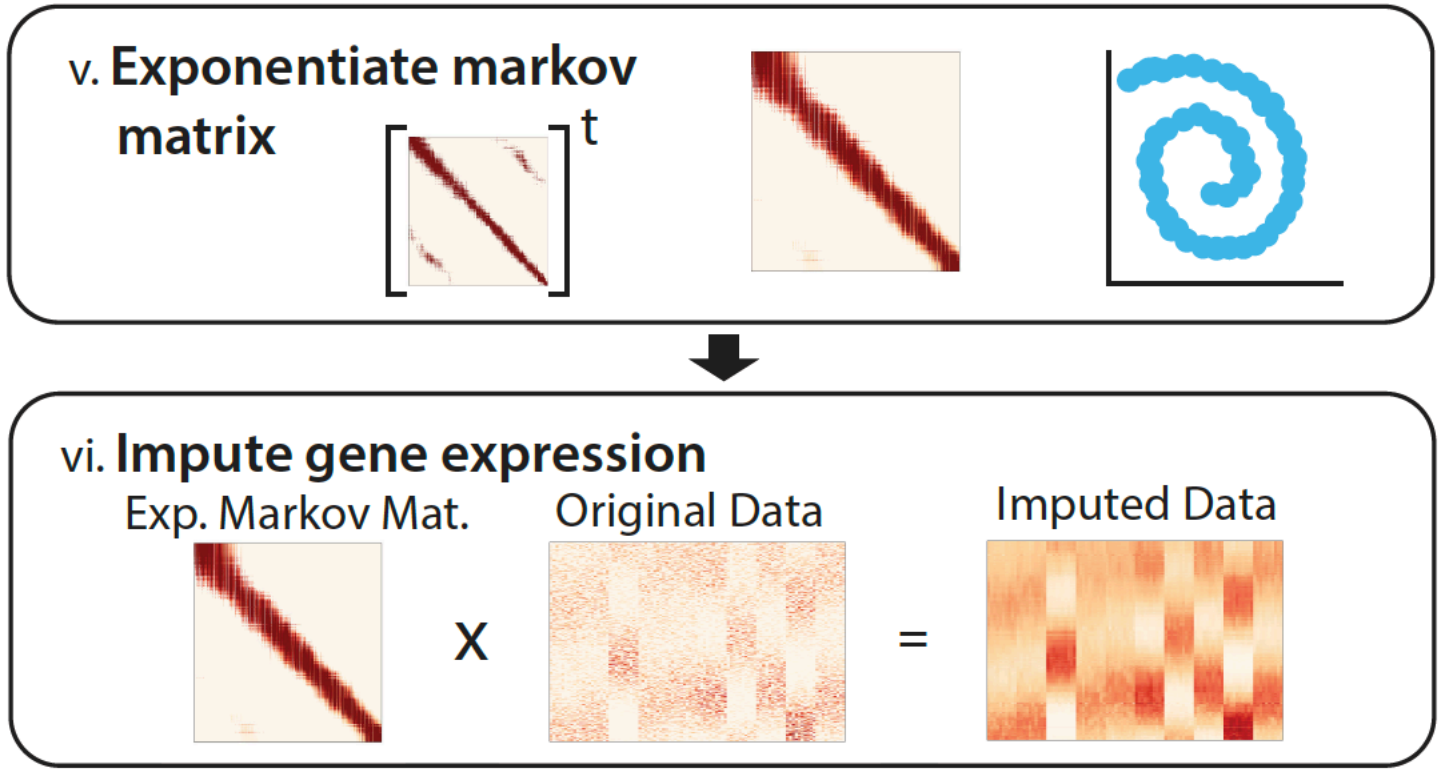

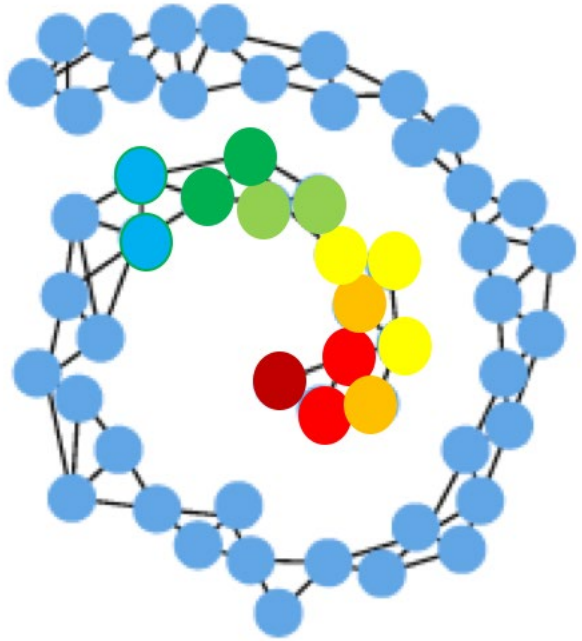

van Dijk et al. Cell 2018

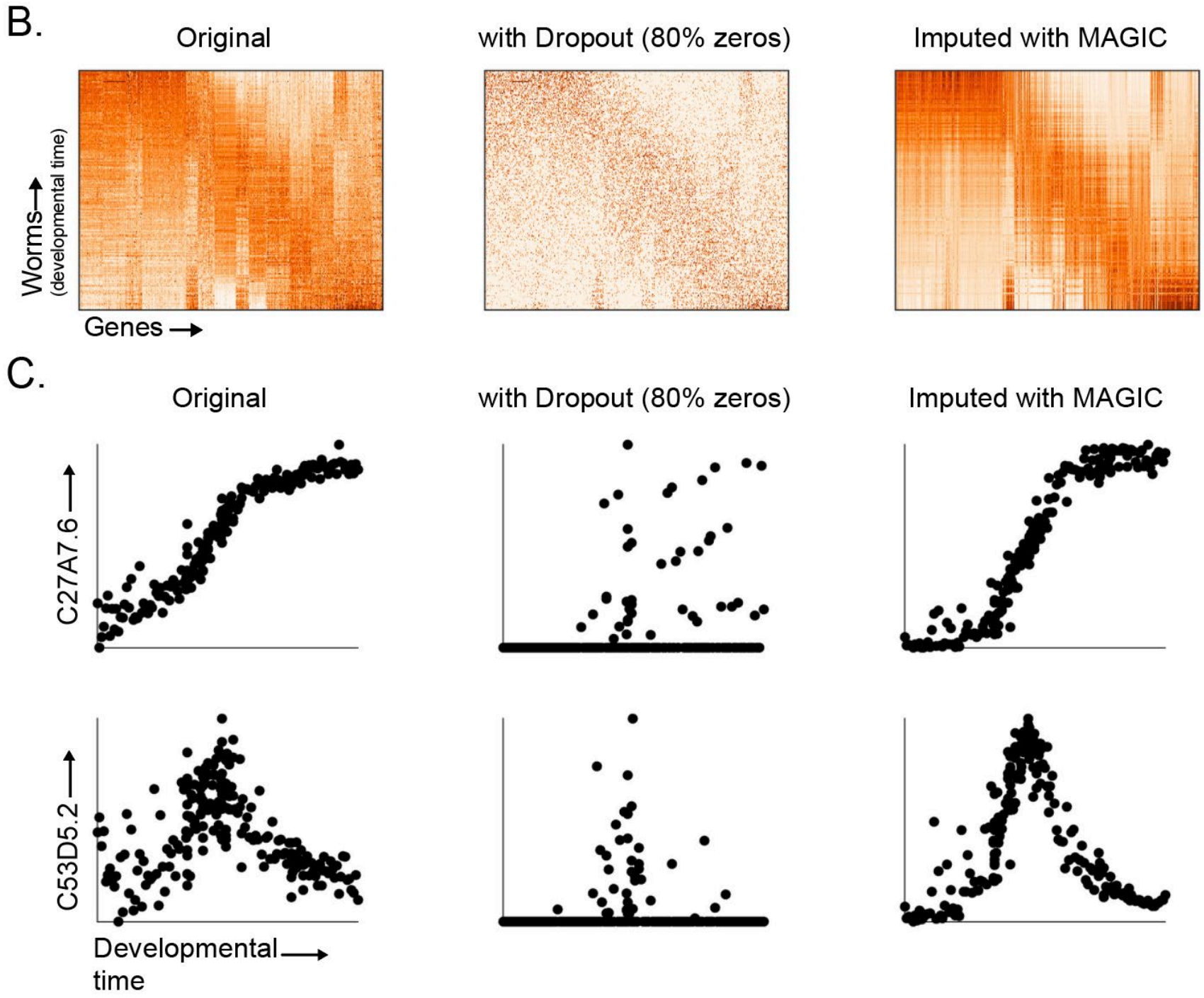
B.
Original
with Dropout (80% zeros)
Imputed with MAGIC
Worms
(developmental time)
Genes
C.
Original
with Dropout (80% zeros)
Imputed with MAGIC
C27A7.6
C53D5.2
Developmental
time

Points eventually converge

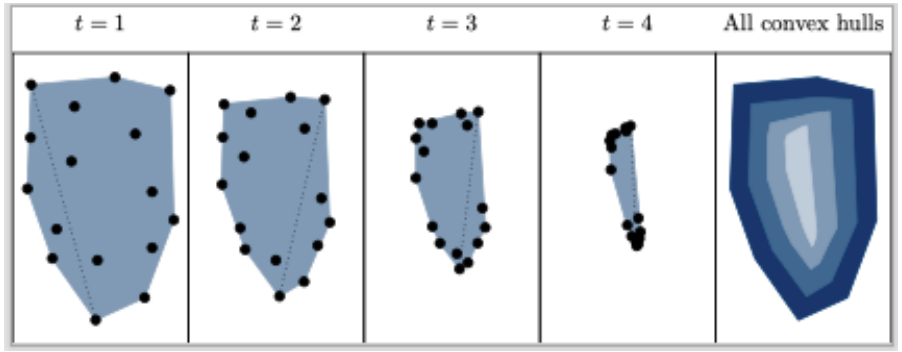

- Application of a **positive diffusion operator** to a datapoint makes it a convex combination of the points in the dataset, and thus it goes into the interior of the current data convex hull
- ➔The convex hull shrink
- Shrinks at a rate proportional to ∂ which is the smallest value in the kernel

Spectral Convergence

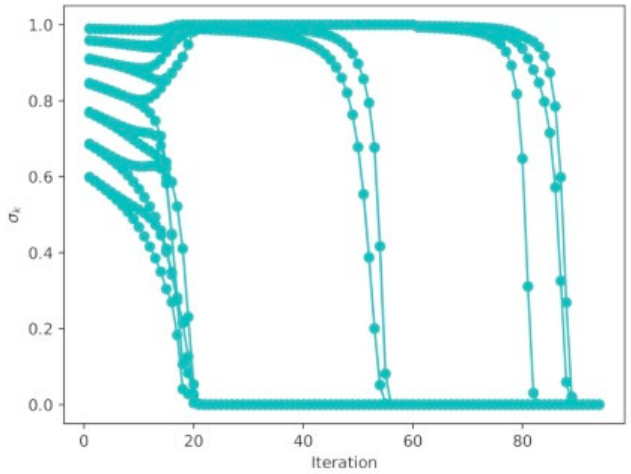

Lemma *For the operator $\mathbf{P}_t$ and its second largest eigenvalue $\lambda_{t,2}$, we have the following bound on the norm of $H_t(\mathbf{P}_t f)$*

$$\|H_t(\mathbf{P}_t f)\|_{d_t} \leq \lambda_{t,2} \|H_t(f)\|_{d_t},$$

for all functions $f \in \mathbb{R}^N$.

- When the diffusion operator is applied to a function (i.e., here the features of data, the first non-trivial eigenvalue (also called Fiedler value) is a bound on the resultant magnitude
- We can just **select** the bandwidth of the diffusion kernel such that the Fiedler value is bounded away from 1!

Condensation Homology

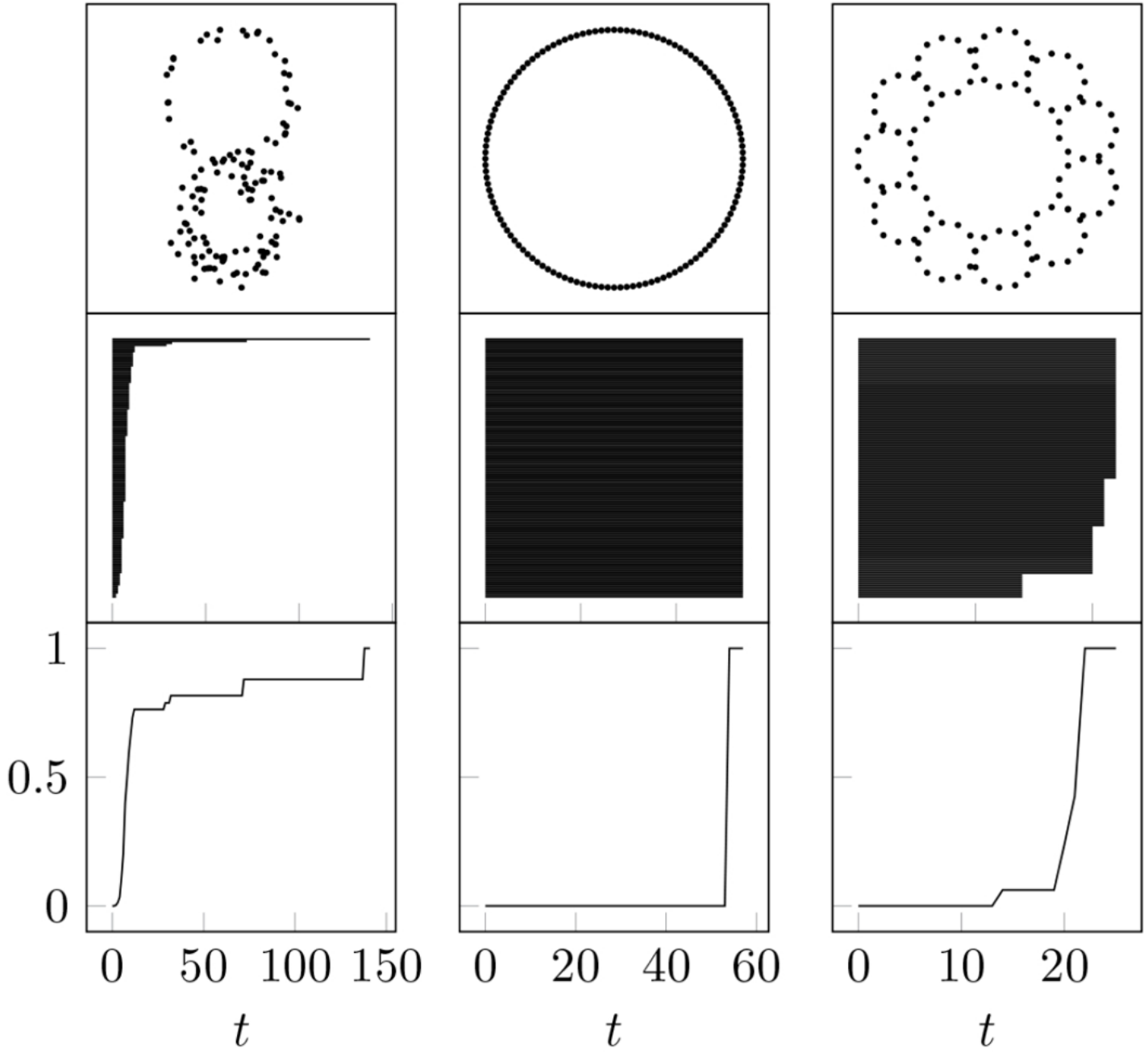

VR Homology (sequence)

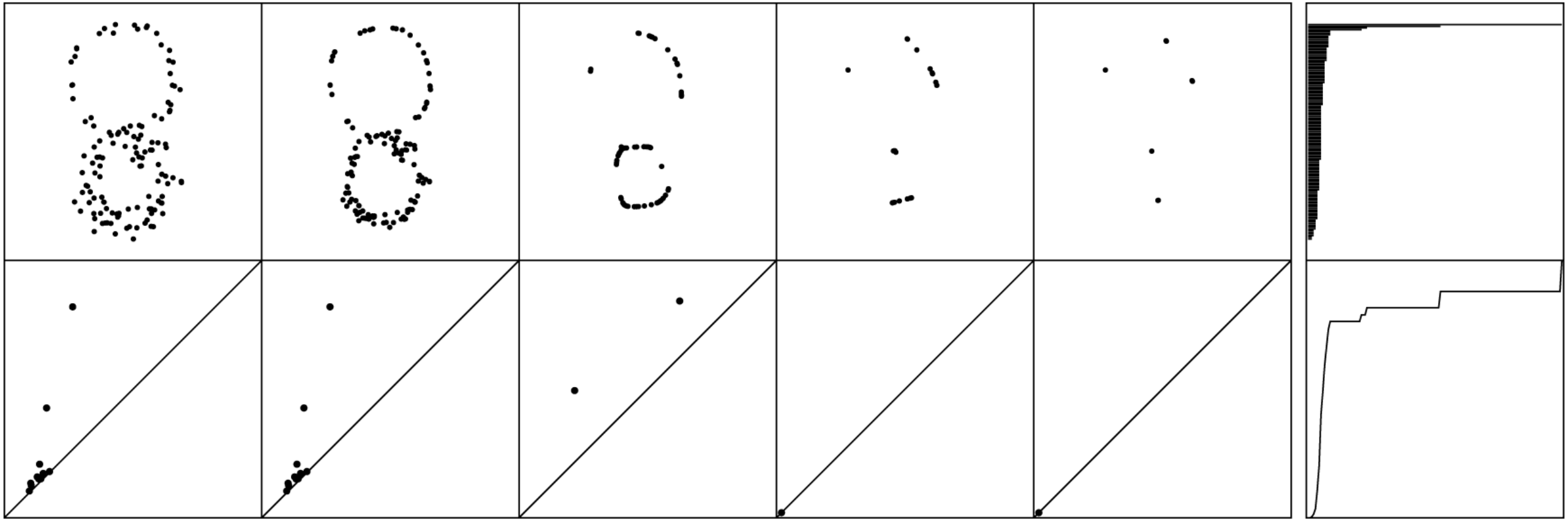

(a) (b)

PHATE/C-PHATE/T-PHATE

(Moon K et al. Nature Biotechnology 2019,
Kuchroo et al. Nature Biotechnology 2022,
Busch Et al. Nature Computational Science 2023
Moyle et al. Nature 2021)

Erica Busch
Manik Kuchroo
Jessie Huang
Kevin Moon
David van Dijk
Zheng Wang
Scott Gigante
Dan Burkhardt
William Chen
Natalia Ivanova
Guy Wolf
Akiko Iwasaki
Nick Turke-Browne

Main idea: a metric-preserving dimensionality reduction algorithm that naturally emphasizes trajectory structure

Structure/Geometry Preservation

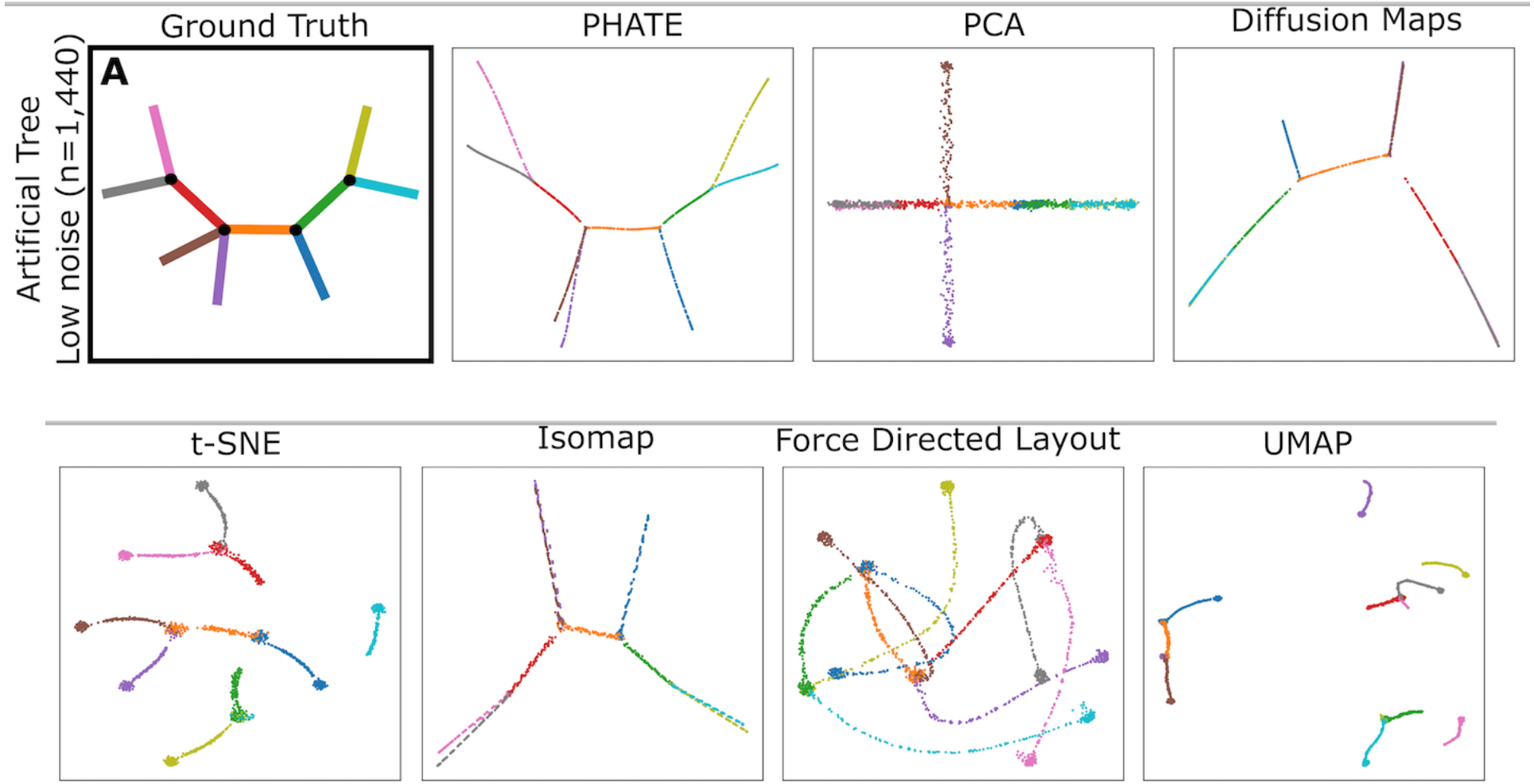

The PHATE Algorithm

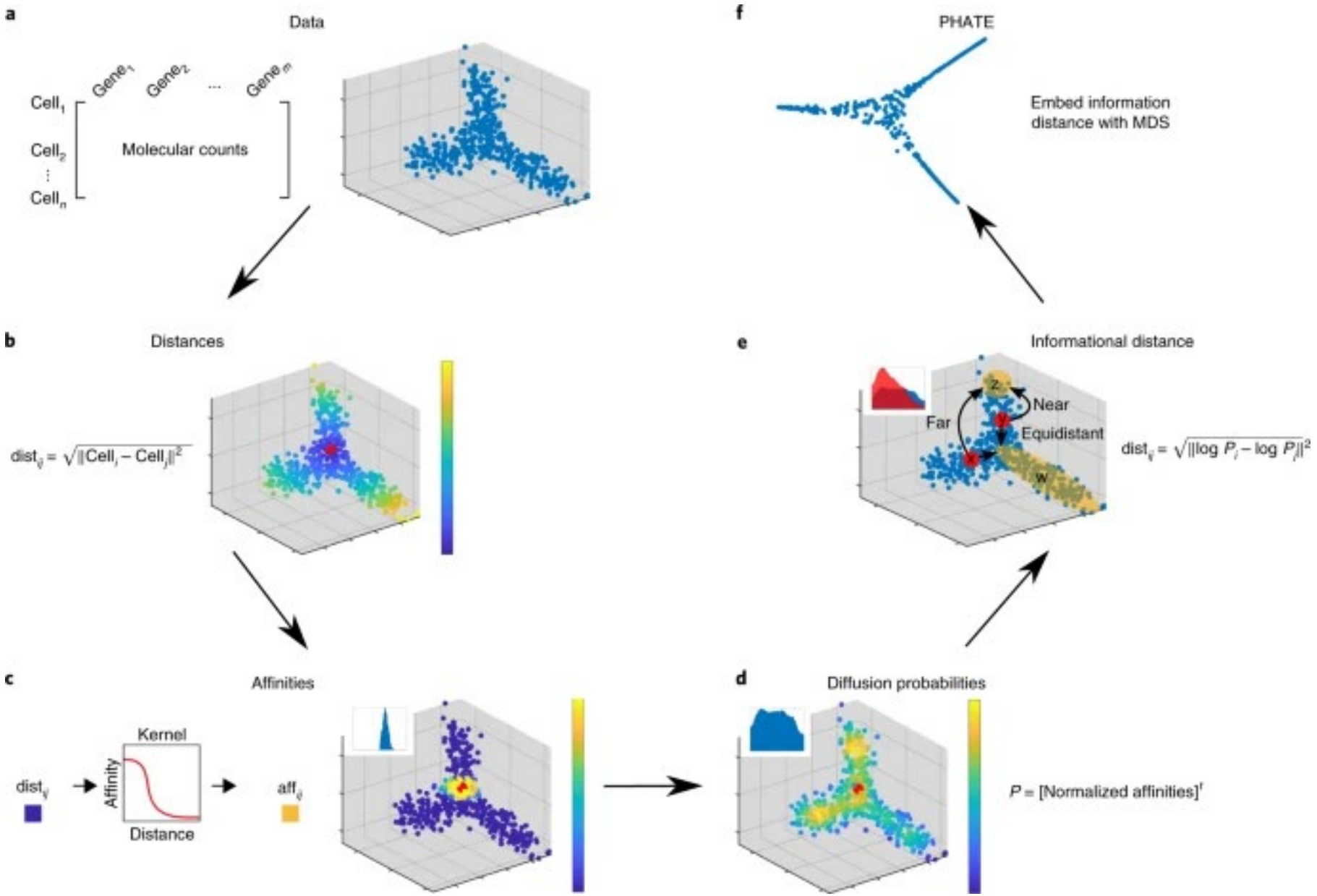

Stem Cell Development

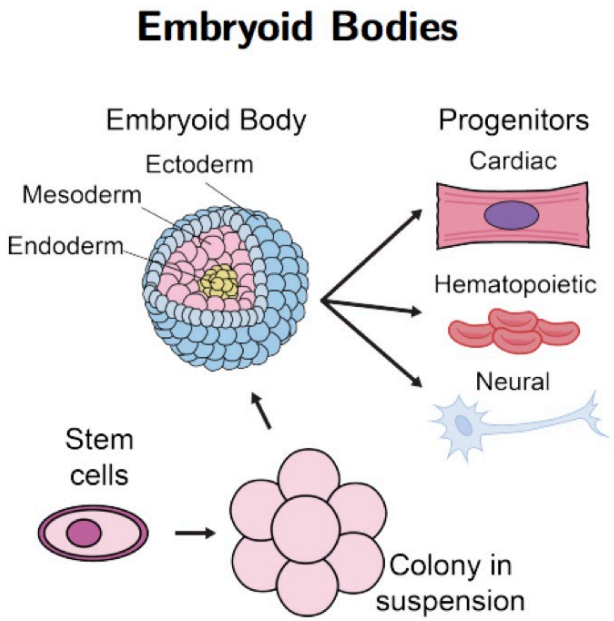

27 day time course

scRNA-seq

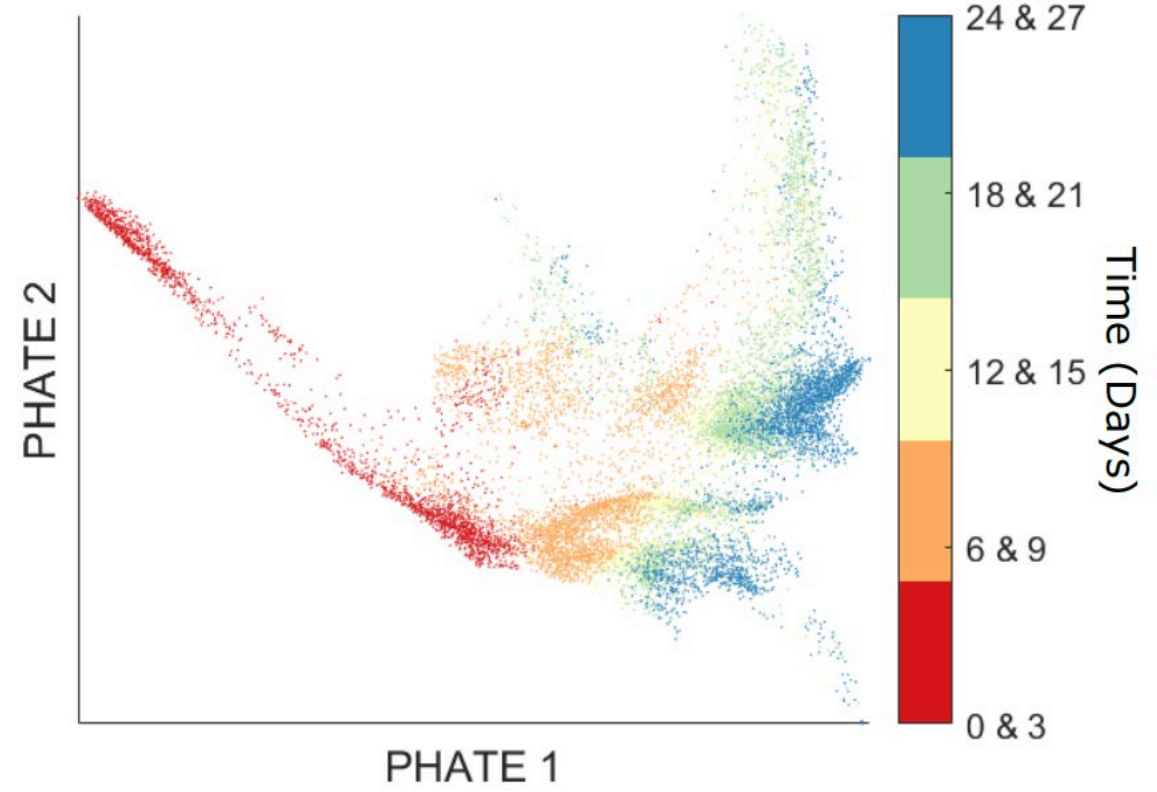

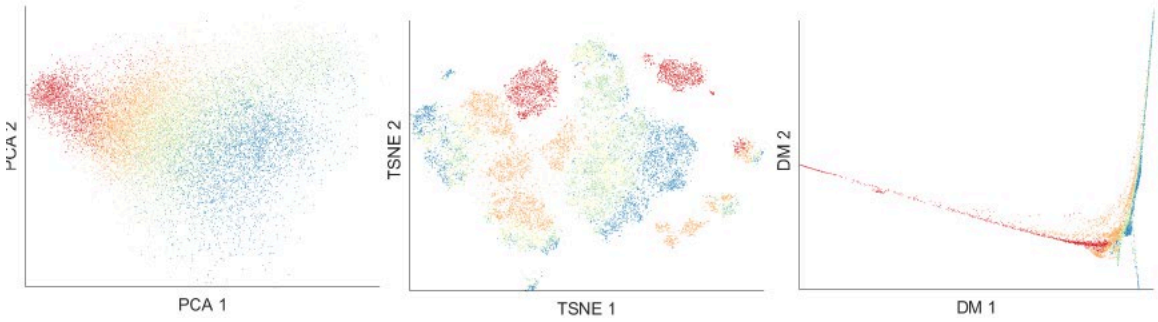

PCA tSNE Diffusion Maps

Temporal PHATE

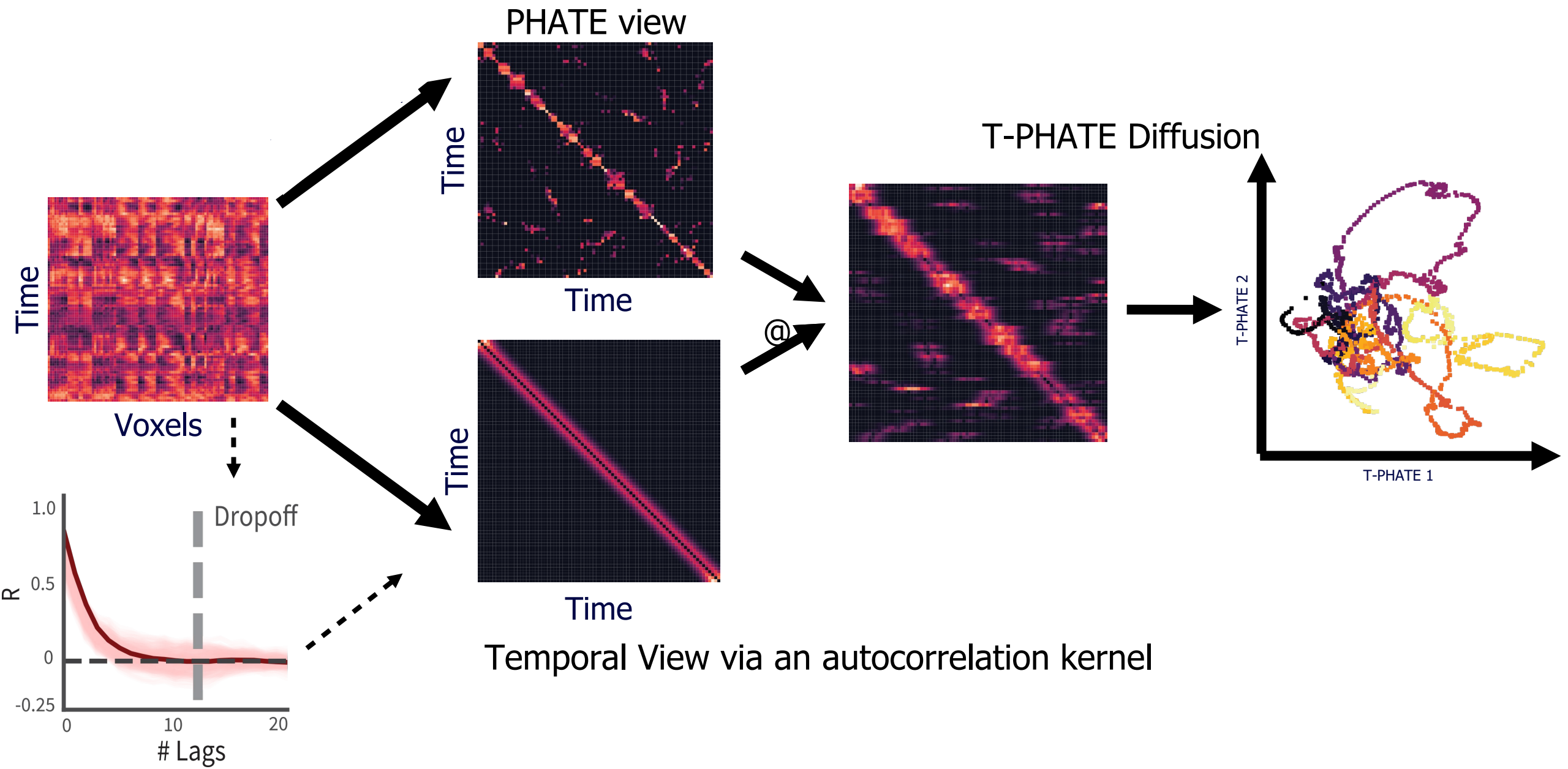

Temporal View via an autocorrelation kernel

Manifold preservation

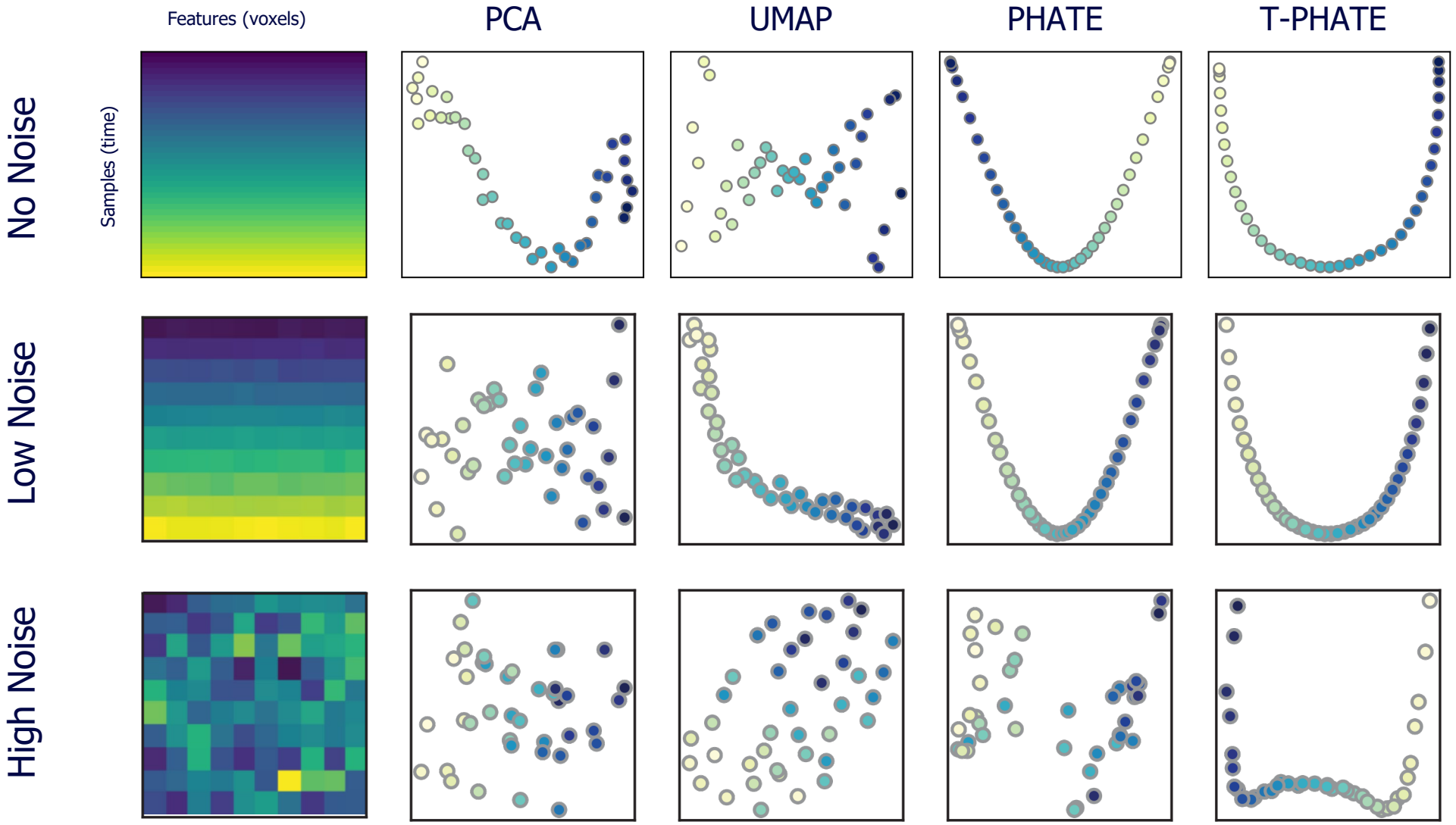

Comparison of techniques

Embeddings of multi-voxel response patterns for a single subject during movie viewing

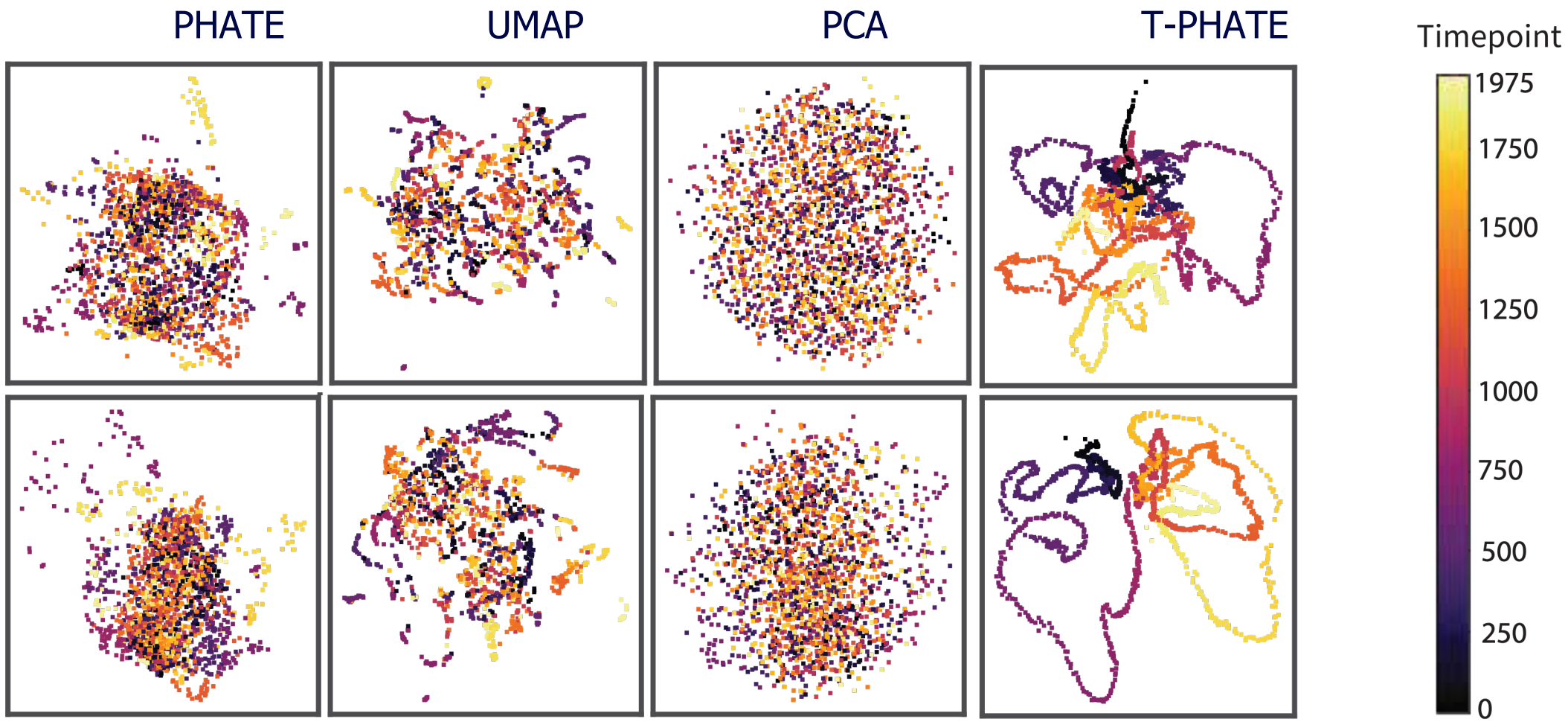

C-PHATE

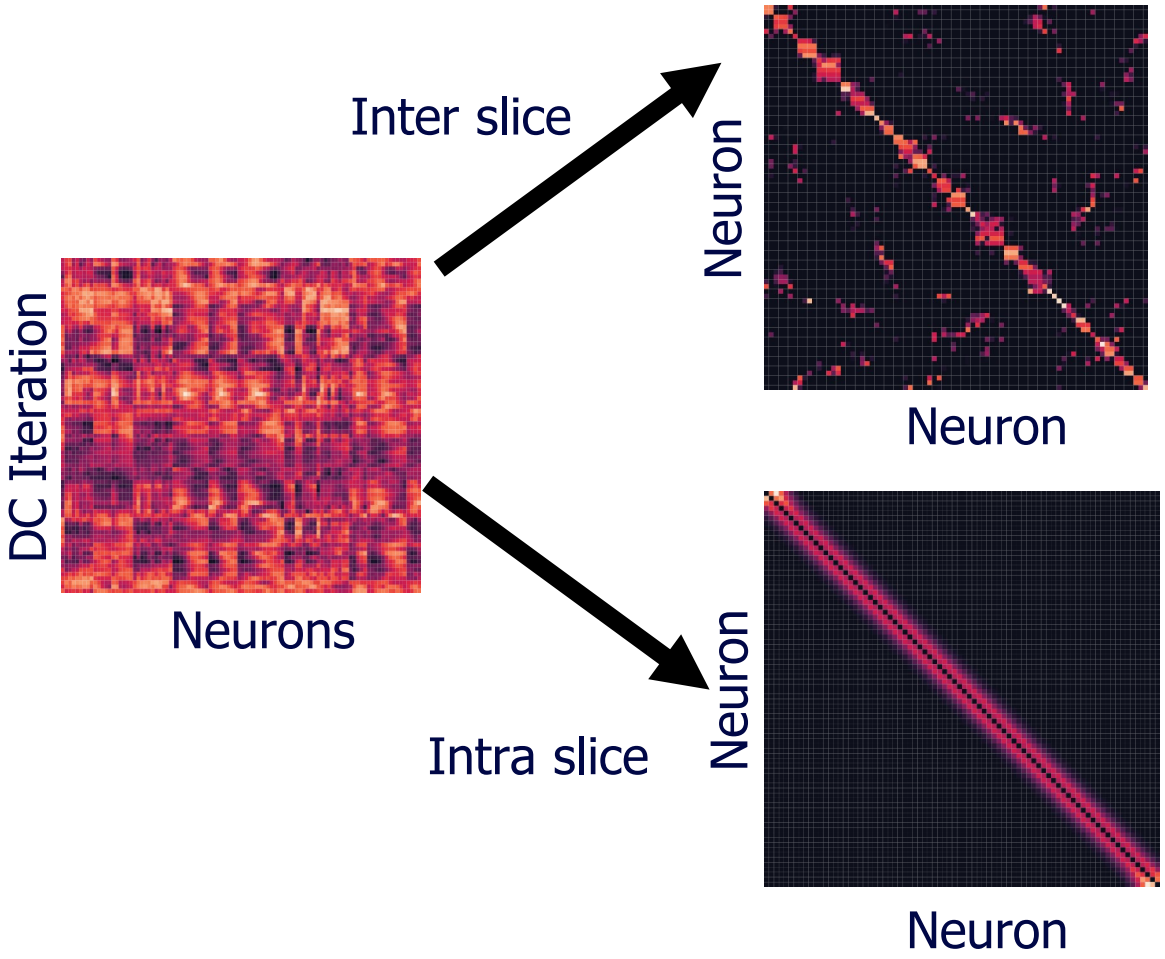
Inter slice
Neuron
Neuron
DC Iteration
Neurons
Intra slice
Neuron
Neuron

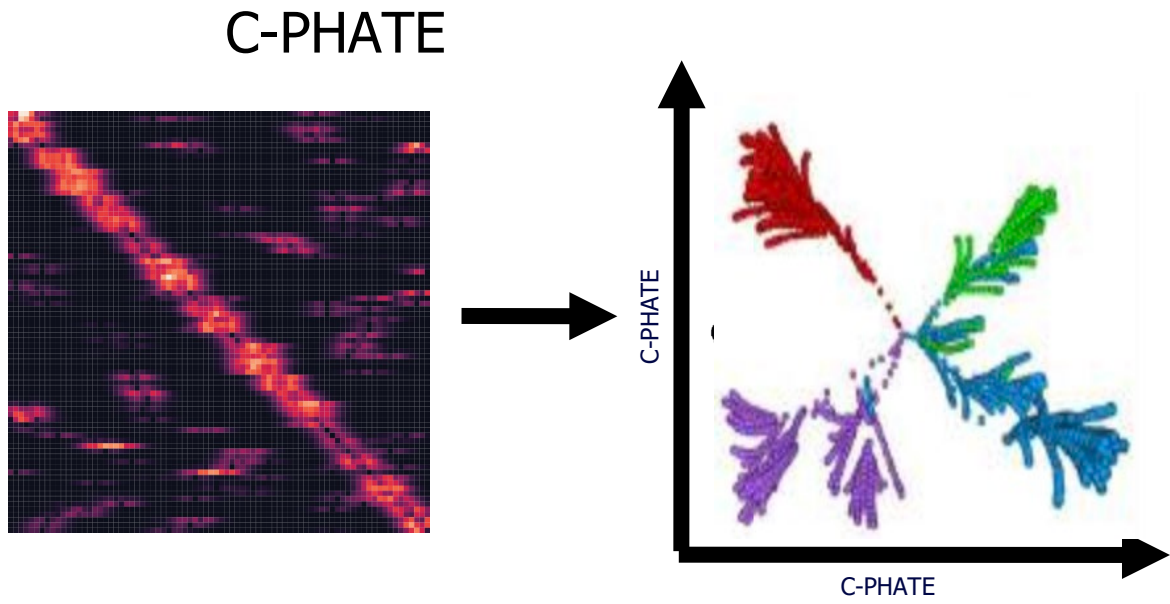
C-PHATE
C-PHATE
C-PHATE

Cellular analysis on retinal cells

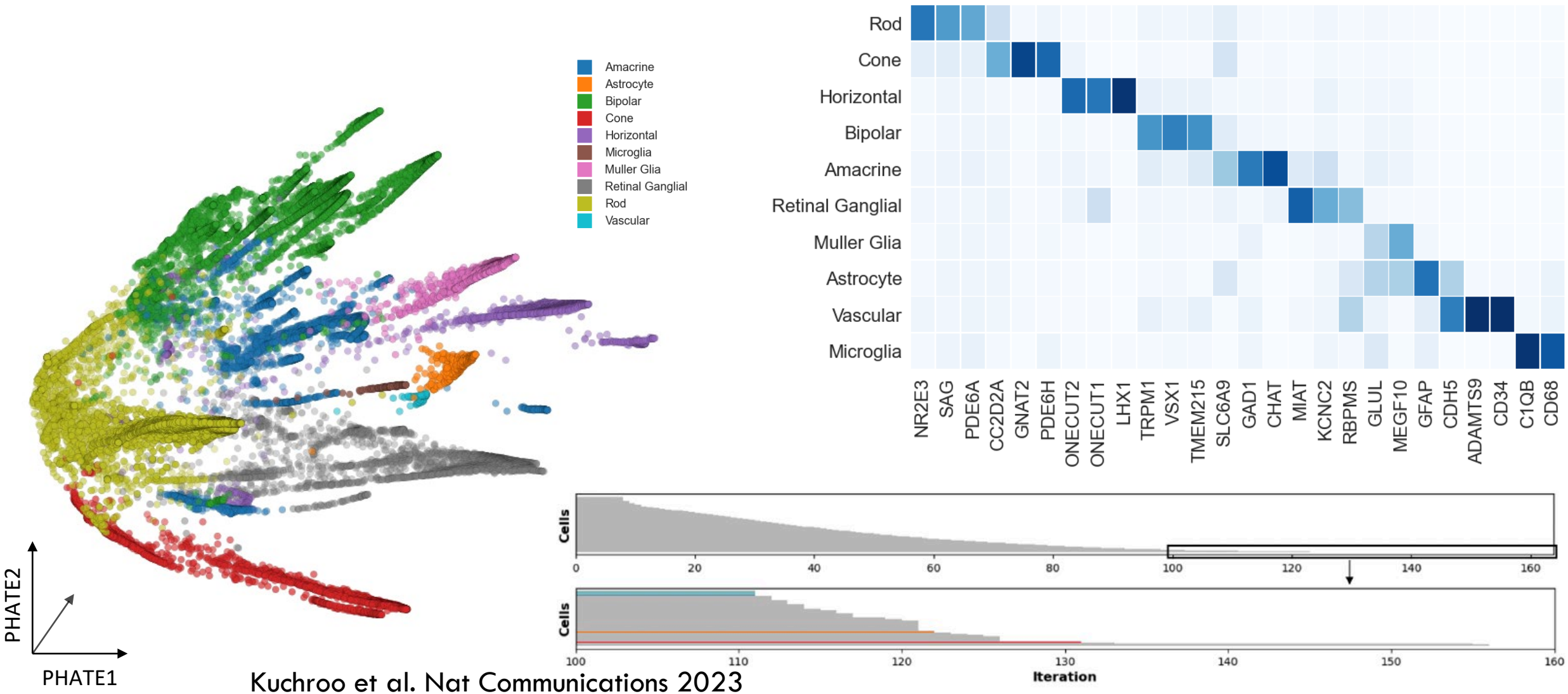

Kuchroo et al. Nat Communications 2023

Identification of activated astrocyte state enriched for each AMD phase

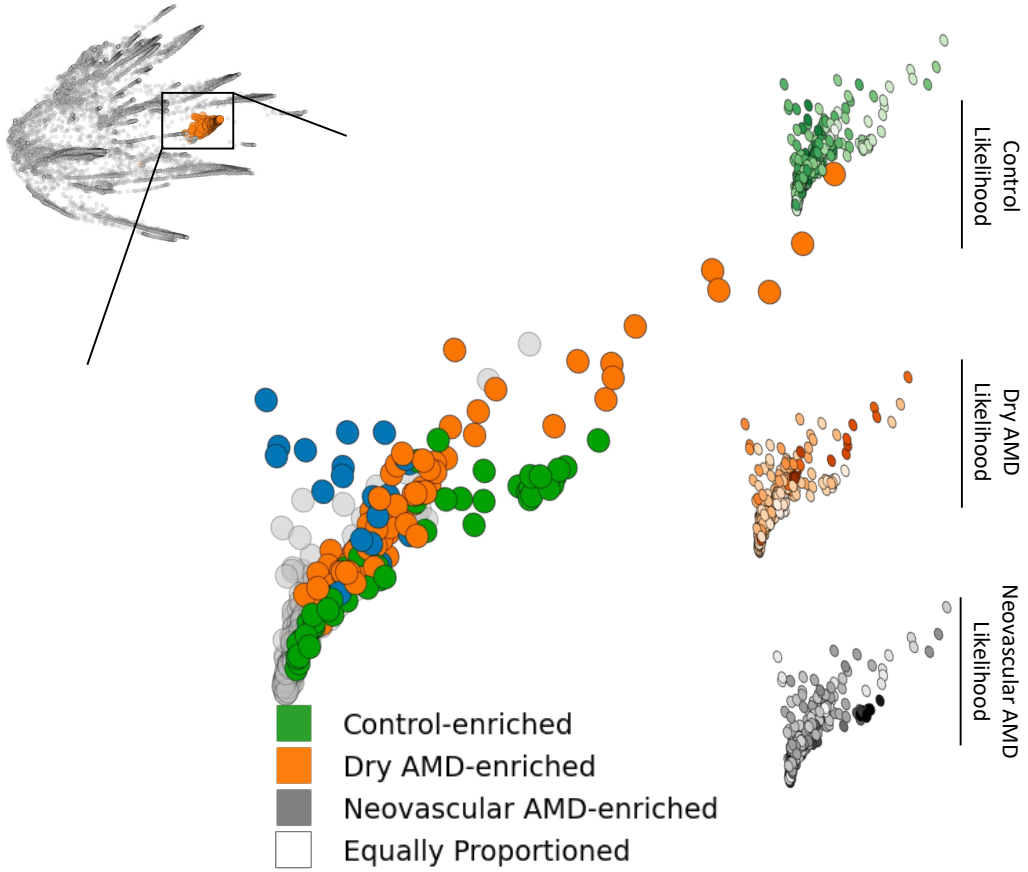

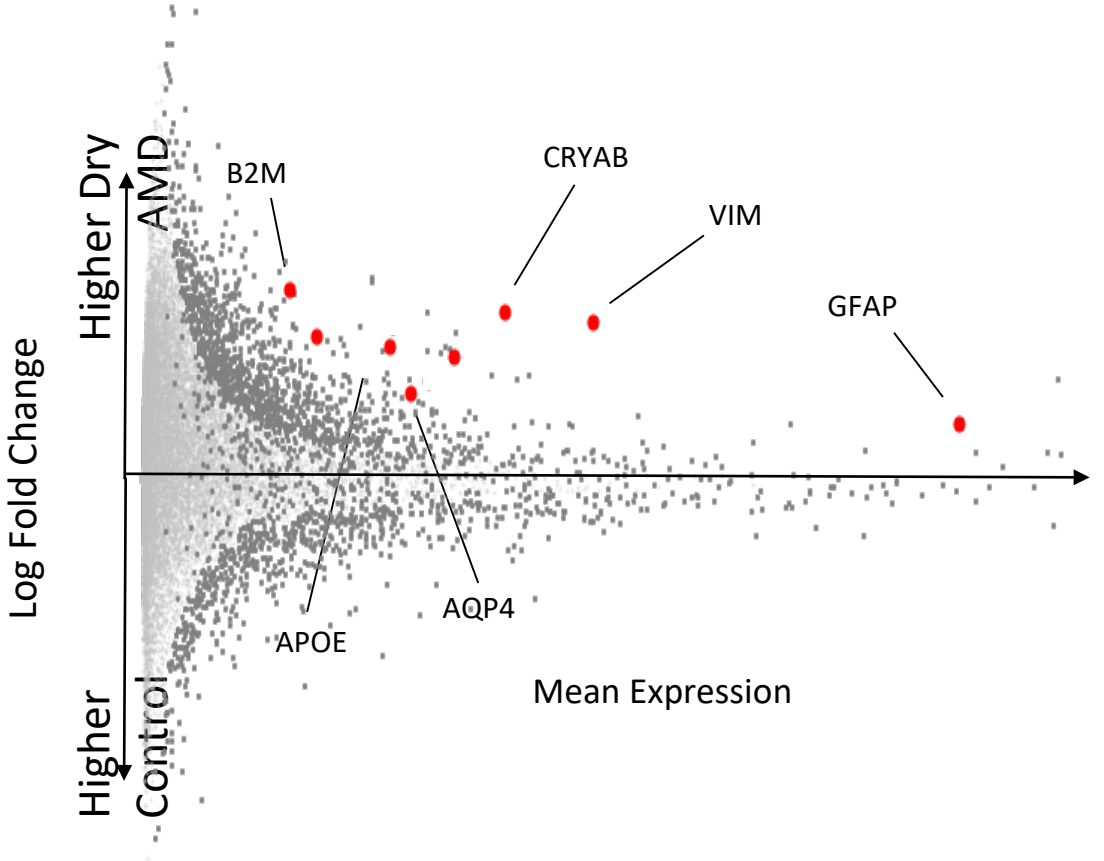

Activated astrocyte state enriched across early neurodegenerative diseases

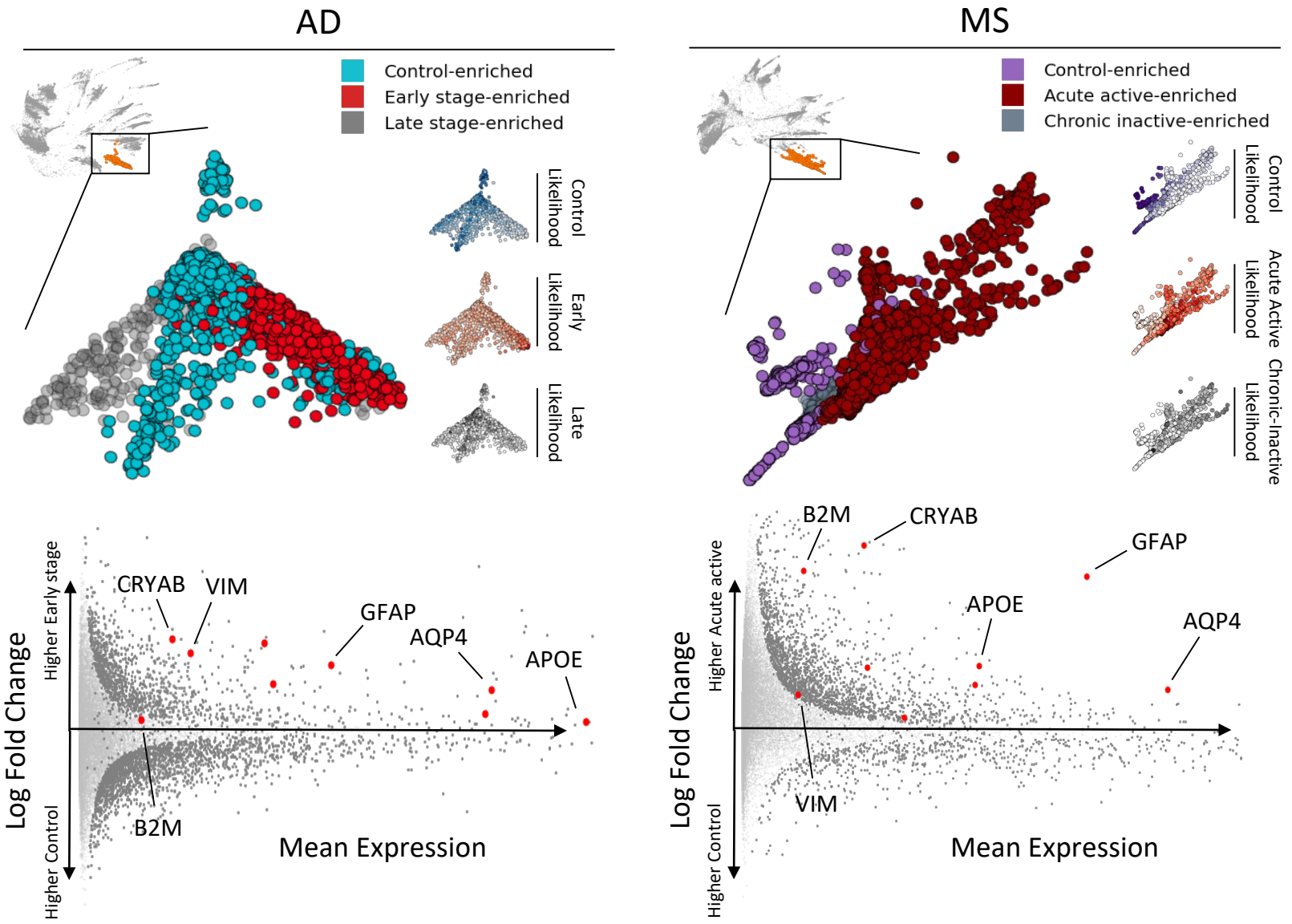

C elegans Neuropil

- Nerve ring or neuropil contains 181 neurons
- Lineage and morphology are known
- Structural principles of organization are unknown
- Studying this with >100,000 instances of neurite-neurite contacts from EM images
- Why contacts rather than synapses?
    - To focus on both structural and functional reasons for organization

Using EM to Understand Neuron Relationships

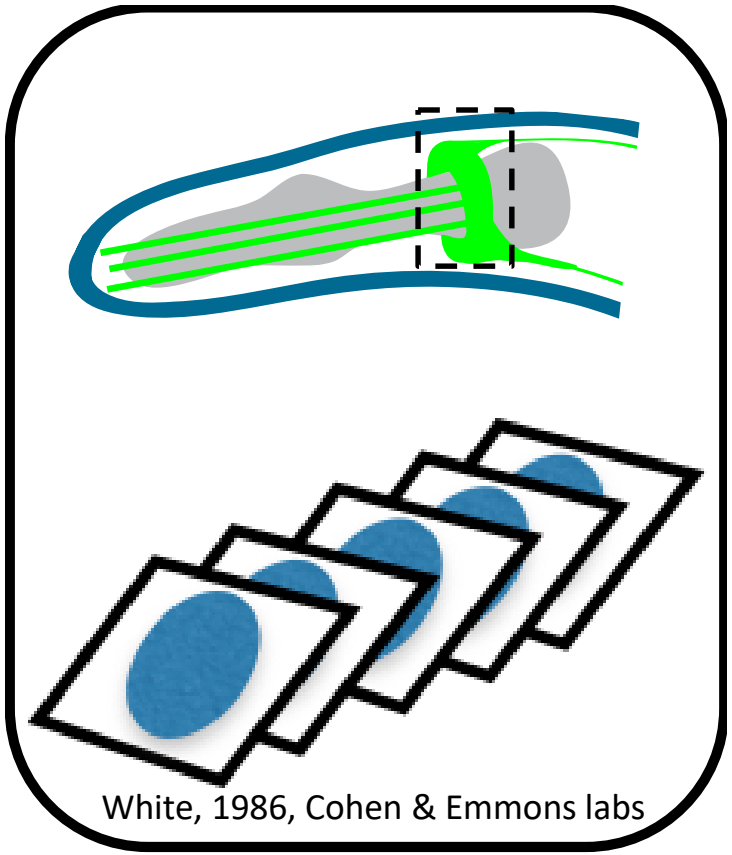

White, 1986, Cohen & Emmons labs

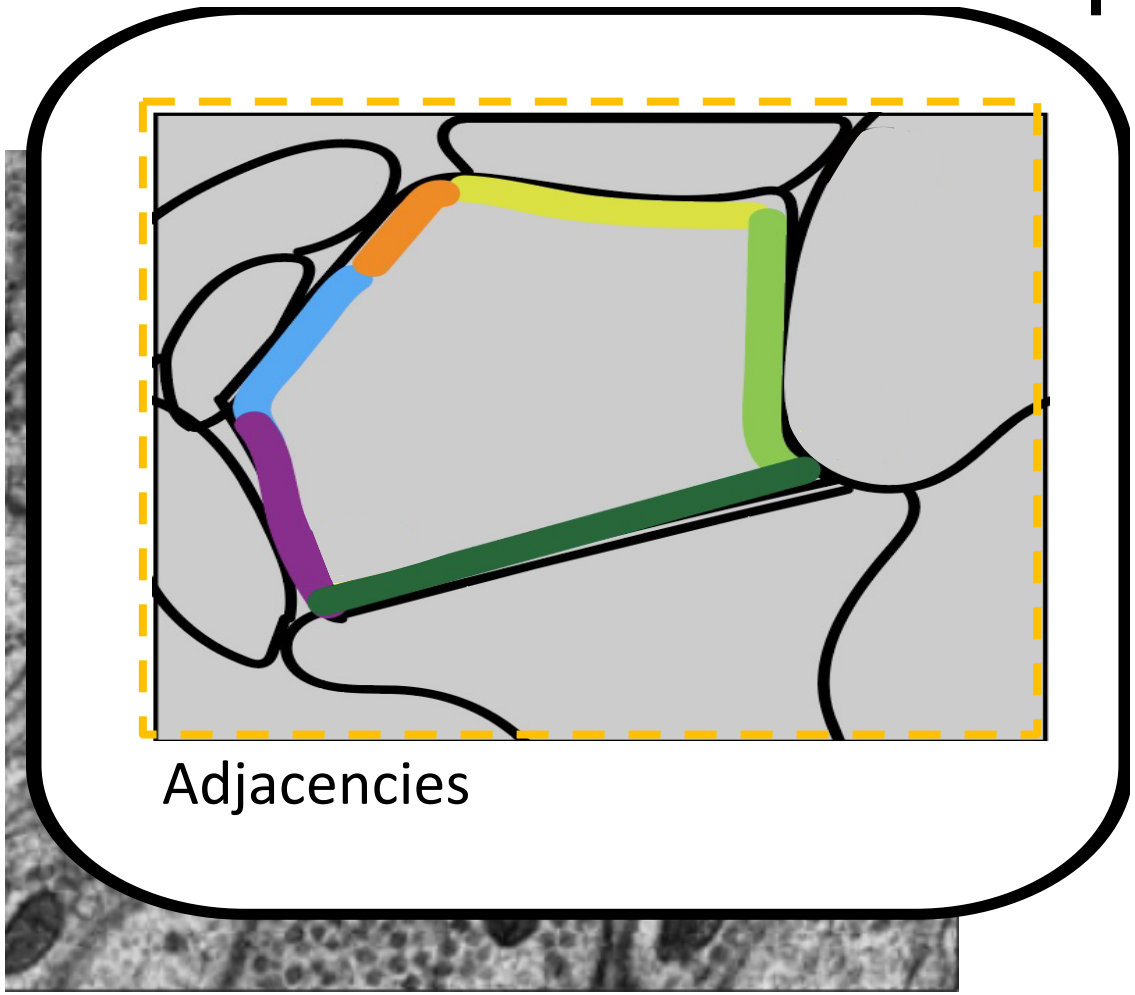

Adjacencies

Applying Diffusion Condensation to Worm Brain Adjacency

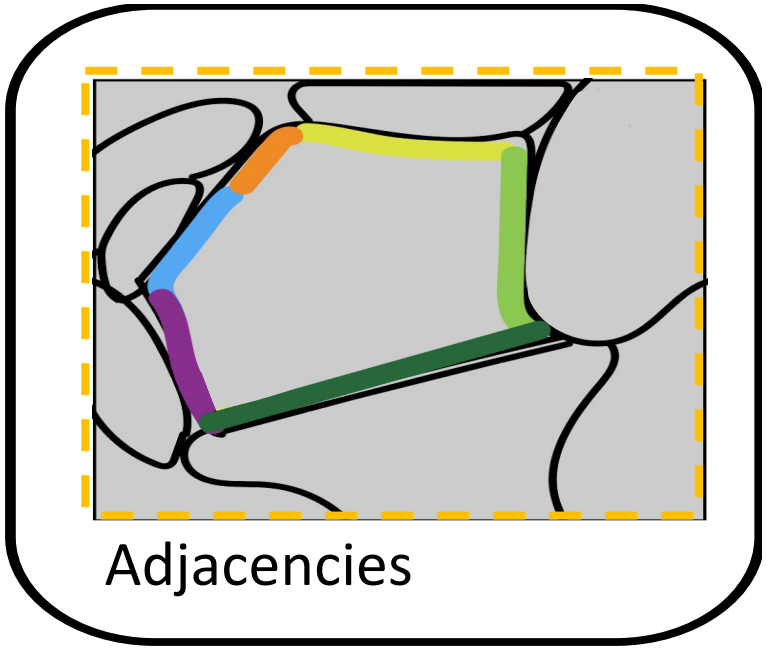

$$\text{Contact Area Fraction (CAF)} : = \phi_{ij} = \frac{2 * SA(i \cap j)}{SA(i) + SA(j)}$$

Extent of contact between pairs of neurons create adjacency matrix

Contact-based “coordinates” for neurons

- Use MDS to go from contact adjacencies to coordinates
- In the “spectral view” these are features of the vertices

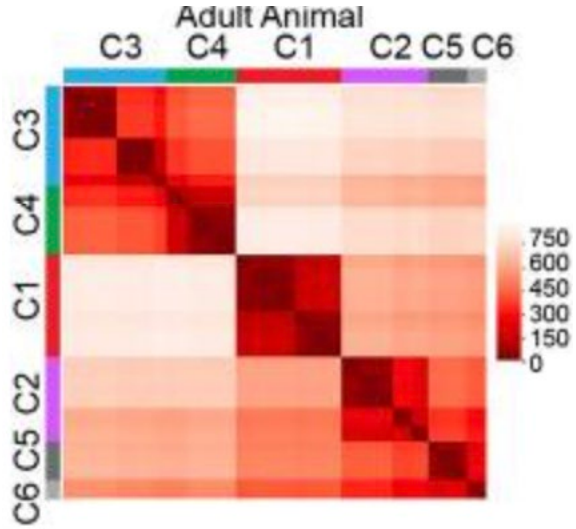

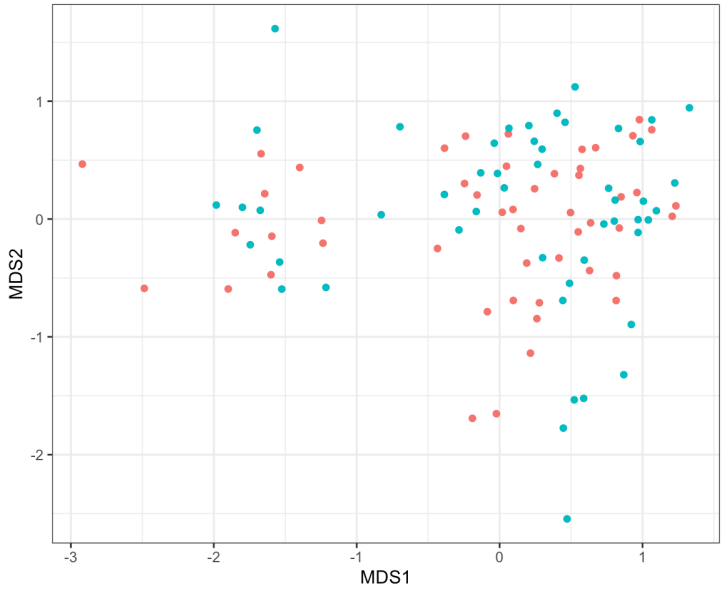

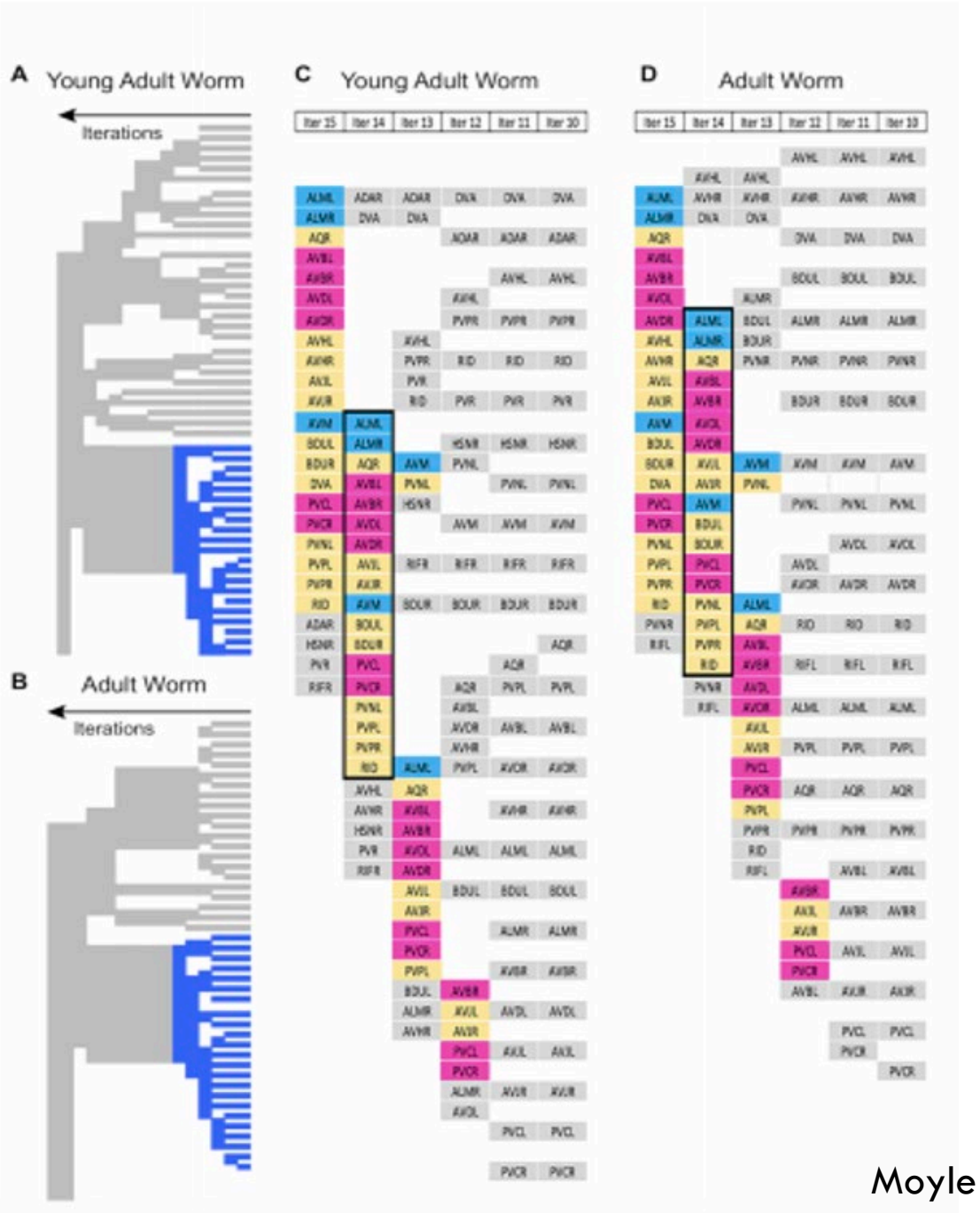

Provides a continuously hierarchical tree where connections are based on extent of adjacency

The “length” of the branches Indicates persistence

Moyle et a. Nature 2021

Highest modularity level (4-clusters)

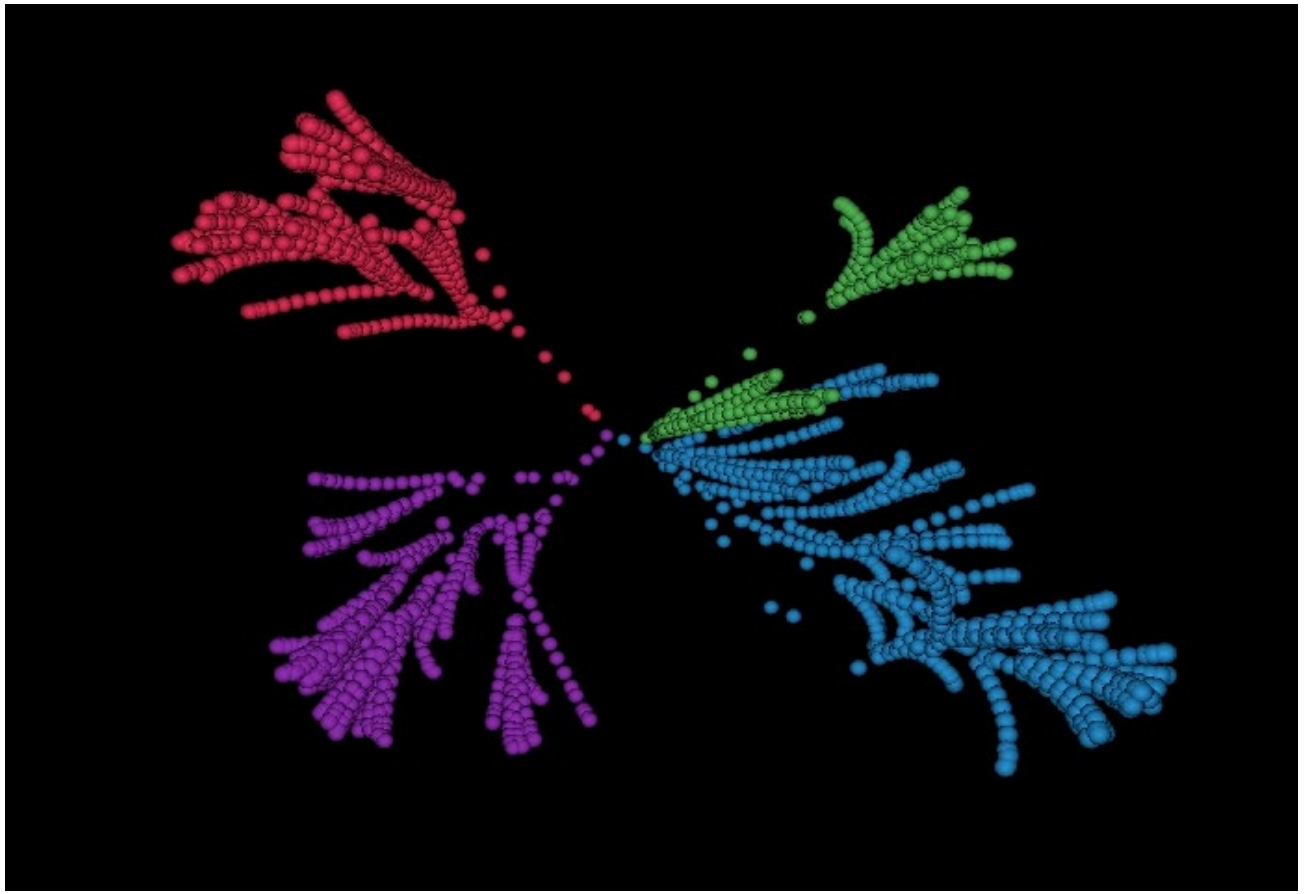

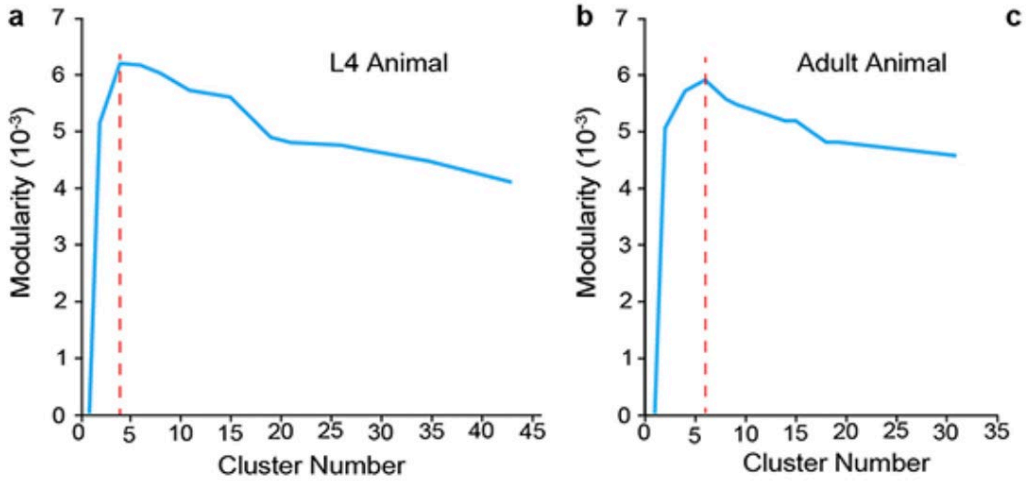

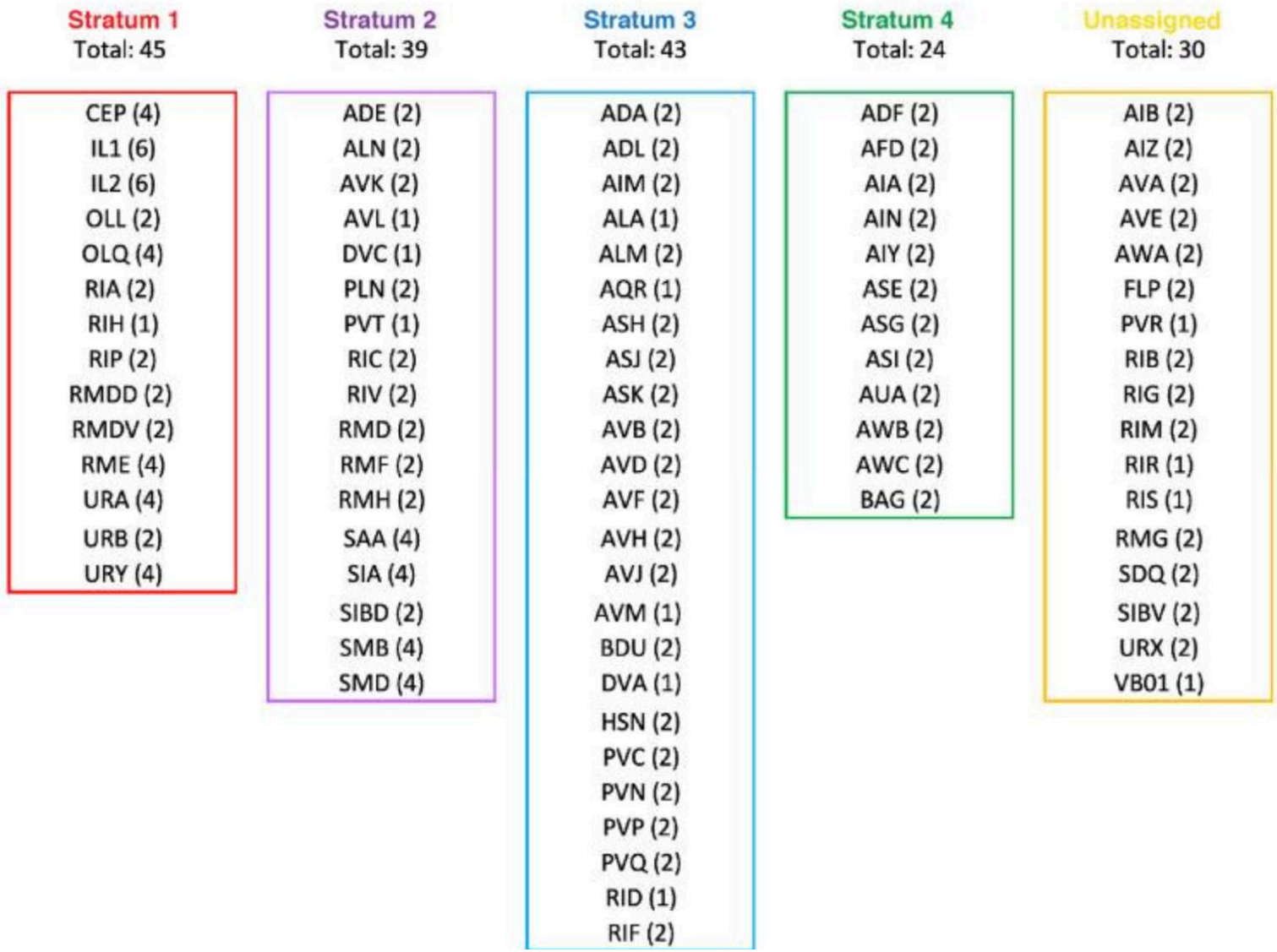
Stratum 1
Total: 45
CEP (4)
IL1 (6)
IL2 (6)
OLL (2)
OLQ (4)
RIA (2)
RIH (1)
RIP (2)
RMDD (2)
RMDV (2)
RME (4)
URA (4)
URB (2)
URY (4)
Stratum 2
Total: 39
ADE (2)
ALN (2)
AVK (2)
AVL (1)
DVC (1)
PLN (2)
PVT (1)
RIC (2)
RIV (2)
RMD (2)
RMF (2)
RMH (2)
SAA (4)
SIA (4)
SIBD (2)
SMB (4)
SMD (4)
Stratum 3
Total: 43
ADA (2)
ADL (2)
AIM (2)
ALA (1)
ALM (2)
AQR (1)
ASH (2)
ASJ (2)
ASK (2)
AVB (2)
AVD (2)
AVF (2)
AVH (2)
AVJ (2)
AVM (1)
BDU (2)
DVA (1)
HSN (2)
PVC (2)
PVN (2)
PVP (2)
PVQ (2)
RID (1)
RIF (2)
Stratum 4
Total: 24
ADF (2)
AFD (2)
AIA (2)
AIN (2)
AIY (2)
ASE (2)
ASG (2)
ASI (2)
AUA (2)
AWB (2)
AWC (2)
BAG (2)
Unassigned
Total: 30
AIB (2)
AIZ (2)
AVA (2)
AVE (2)
AWA (2)
FLP (2)
PVR (1)
RIB (2)
RIG (2)
RIM (2)
RIR (1)
RIS (1)
RMG (2)
SDQ (2)
SIBV (2)
URX (2)
VB01 (1)

Anatomical Significance

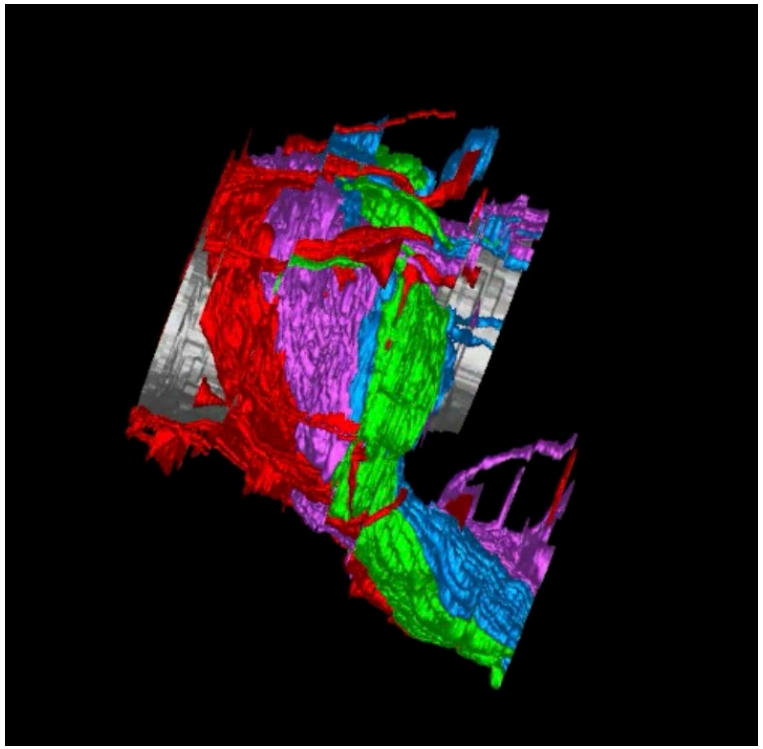

- These four layers or strata stack along the anterior-posterior axis of the animal, encircling the pharynx isthmus
- Image looks “tightly bundled”
- Computational method indicates separation into 4

Structural Encasing

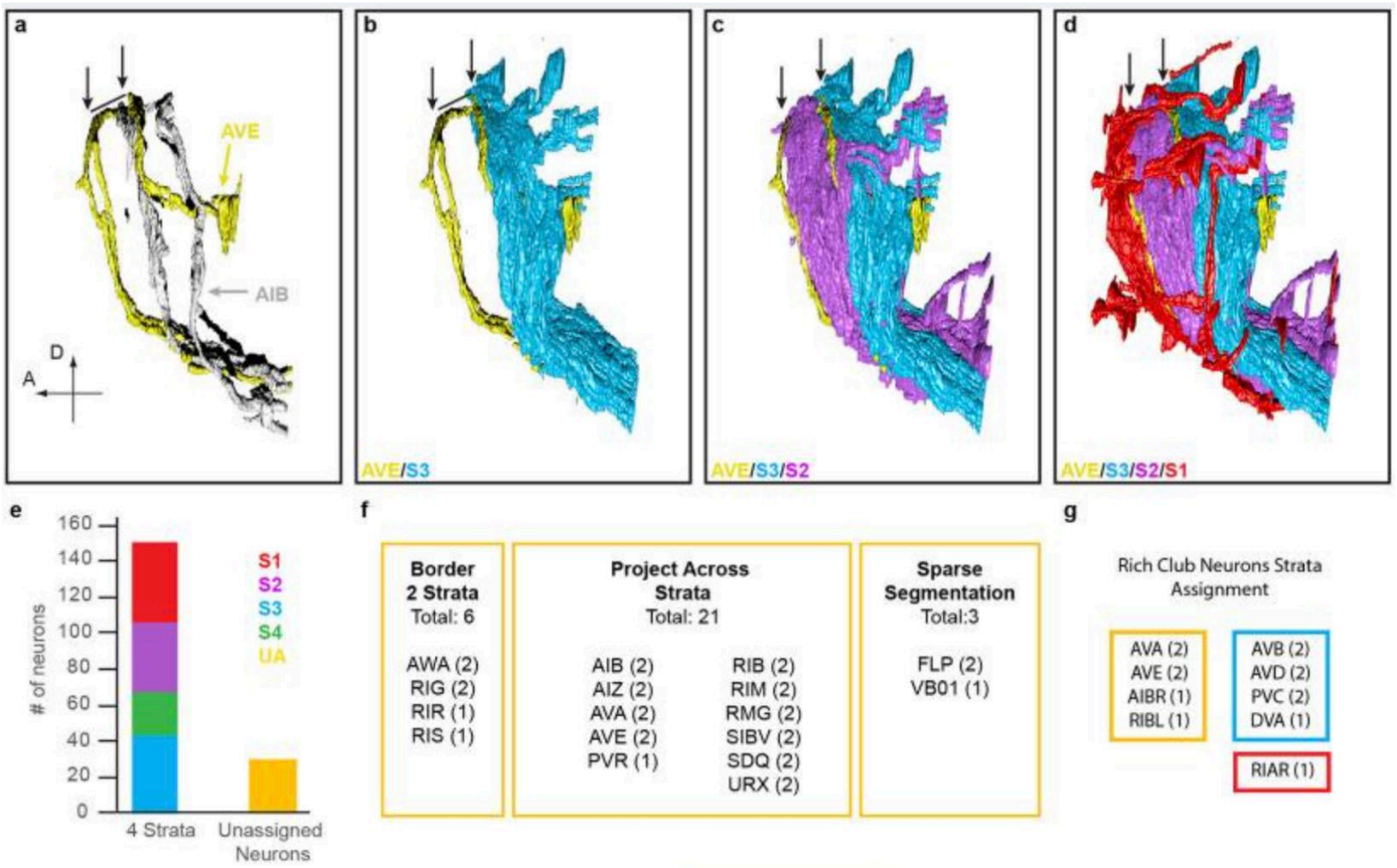

Sensory separation

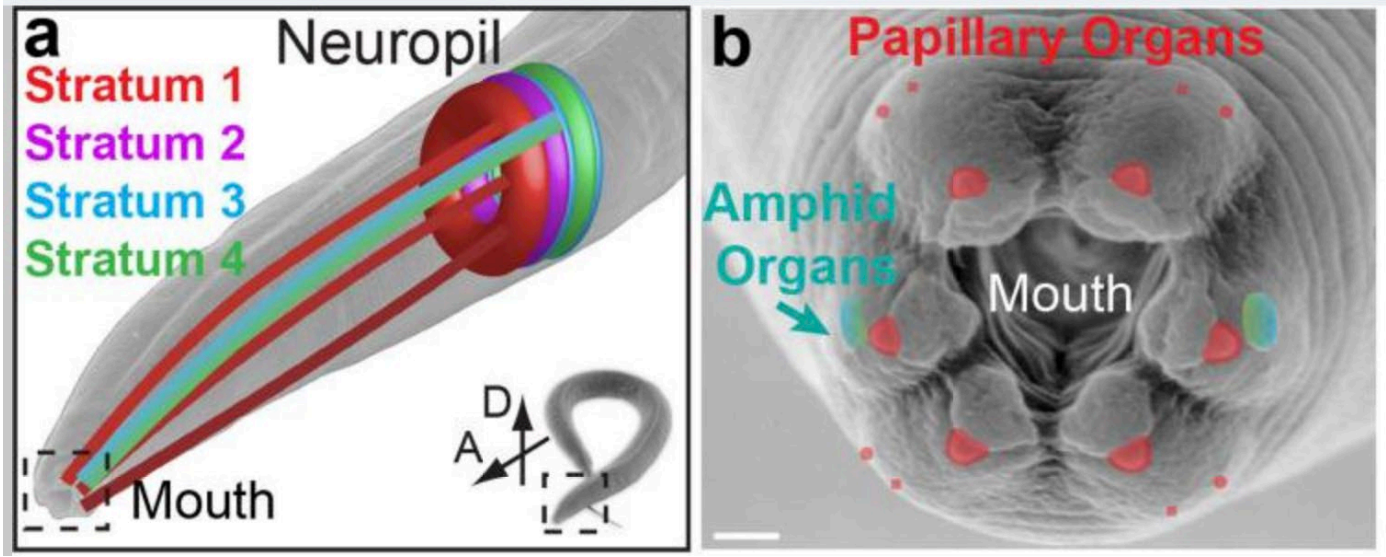

- Papillary axons project to S1 (red)
- No axons to S2 (fuschia)
- Amphidial axons to S3/4 (green/blue)
- Indicate functional segregation of sensory information in the nerve ring

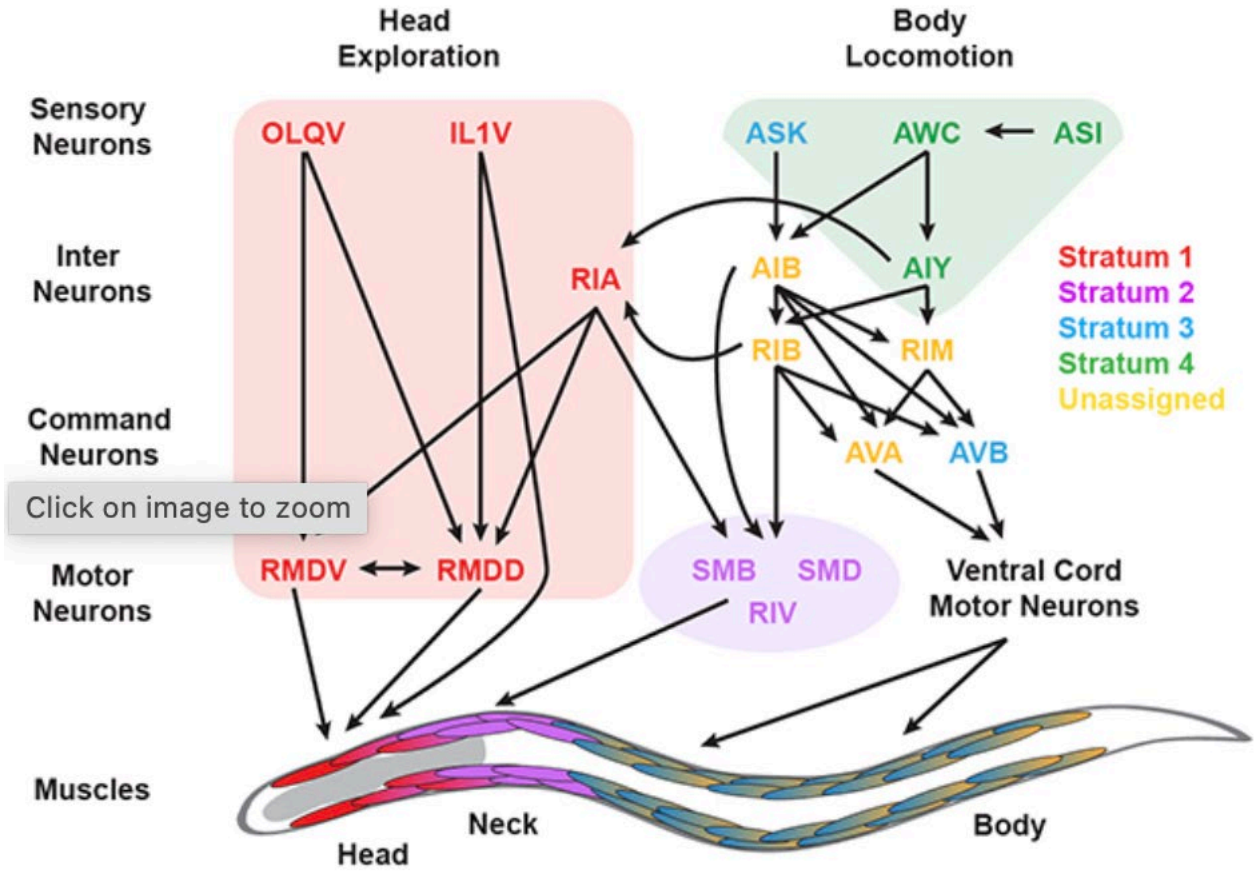

- Within S1 mechanosensory circuits control head withdrawal behaviors
- These include sensory cells which go into motor neurons

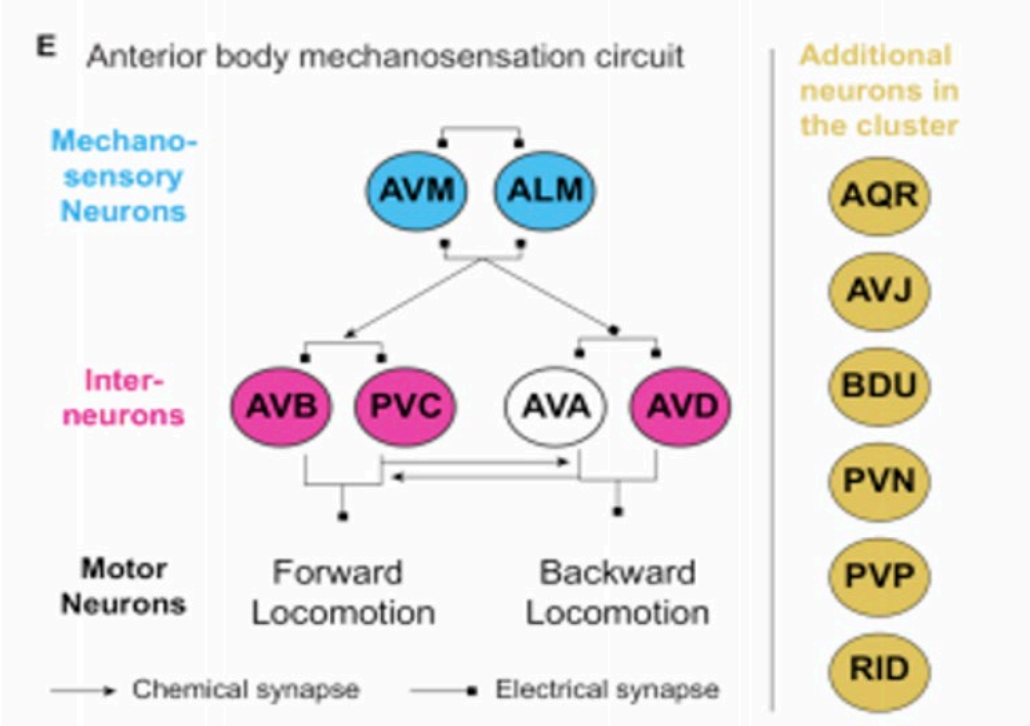

Developmental ordering

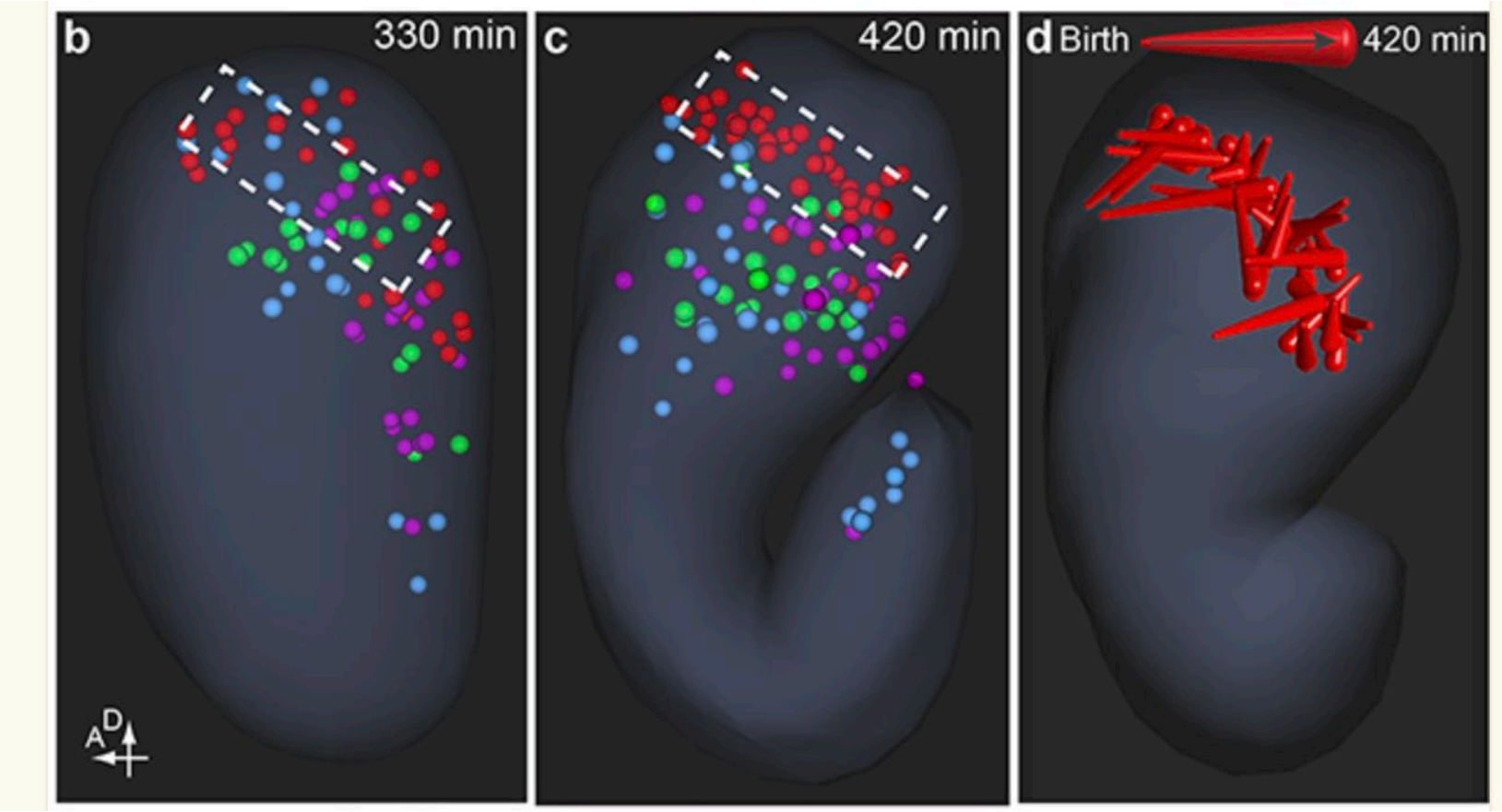

Four dimensional in-vivo imaging

Cell bodies of S1 migrate to the anterior part of the embryo head
Then S2-S4 migrate to the posterior part of the head

The allometry question

- Does the brain just ”scale up” over development?
- I.e., do neurons just become bigger?

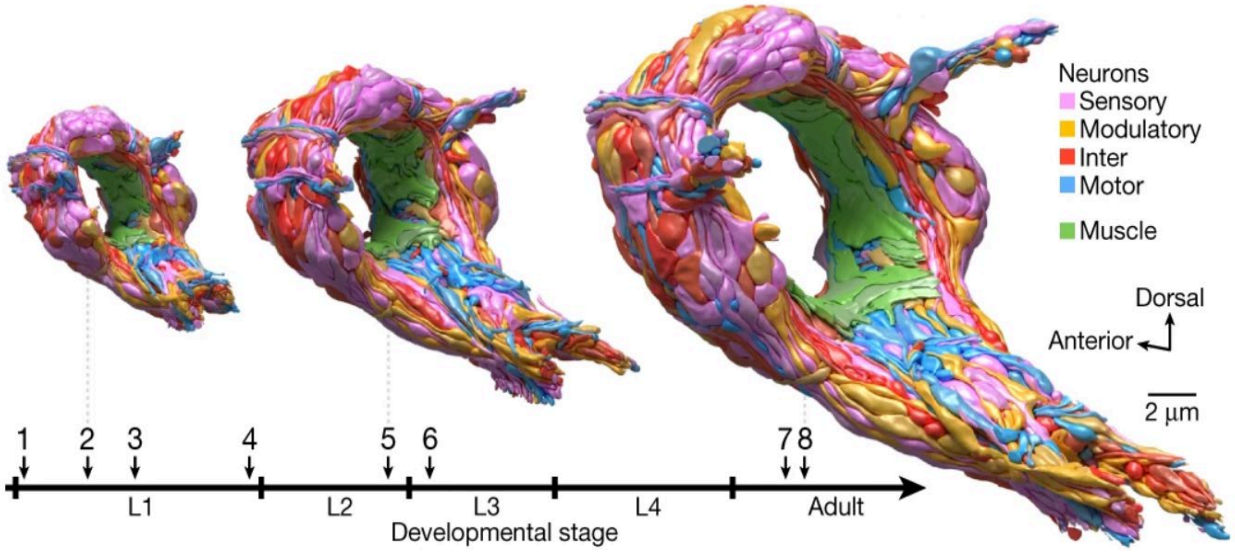

Witvliet, Zhen 2021.

TDA to study allometry

- Diffusion condensation has a first order homology based on the clusters that emerge
- Using contact area fraction we have invariance to allometric scaling
- So similarity in persistence indicates allometry if SA is larger!

$$\text{Contact Area Fraction (CAF)} : = \phi_{ij} = \frac{2 * \alpha * SA(i \cap j)}{\alpha * SA(i) + \alpha * SA(j)} = \phi_{ij} = \frac{2 * SA(i \cap j)}{SA(i) + SA(j)}, \quad \text{where } \alpha \text{ is the scaling factor}$$

Persistence diagram

A fingerprint of the epsilon (ε) values at the birth and death of merge events.

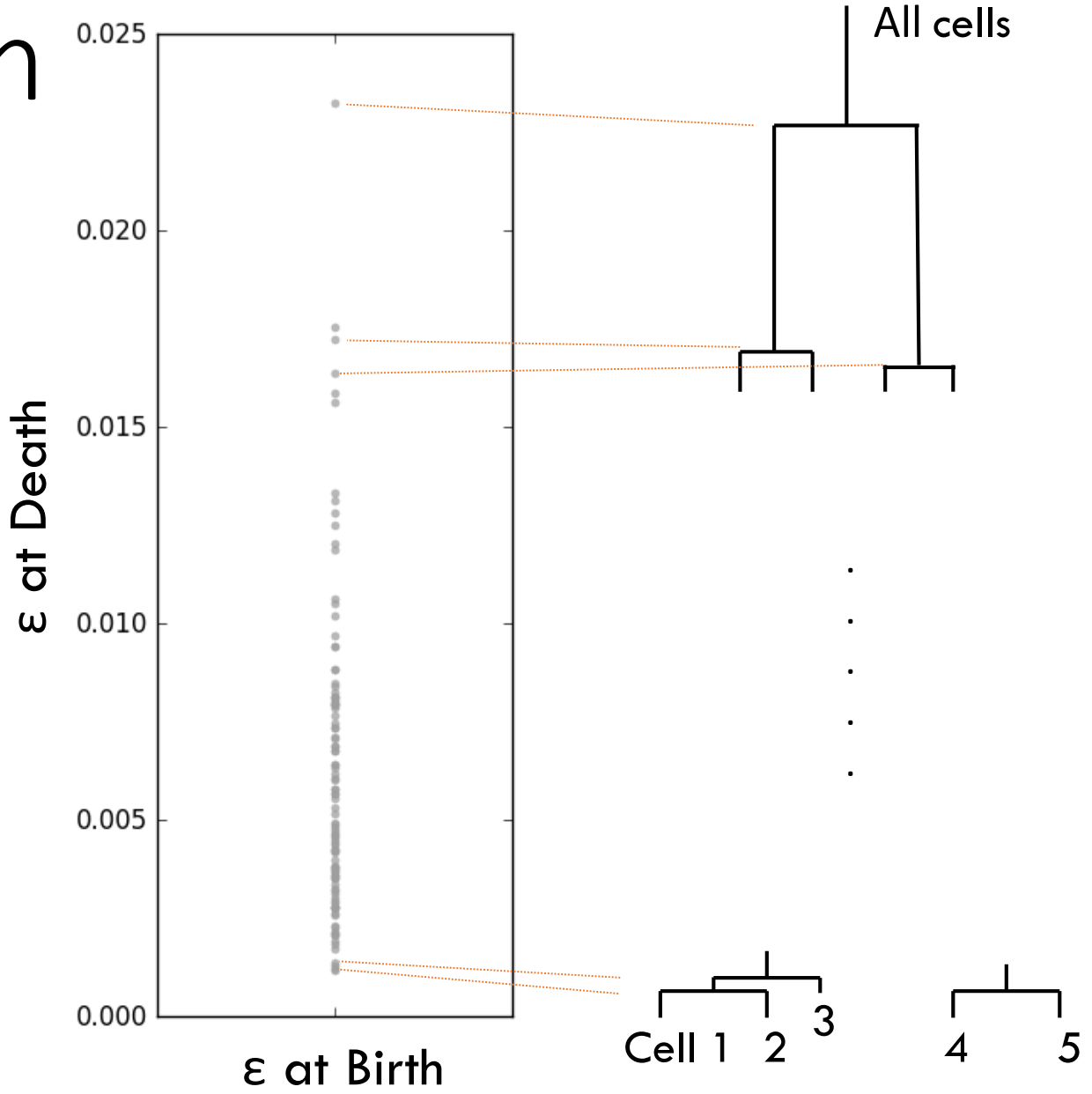

Similarity between persistence

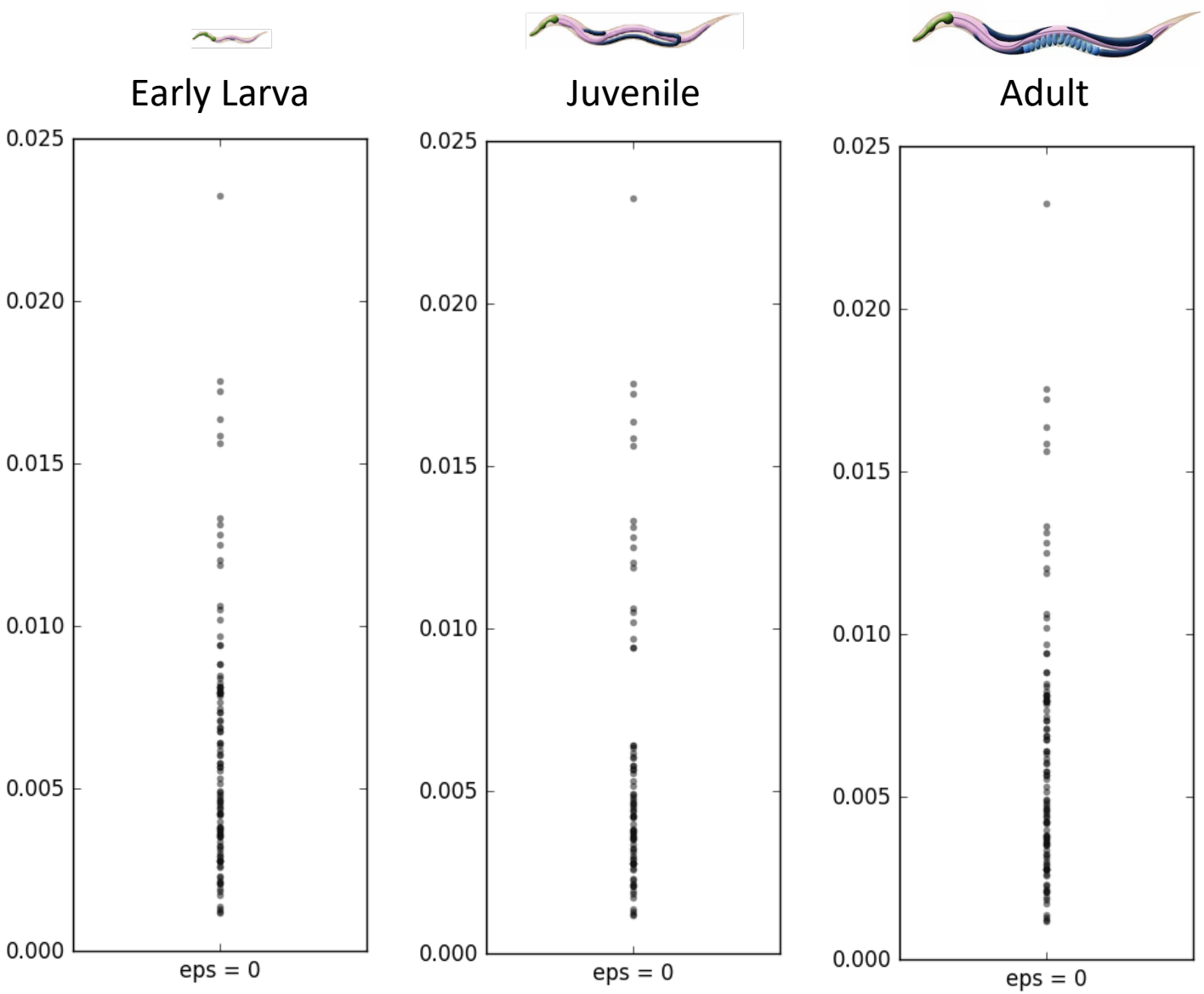

Wasserstein distance:
Measure of the similarity of persistence diagrams.

2-Wassstein

The nerve ring scales allometrically at a systems level

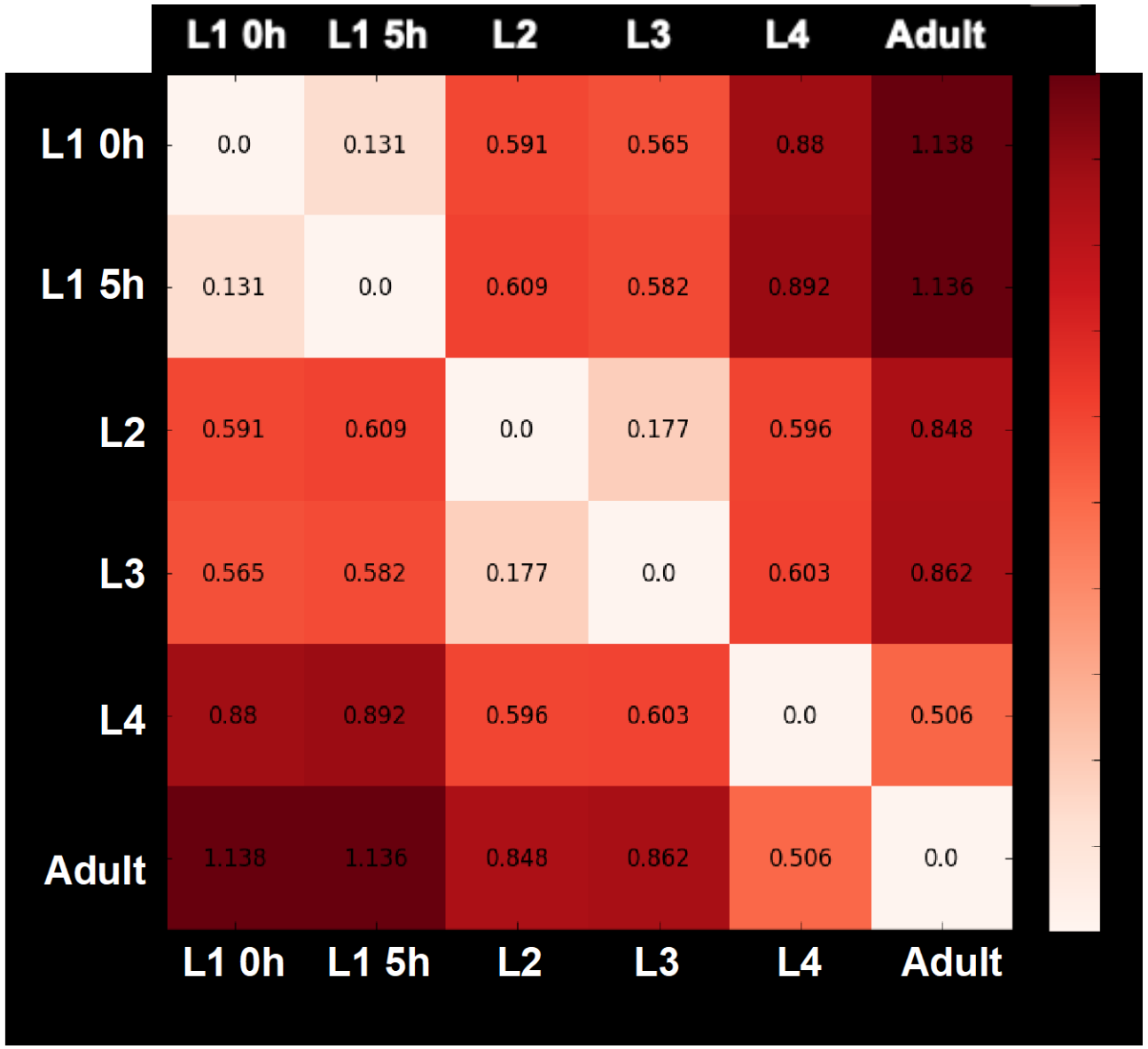

- The relationship landscape of the nerve ring is an allometrically scaling system.
- At at similar ages, relationships are more similar.
- The level of allometry increases as the worm matures.
- There are biologically interesting ‘jumps’ between specific developmental stages.

Stereotypical brain regions show non-uniform levels of relationship persistence

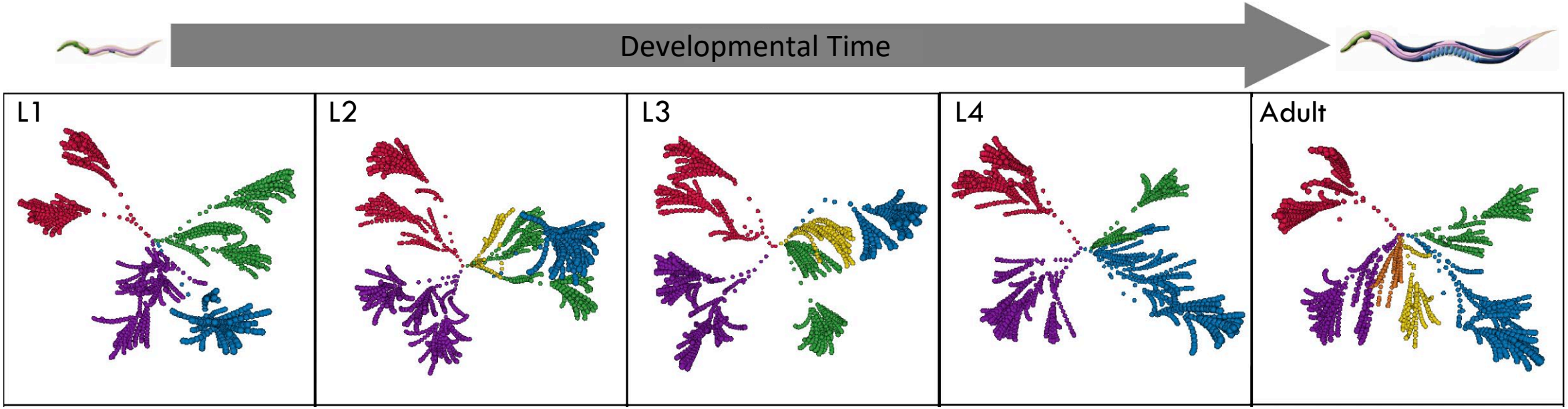

- 4 Layers is the most. Modular stage
- Present since early development
- Map to the same A-P regions
- Variability in the level of relationship persistence across regions

Non-uniform levels of allometric change across brain regions

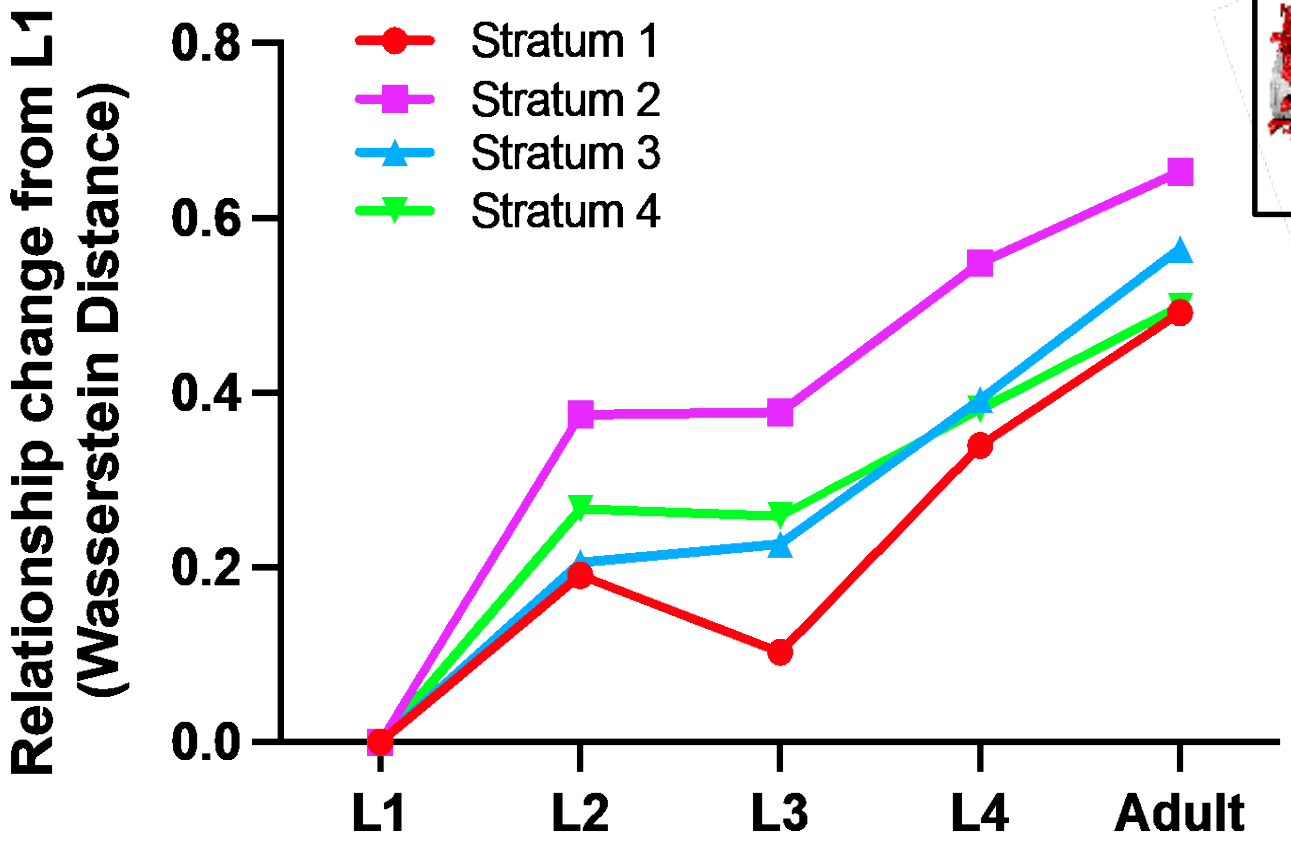

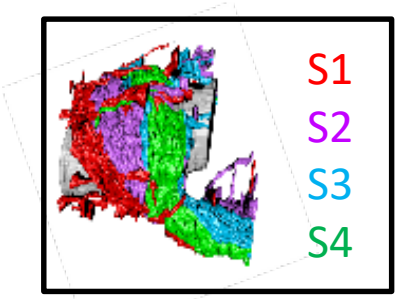

- S1 has the most persistent relationships.
- S2 shows the greatest allometric relationship changes.
- S3 and S4 share similar levels of allometric change, but unique to

1. Growth of wide platforms
2. Most persistent relationships in the nerve ring
3. Expand platforms locally to support the addition of synapses in reflex circuitry

Retains essential reflex circuitry while strengthening NMJ connections

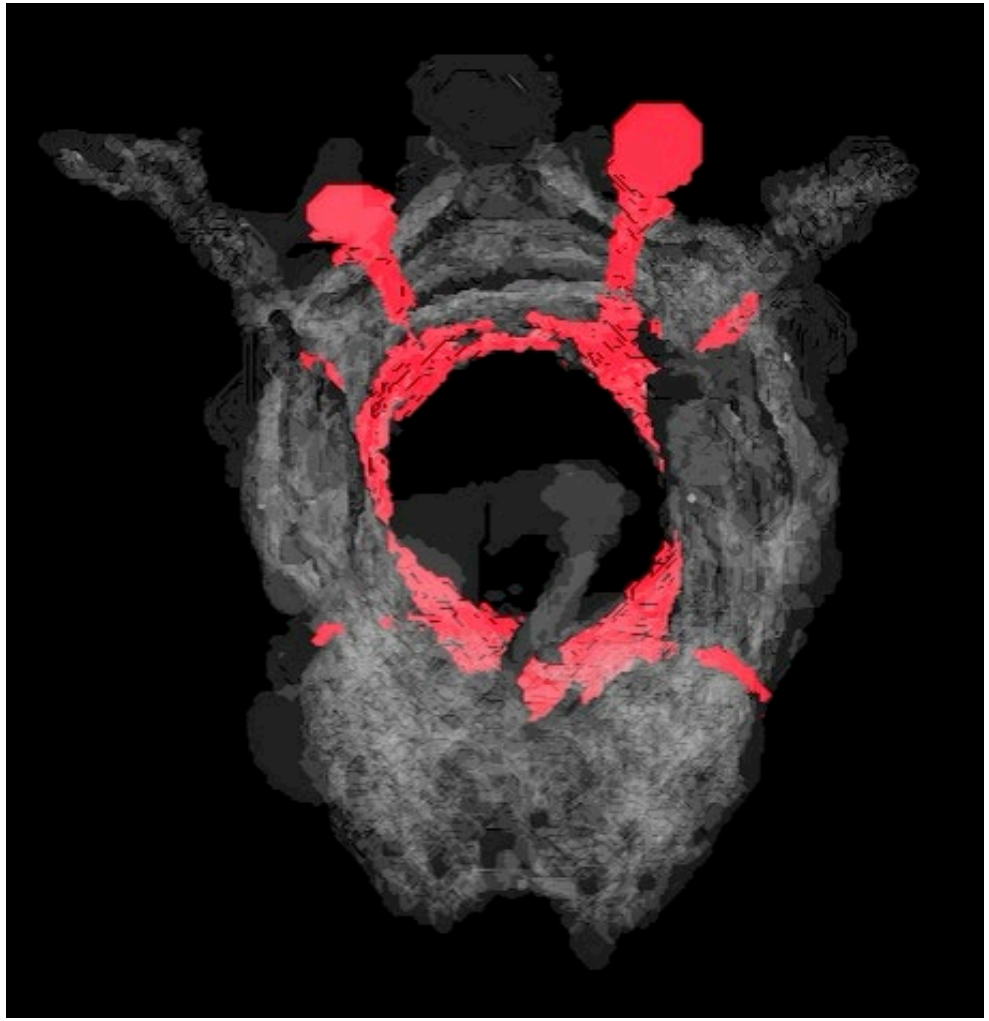

Summary

- EM-derived adjacencies can be used to study the worm nervous system organization
- Diffusion condensation is a new kind of “manifold filteration” for graphs that are thought to lie on manifolds
- This method helps to delineate delineating circuitry at various levels of granularity
- TDA can be used to study allometry (scaling up)
  - Varying levels of allometry

Structural vs Functional Connectivity

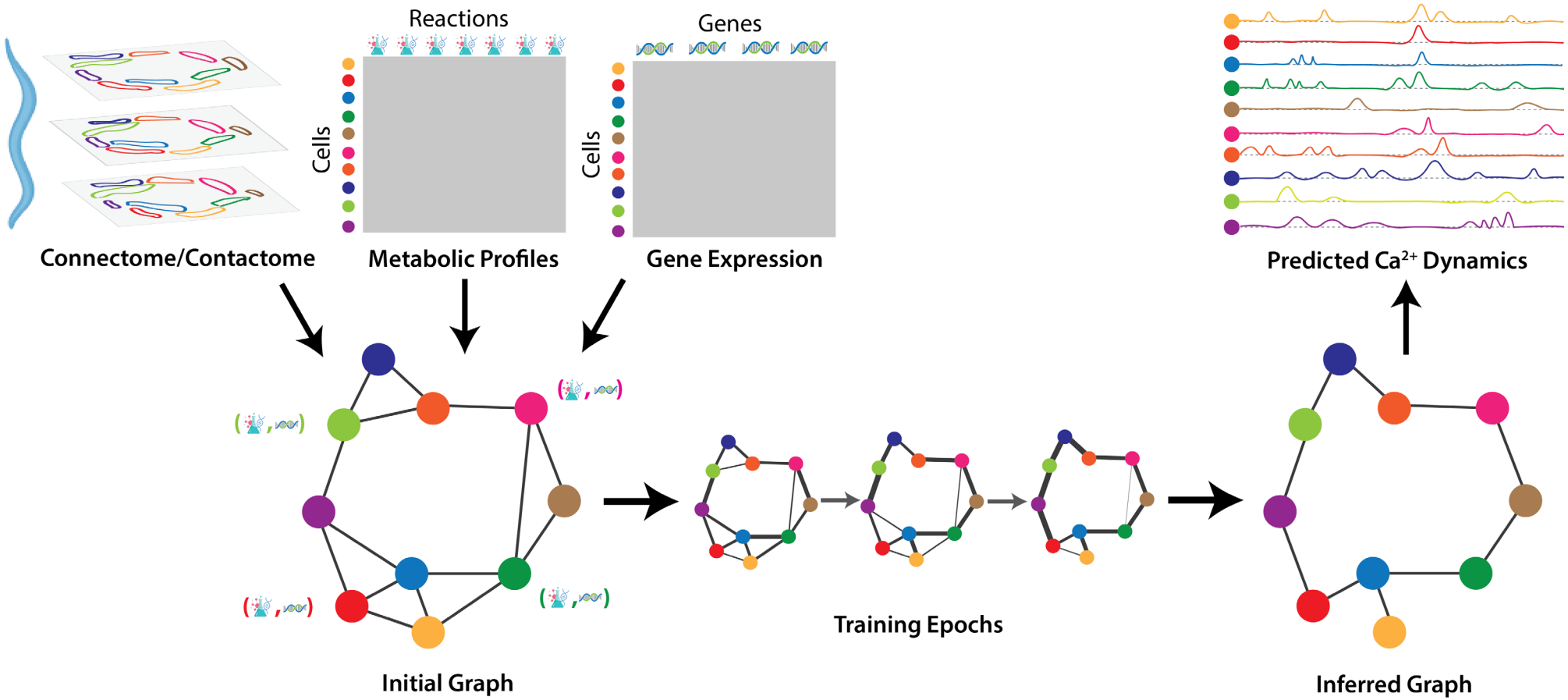

Regulatory Temporal Interaction Network Inference (RiTINI)

(Bhaskar, Magruder, et al. 2023, Learning On Graphs (LOG))

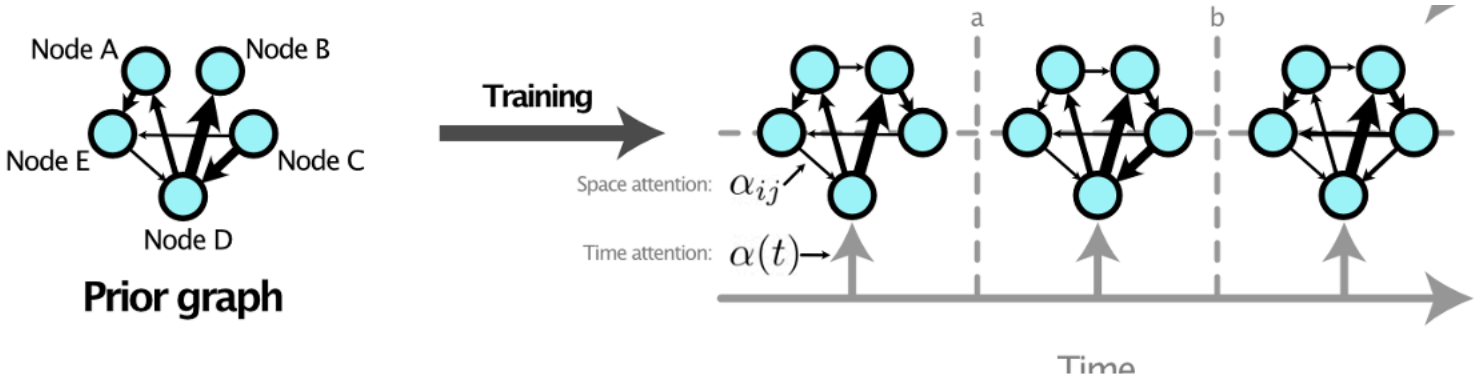

Dhananjay Bhaskar
Sumner Magruder
Edward De Brouwer
Frederik Wenkel
Guy Wolf

Main idea: Learn a dynamic interaction graph that matches the regulatory network

Using dynamic activity prediction as a task

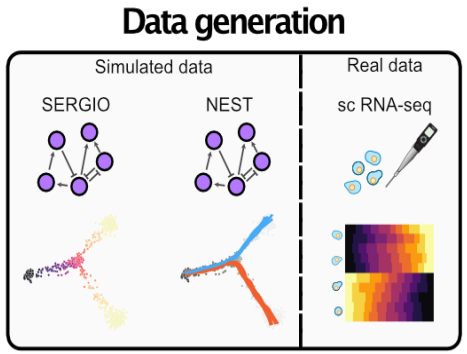

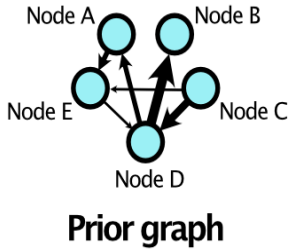

Prior graph

Predicting next requires a change in attention

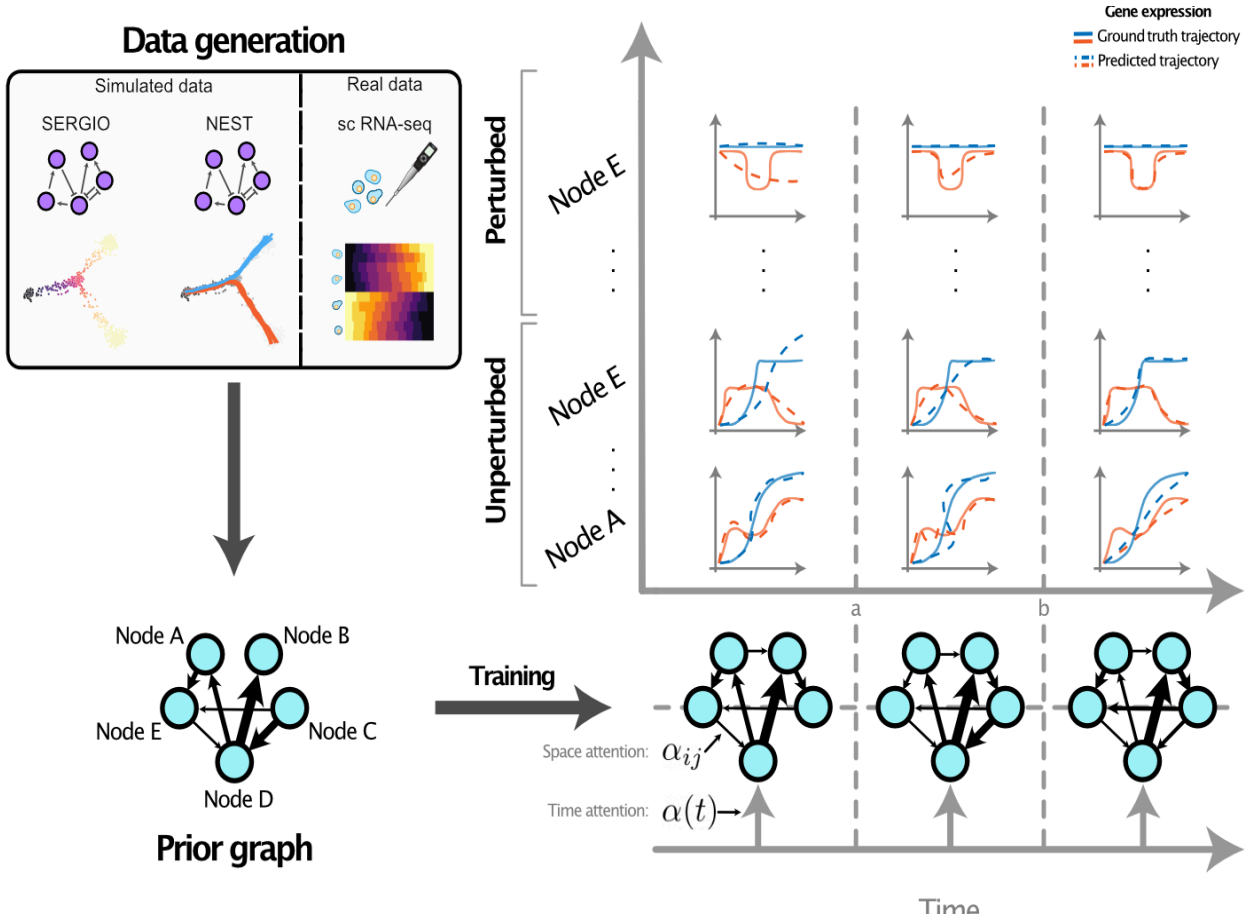

Attention readouts then create dynamic graph

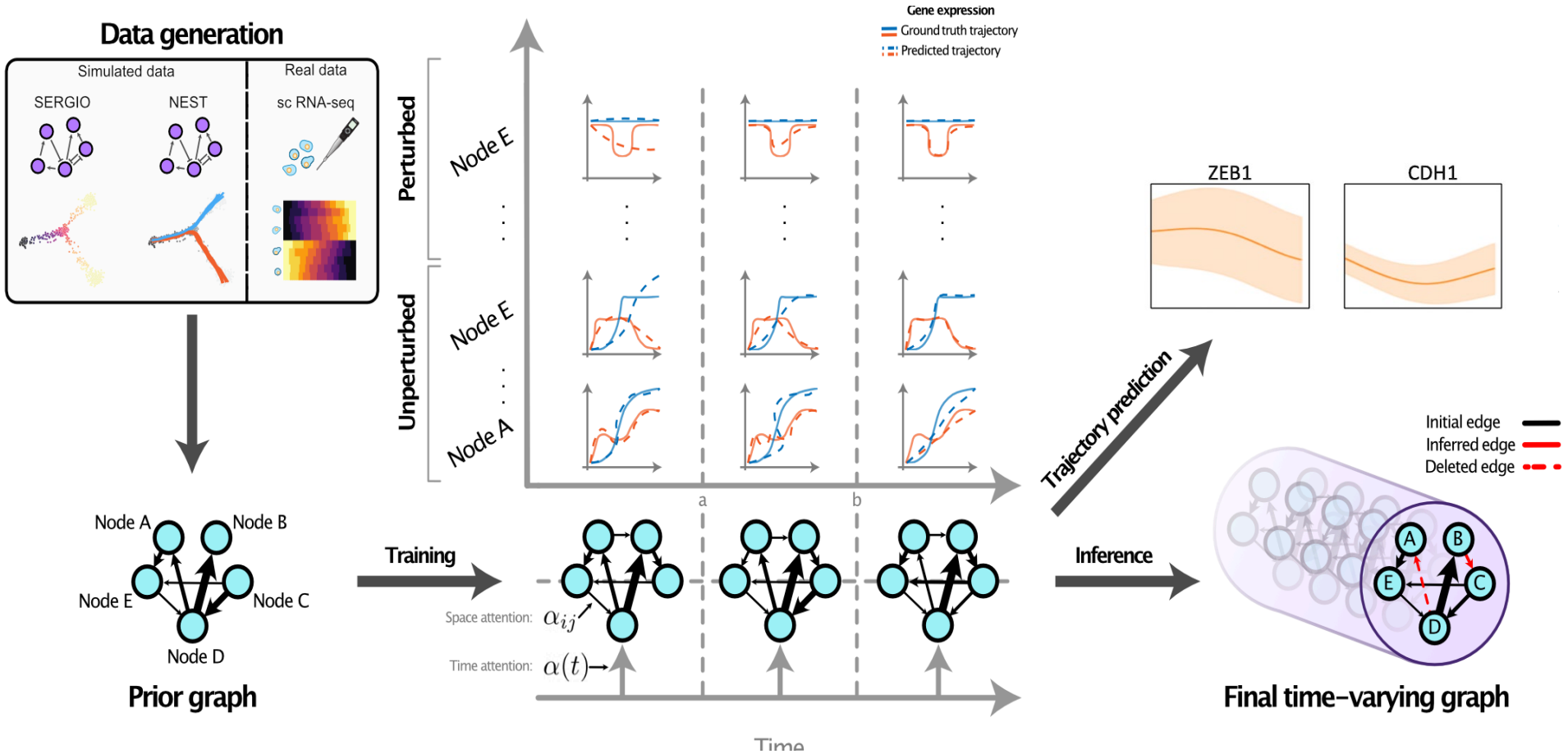

Space-time attention mechanism

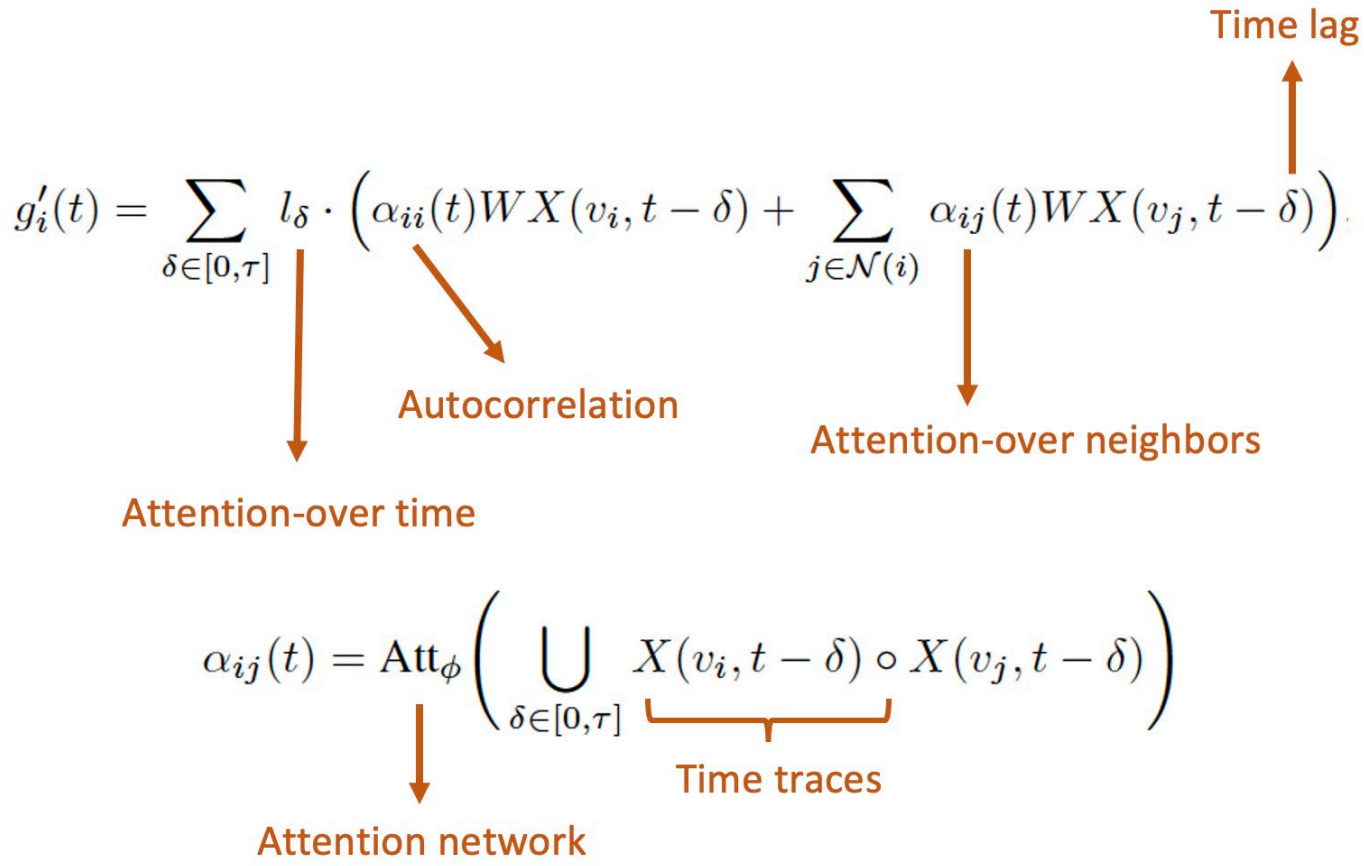

1. Attention network gives time-varying graph
2. Supports hysteresis, time attention can look at a specific point in time or over an interval
3. Outputs instantaneous derivative

RITINI Loss function

$$\frac{d}{dt}g_i(t) = f_\theta(g_i(t), t)$$

The graph attention network outputs a derivate which is then integrated with an ODE solver:

$$\hat{X}(v_i, t) = \text{ODESolve}(f_\theta, g_i'(t_0), t_0, t_1) \quad \forall t \in (t_0, t_1]$$

The final loss function also enforces closeness to a prior graph $\mathcal{E}_\mathcal{P}$ and sparsity to tackle lack of identifiability in this problem:

$$\mathcal{L}(t) = \underbrace{\sum_i \|\hat{X}(v_i, t) - X(v_i, t)\|}_{\text{MSE between ground truth and predicted dynamics}} + \lambda_1 \underbrace{\sum_{i,j} \|\alpha_{ij}(t) - \mathcal{E}_\mathcal{P}\|_F}_{\text{closeness to prior}} + \underbrace{\lambda_2 |\alpha(t)|_1}_{\text{sparsity}}$$

In silico perturbations—also used in training

- If a timed perturbation is applied then its effects propagate through the network
- This elucidates the structure of the network

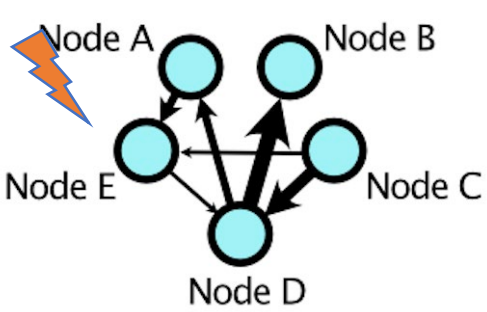

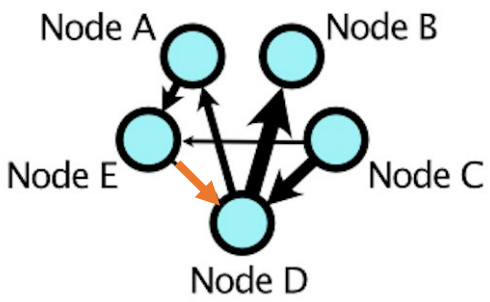

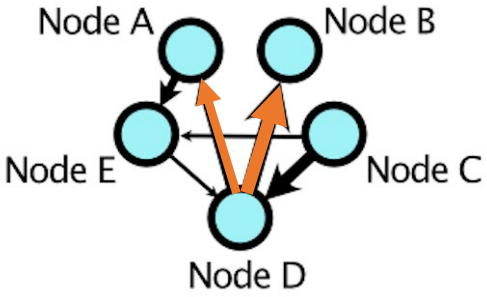

Validation with SERGIO

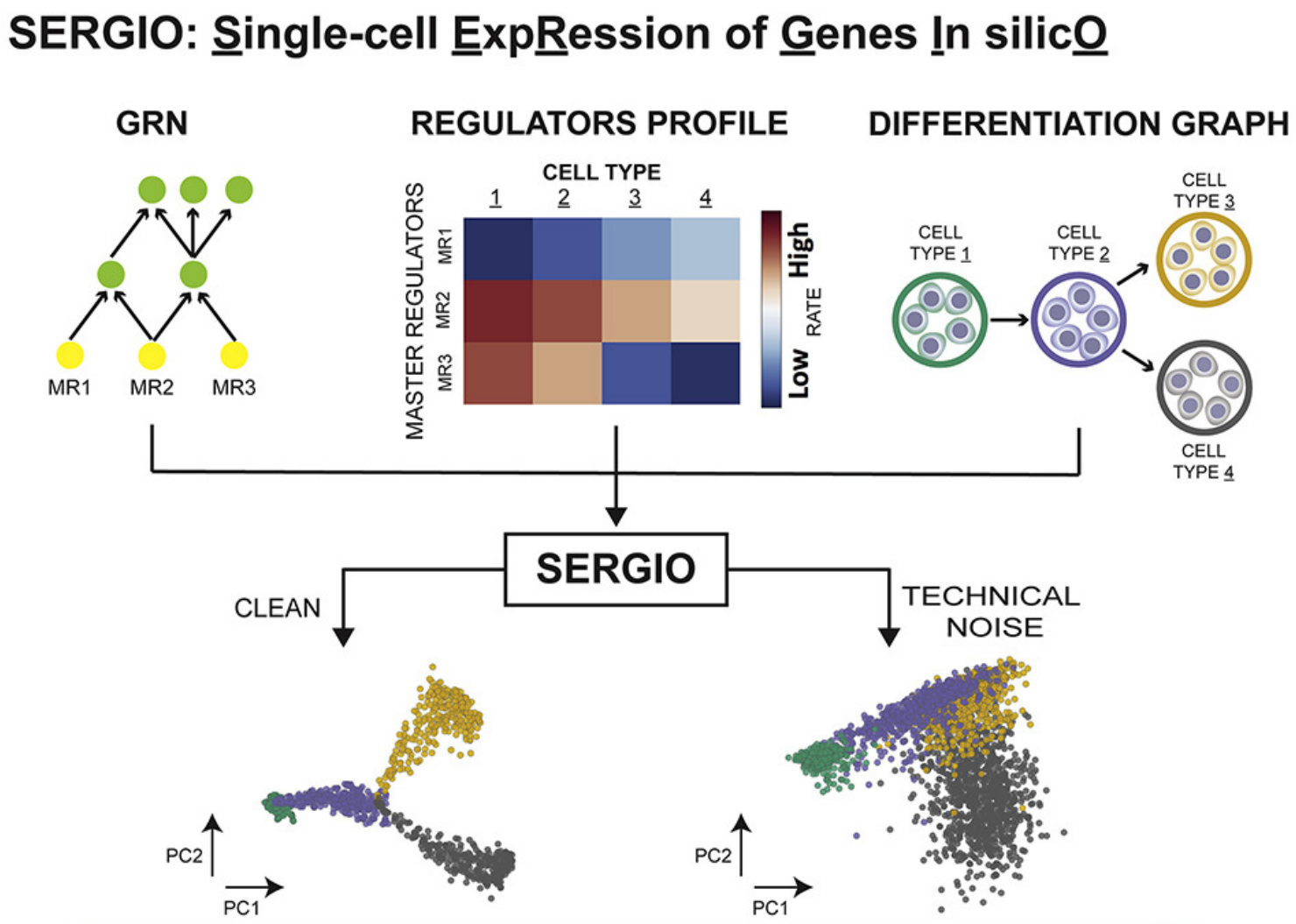

Dibaeinia and Sinha, Cell Systems, 2020

Synthetic Differentiation Dataset

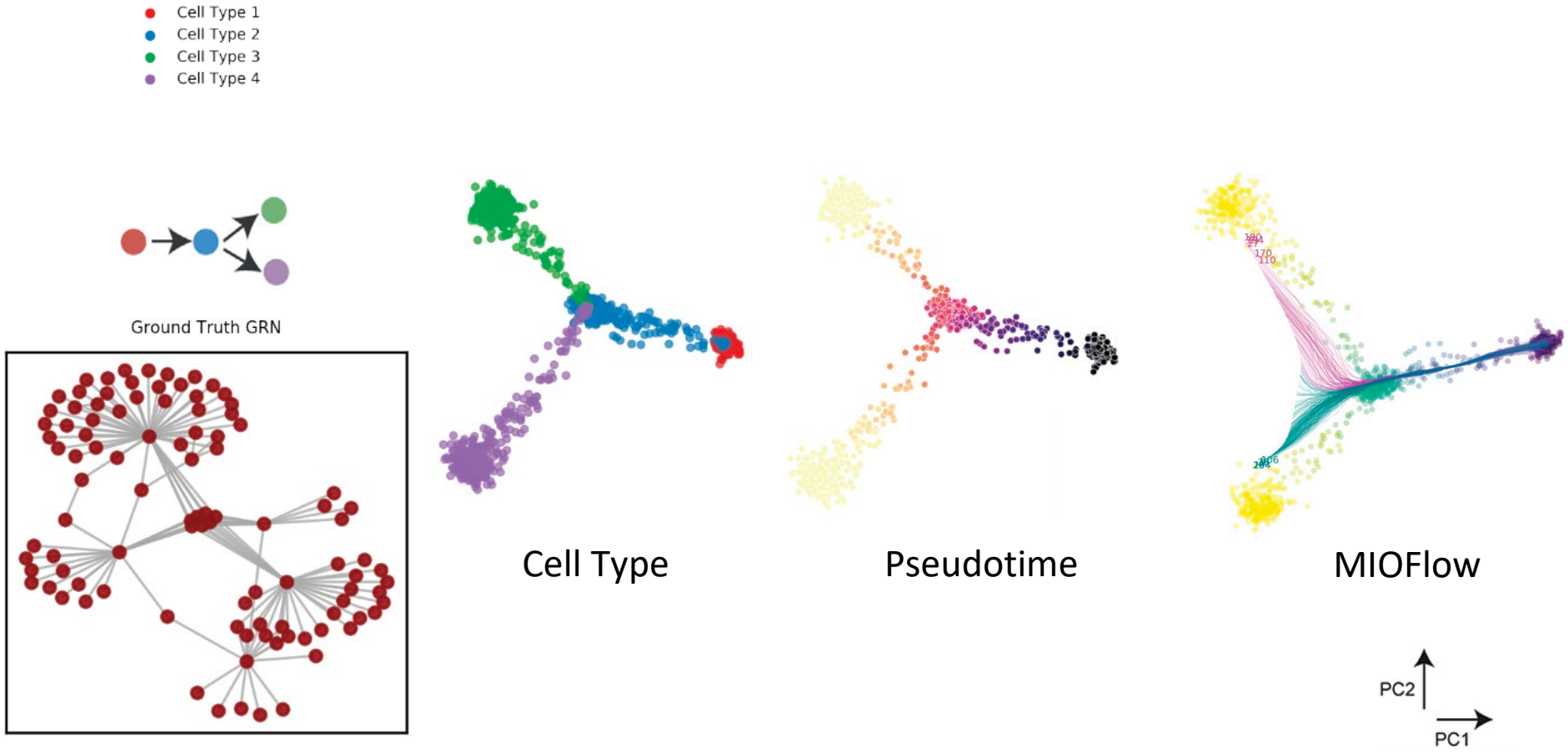

Synthetic Differentiation Dataset

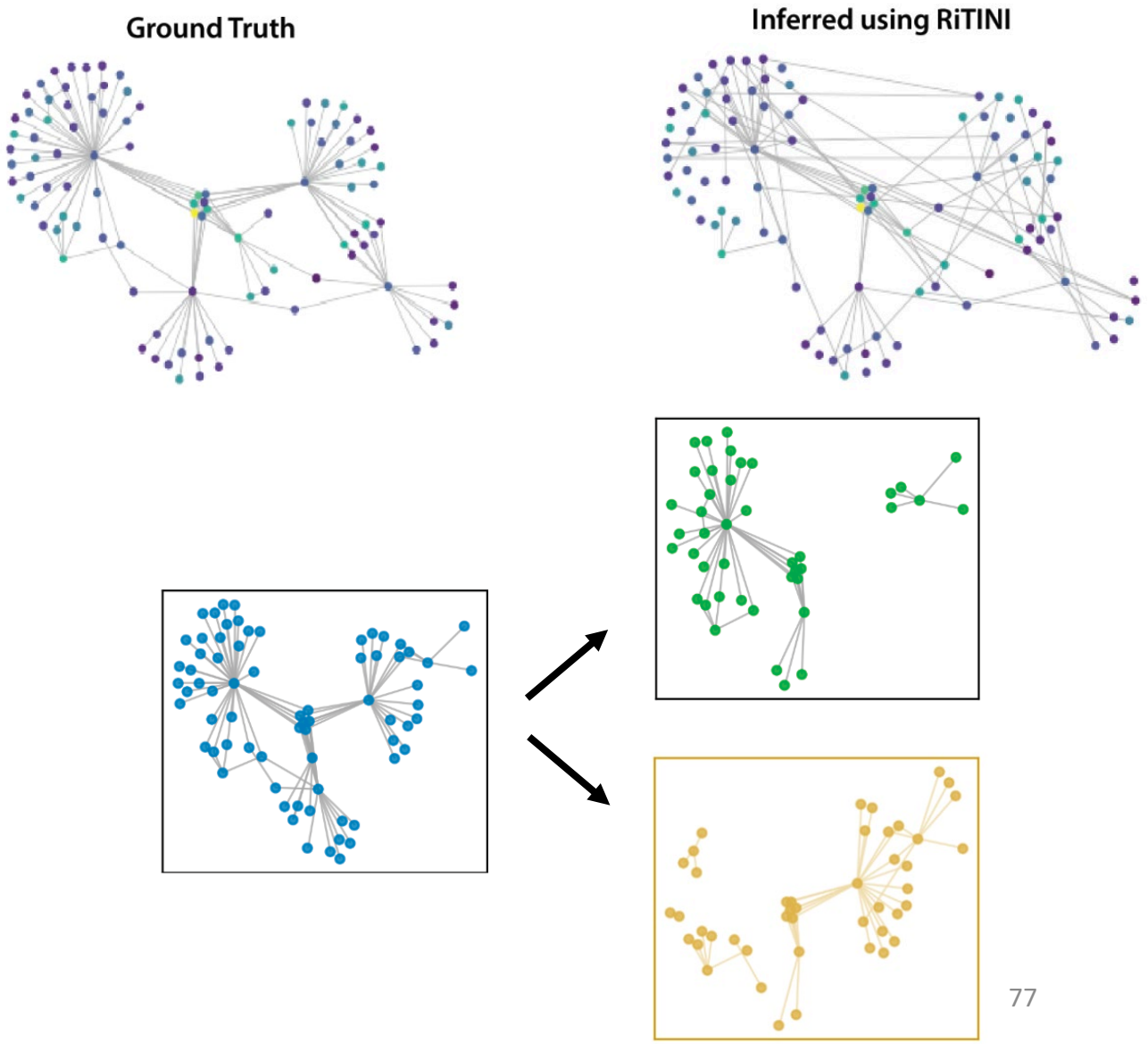

Quantitative Evaluation

Method	Dataset						
	Dynamical System	Neuronal Network (NEST)			Gene Regulatory Network (SERGIO)		
$(\lvert\mathcal{V}\rvert, \lvert\mathcal{E}\rvert) =$	$(5, 5)$	$(40, 78)$	$(50, 126)$	$(75, 308)$	$(100, 137)$	$(150, 329)$	$(200, 507)$
GC [41]	2.6 ± 1.0	28.8 ± 3.3	39.2 ± 2.3	75.4 ± 9.2	51.2 ± 3.3	109.0 ± 6.4	158.8 ± 12.6
OCE [42]	4.4 ± 1.6	72.8 ± 3.5	109.6 ± 4.2	255.6 ± 7.3	138.6 ± 3.5	293.4 ± 2.9	449.8 ± 1.1
PC [43, 44]	4.4 ± 1.4	75.8 ± 2.1	117.8 ± 3.9	284.6 ± 3.2	140.4 ± 3.9	317.2 ± 3.7	495.6 ± 6.5
mTE [45]	4.6 ± 1.7	64.2 ± 3.5	100.0 ± 7.6	232.2 ± 7.1	126.4 ± 2.4	261.0 ± 2.2	397.4 ± 8.8
mMI [46]	1.8 ± 0.7	20.6 ± 5.0	$\mathbf{34.6 \pm 5.2}$	82.0 ± 3.9	51.2 ± 3.3	99.8 ± 4.0	162.8 ± 6.2
NRI [47]	$\mathbf{0.5 \pm 0.1}$	$\mathbf{18.3 \pm 4.2}$	43.7 ± 8.6	94.1 ± 3.9	72.1 ± 6.2	106.6 ± 5.4	219.8 ± 13.4
DCRNN [48]	2.2 ± 0.4	44.7 ± 3.8	81.3 ± 9.6	117.0 ± 13.8	158.14 ± 8.6	303.79 ± 12.4	508.25 ± 23.6
GTS [49]	0.8 ± 0.3	23.5 ± 1.3	76.2 ± 11.9	181.7 ± 24.2	215.4 ± 13.8	347.2 ± 19.3	481.8 ± 7.0
NIR [50]	1.3 ± 0.1	22.5 ± 2.8	39.4 ± 1.9	106.2 ± 4.7	62.7 ± 3.2	86.3 ± 2.8	159.2 ± 11.6
RiTINI	2.2 ± 1.6	25.4 ± 2.8	35.2 ± 2.3	$\mathbf{69.6 \pm 7.7}$	$\mathbf{44.6 \pm 6.2}$	$\mathbf{83.6 \pm 4.2}$	$\mathbf{128.0 \pm 4.3}$
RiTINI (w/o hysteresis)	0.6 ± 0.4	22.4 ± 1.7	38.0 ± 6.9	91.3 ± 5.2	63.6 ± 8.2	118.3 ± 9.3	205.7 ± 8.3
RiTINI (w/o neural ODE)	1.7 ± 0.3	48.1 ± 3.0	72.4 ± 8.8	129.3 ± 9.4	114.2 ± 3.1	168.0 ± 12.6	329.7 ± 22.5

Table 1: Mean and standard deviation of the graph edit distance between the inferred graph and the ground truth, across 5 different simulations with perturbations (lower is better).

Cellular Embryonic Stem Cell Differentiation

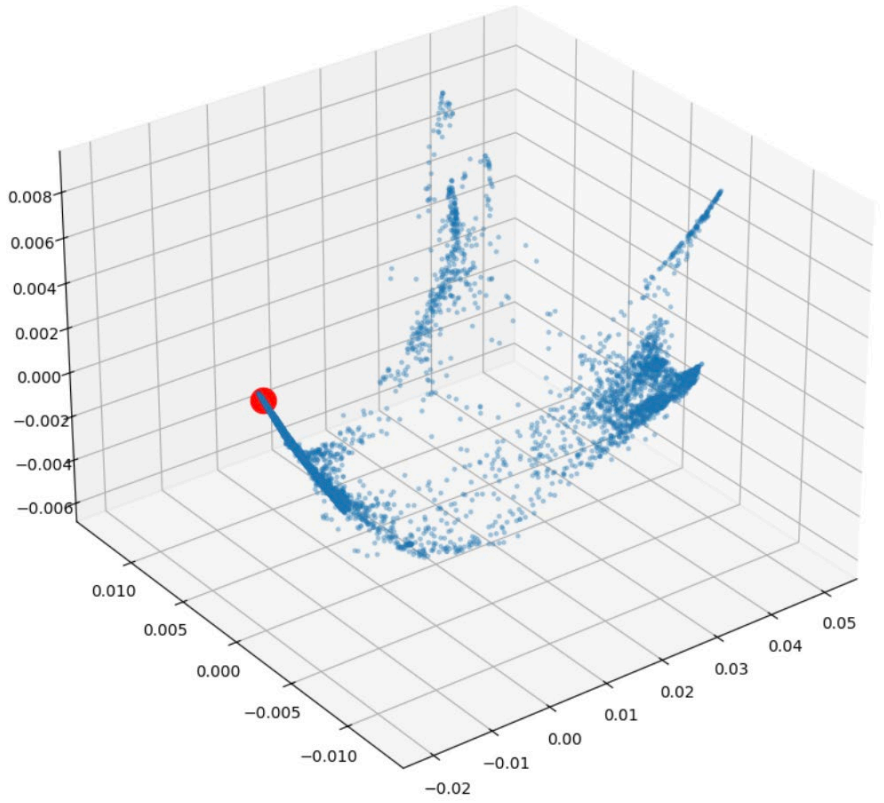

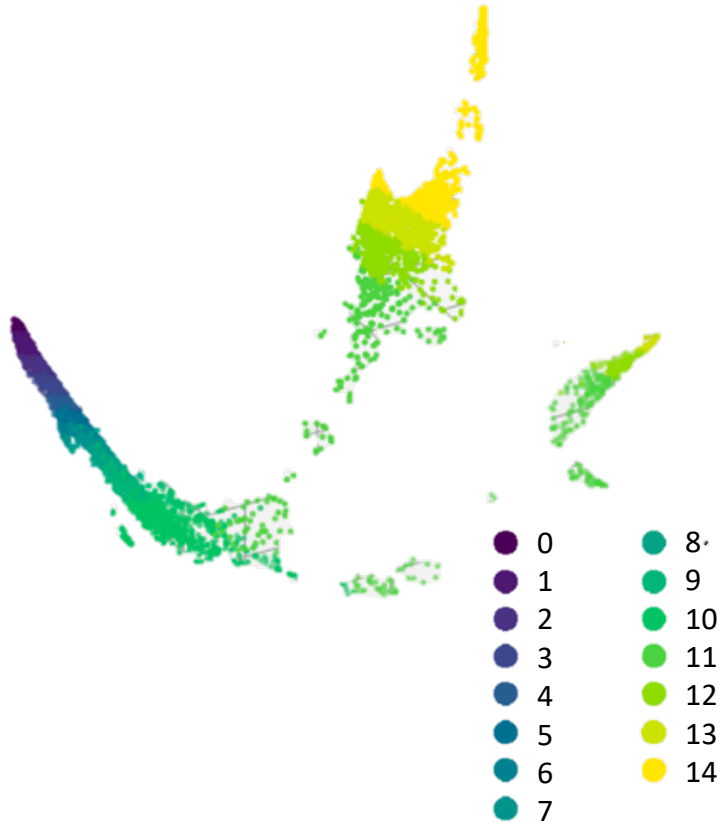

Branch Segmentation

ESC

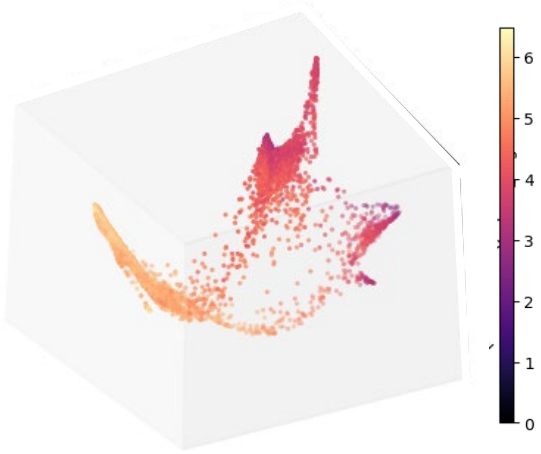

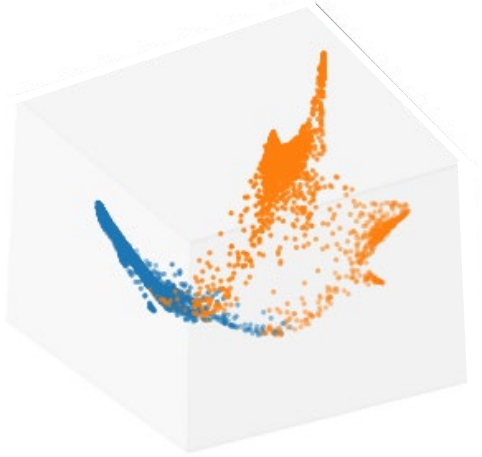

Neural Progenitors

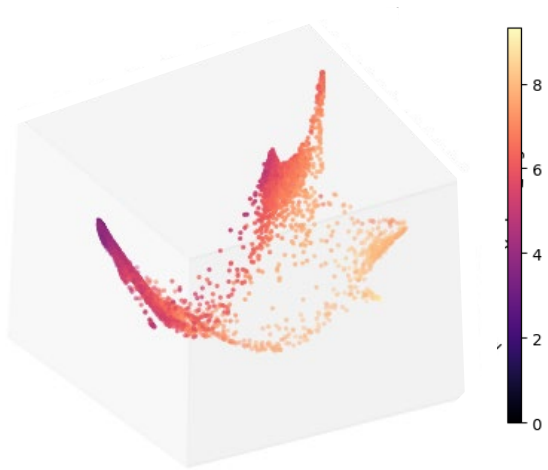

Neural Crest

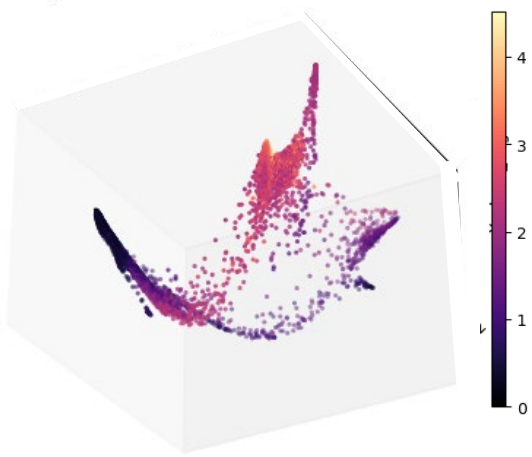

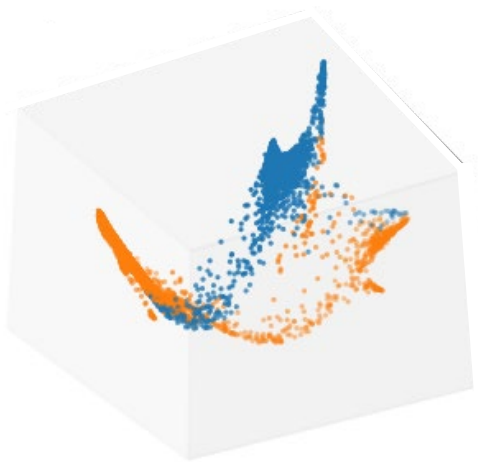

Trajectory Inference from MIOflow Neural ODE

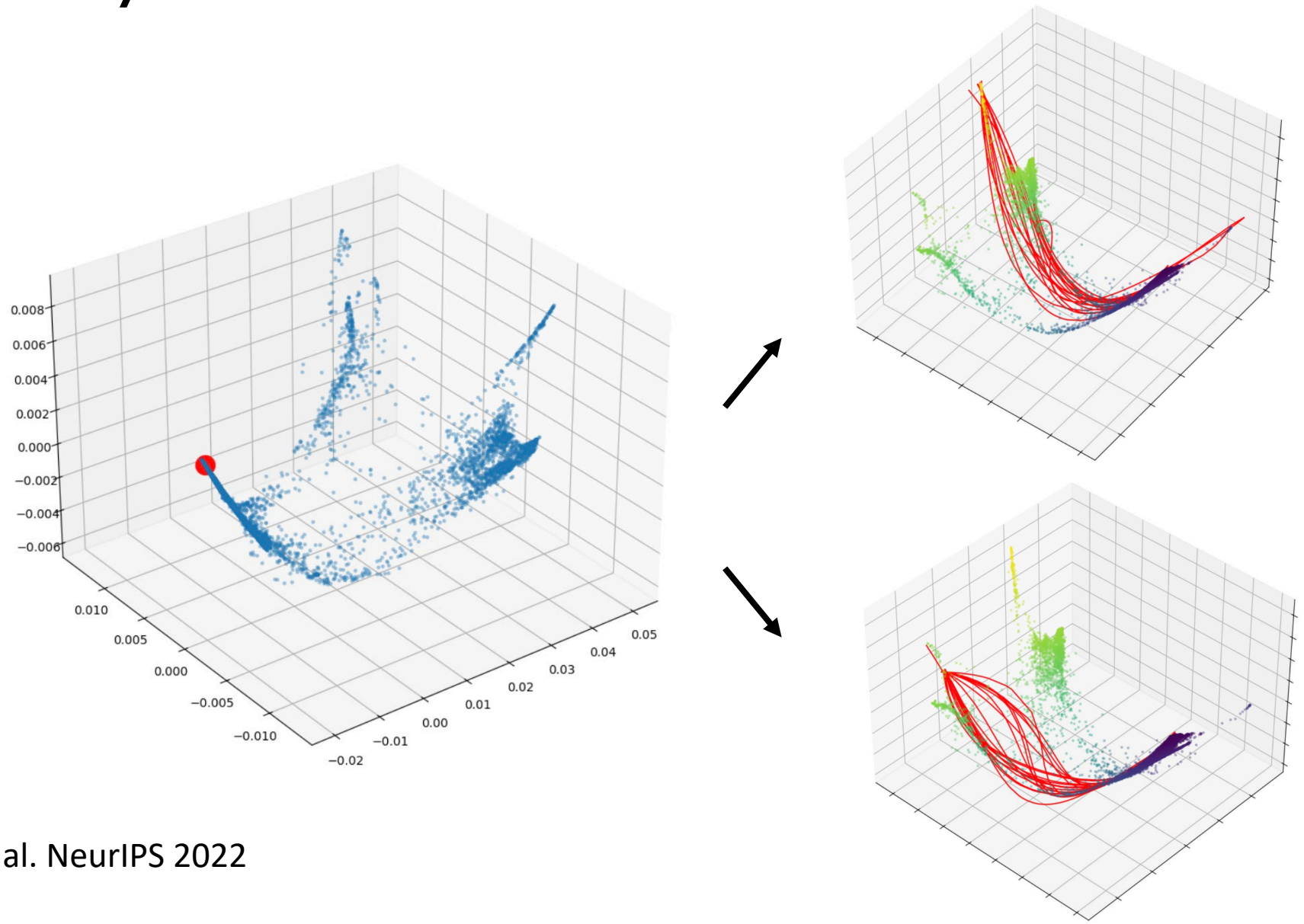

Huguet et al. NeurIPS 2022

Inferred Gene Regulatory Network

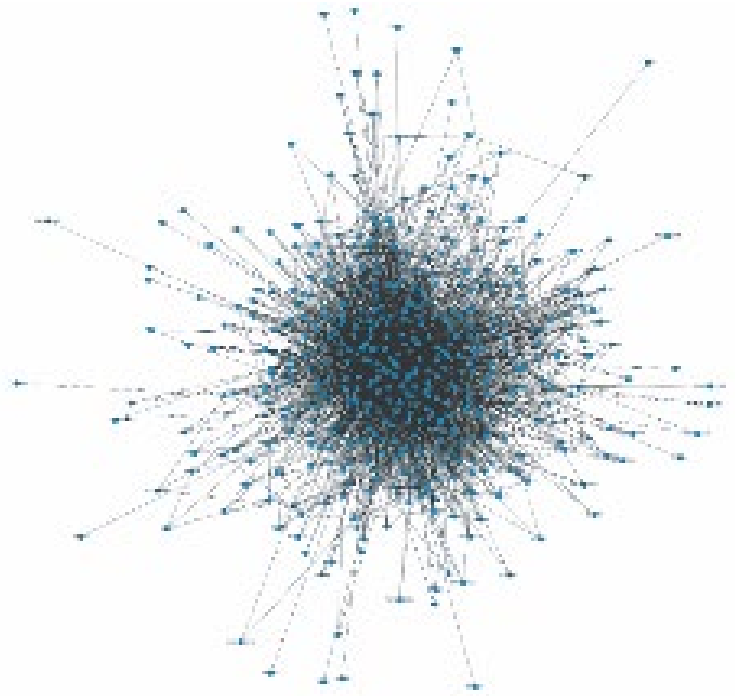

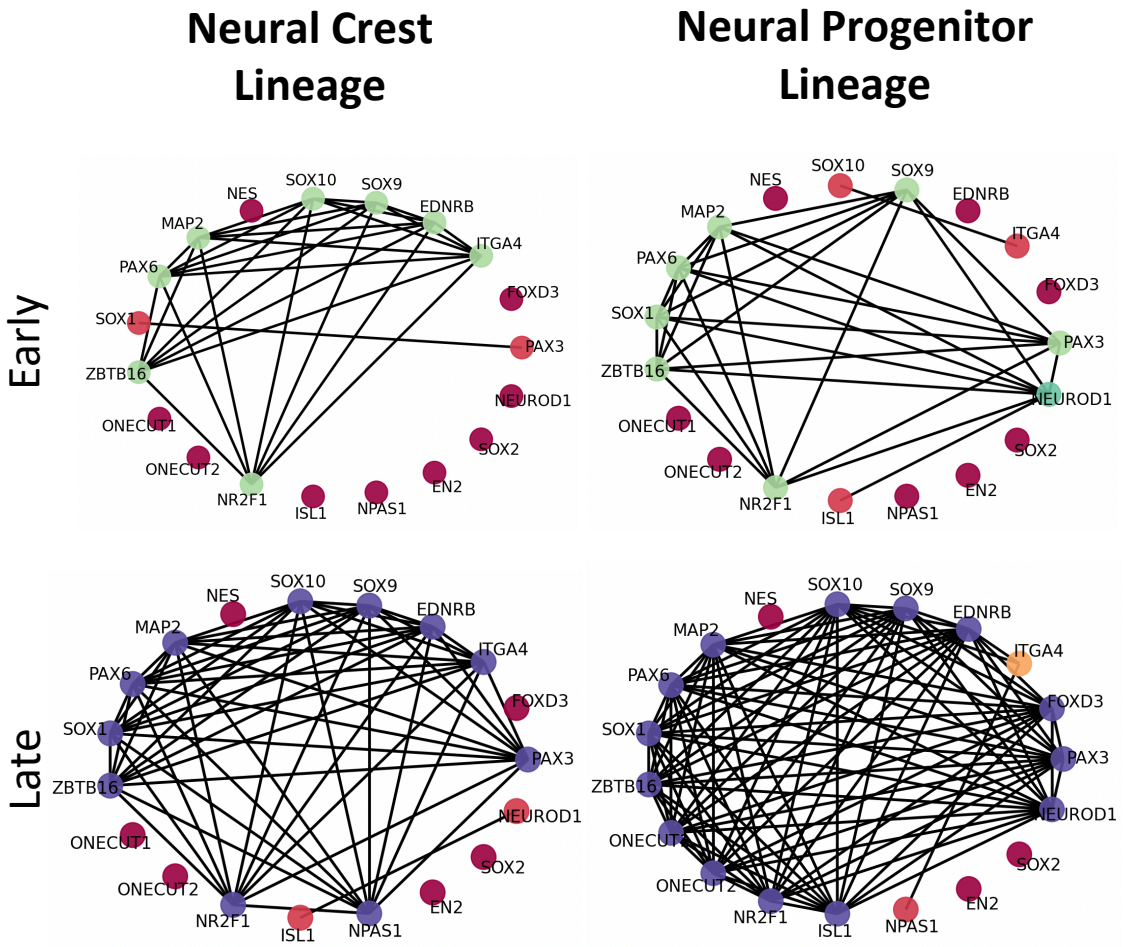

In Silico Perturbations-top ranked perturbations

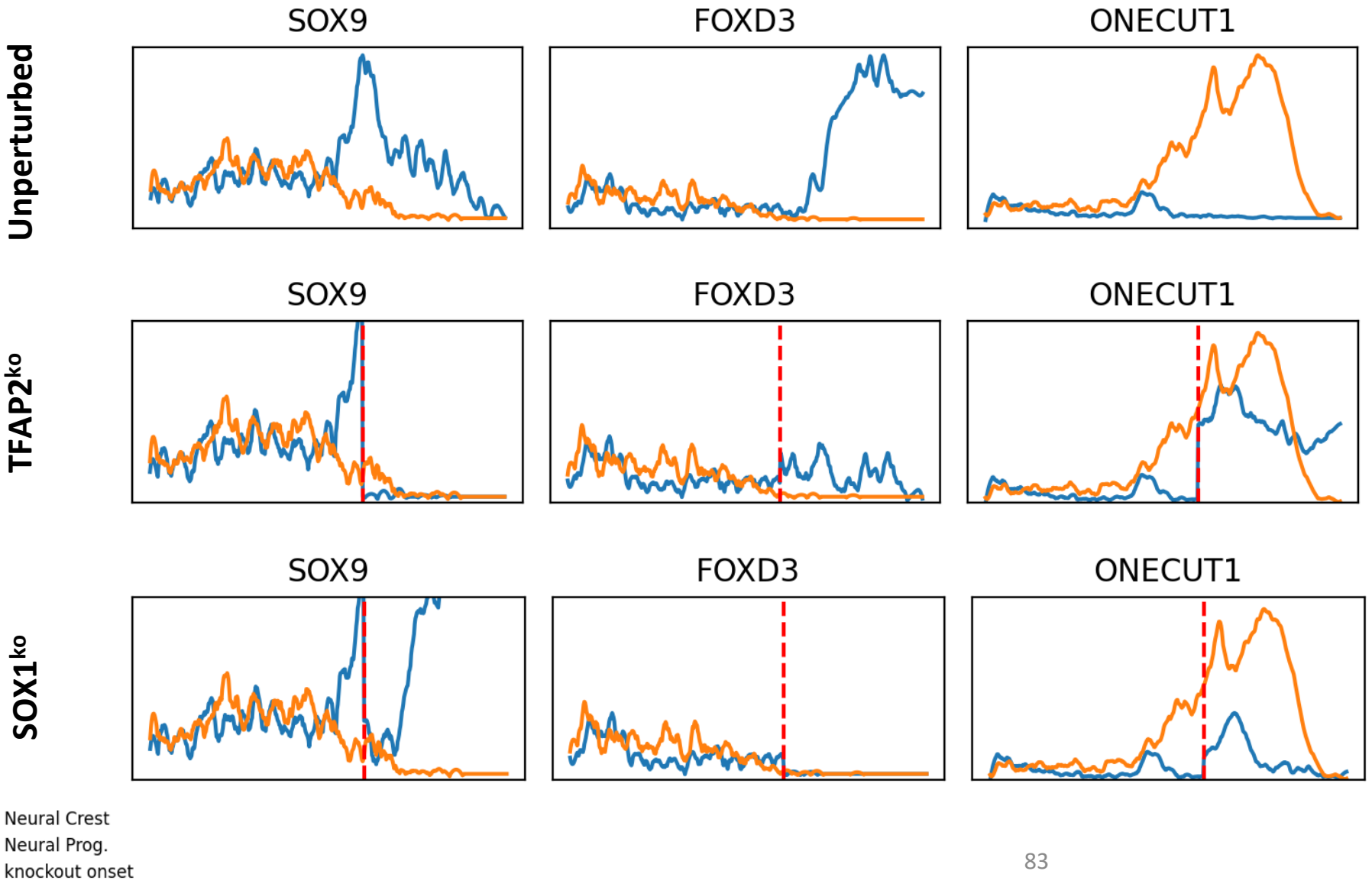

NEST Simulations

Network of coupled Wilson-Cowan oscillators

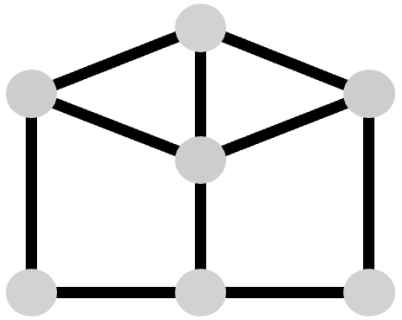

$$\frac{dr_{\mathrm{E}}}{dt} = \left(\alpha_{\mathrm{E}} \cdot S_{\mathrm{E}}(w_{\mathrm{EE}} \cdot r_{\mathrm{E}} - w_{\mathrm{EI}} \cdot r_{\mathrm{I}}) - \theta_{\mathrm{E}} - r_{\mathrm{E}}\right) / \tau_{\mathrm{E}}$$

$$\frac{dr_{\mathrm{I}}}{dt} = \left(\alpha_{\mathrm{I}} \cdot S_{\mathrm{I}}(w_{\mathrm{IE}} \cdot r_{\mathrm{E}} - w_{\mathrm{II}} \cdot r_{\mathrm{I}}) - \theta_{\mathrm{I}} - r_{\mathrm{I}}\right) / \tau_{\mathrm{I}}$$

nest::

simulated neural activity

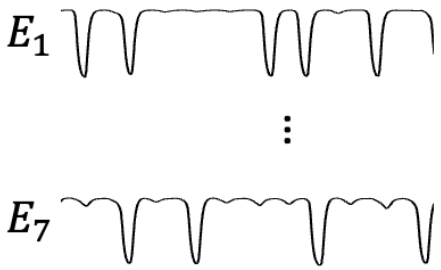

Recover neuronal connectivity

Perturbation simulated

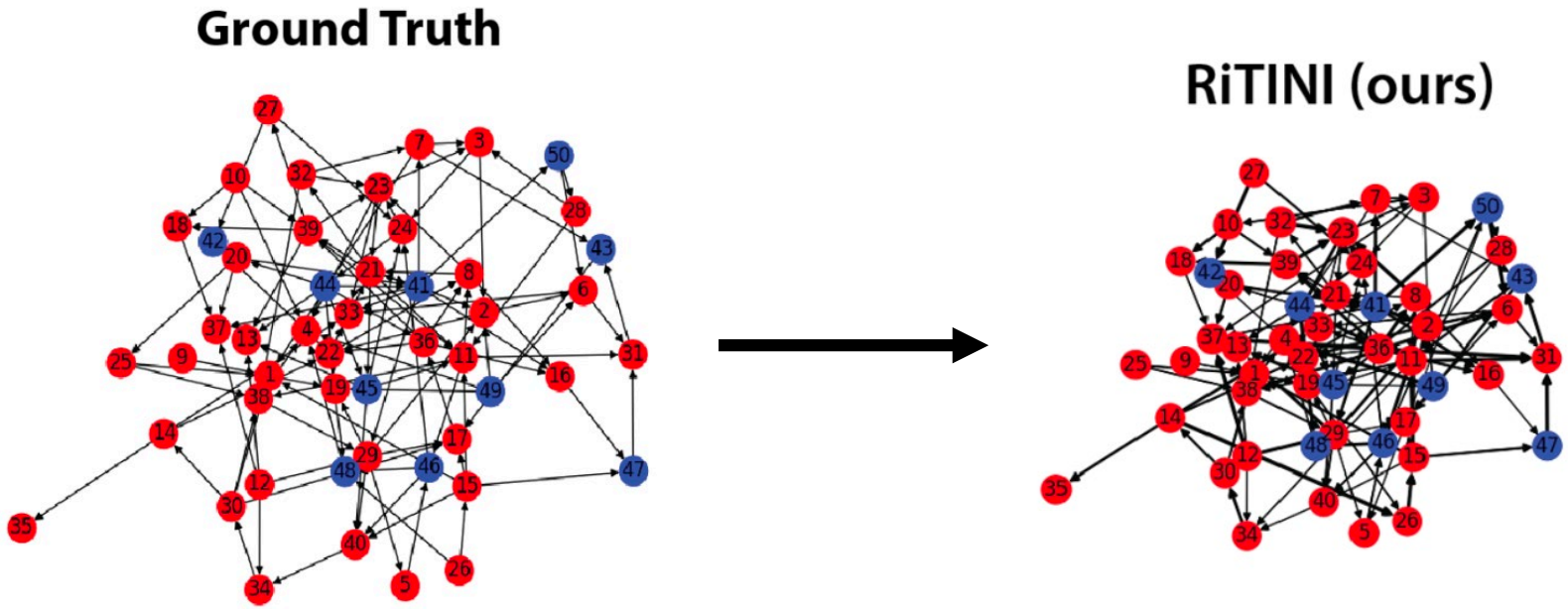

Train using optogenetic stimulations to shift parameters in the equation

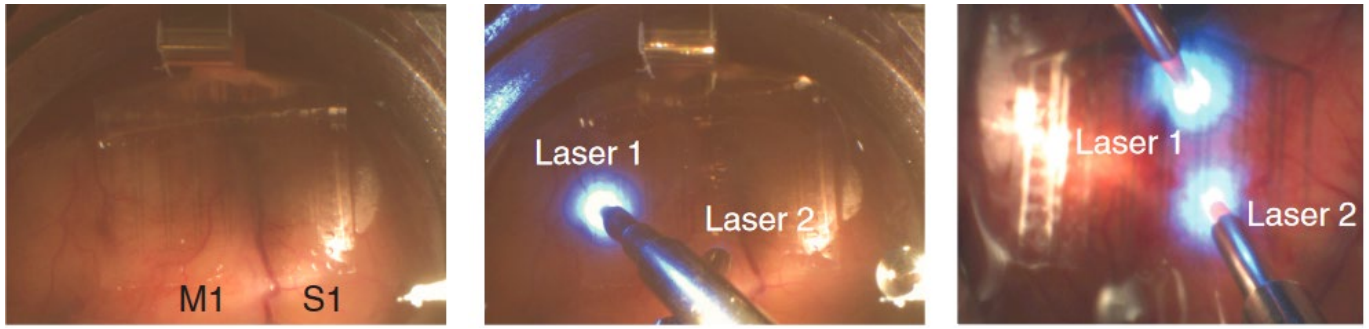

Recovery of ground truth “static”

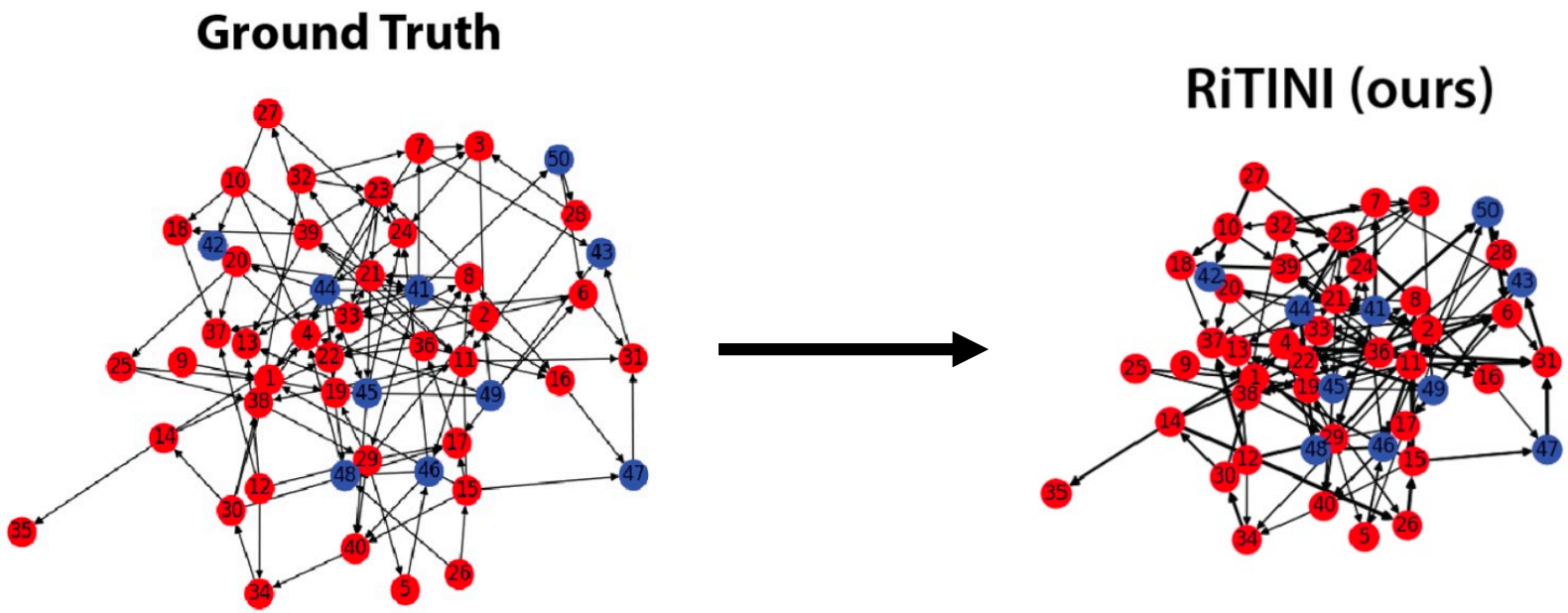

Method	Dataset						
	Dynamical System	Neuronal Network (NEST)			Gene Regulatory Network (SERGIO)		
$(\lvert\mathcal{V}\rvert, \lvert\mathcal{E}\rvert) =$	$(5, 5)$	$(40, 78)$	$(50, 126)$	$(75, 308)$	$(100, 137)$	$(150, 329)$	$(200, 507)$
GC [41]	2.6 ± 1.0	28.8 ± 3.3	39.2 ± 2.3	75.4 ± 9.2	51.2 ± 3.3	109.0 ± 6.4	158.8 ± 12.6
OCE [42]	4.4 ± 1.6	72.8 ± 3.5	109.6 ± 4.2	255.6 ± 7.3	138.6 ± 3.5	293.4 ± 2.9	449.8 ± 1.1
PC [43, 44]	4.4 ± 1.4	75.8 ± 2.1	117.8 ± 3.9	284.6 ± 3.2	140.4 ± 3.9	317.2 ± 3.7	495.6 ± 6.5
mTE [45]	4.6 ± 1.7	64.2 ± 3.5	100.0 ± 7.6	232.2 ± 7.1	126.4 ± 2.4	261.0 ± 2.2	397.4 ± 8.8
mMI [46]	1.8 ± 0.7	20.6 ± 5.0	$\mathbf{34.6 \pm 5.2}$	82.0 ± 3.9	51.2 ± 3.3	99.8 ± 4.0	162.8 ± 6.2
NRI [47]	$\mathbf{0.5 \pm 0.1}$	$\mathbf{18.3 \pm 4.2}$	43.7 ± 8.6	94.1 ± 3.9	72.1 ± 6.2	106.6 ± 5.4	219.8 ± 13.4
DCRNN [48]	2.2 ± 0.4	44.7 ± 3.8	81.3 ± 9.6	117.0 ± 13.8	158.14 ± 8.6	303.79 ± 12.4	508.25 ± 23.6
GTS [49]	0.8 ± 0.3	23.5 ± 1.3	76.2 ± 11.9	181.7 ± 24.2	215.4 ± 13.8	347.2 ± 19.3	481.8 ± 7.0
NIR [50]	1.3 ± 0.1	22.5 ± 2.8	39.4 ± 1.9	106.2 ± 4.7	62.7 ± 3.2	86.3 ± 2.8	159.2 ± 11.6
RiTINI	2.2 ± 1.6	25.4 ± 2.8	35.2 ± 2.3	$\mathbf{69.6 \pm 7.7}$	$\mathbf{44.6 \pm 6.2}$	$\mathbf{83.6 \pm 4.2}$	$\mathbf{128.0 \pm 4.3}$
RiTINI (w/o hysteresis)	0.6 ± 0.4	22.4 ± 1.7	38.0 ± 6.9	91.3 ± 5.2	63.6 ± 8.2	118.3 ± 9.3	205.7 ± 8.3
RiTINI (w/o neural ODE)	1.7 ± 0.3	48.1 ± 3.0	72.4 ± 8.8	129.3 ± 9.4	114.2 ± 3.1	168.0 ± 12.6	329.7 ± 22.5

Table 1: Mean and standard deviation of the graph edit distance between the inferred graph and the ground truth, across 5 different simulations with perturbations (lower is better).

Graph Scattering Homology Trajectory

(D. Bhaskar, J. Moore, F. Gao, et al., Journal of Cell Biology, 2023)

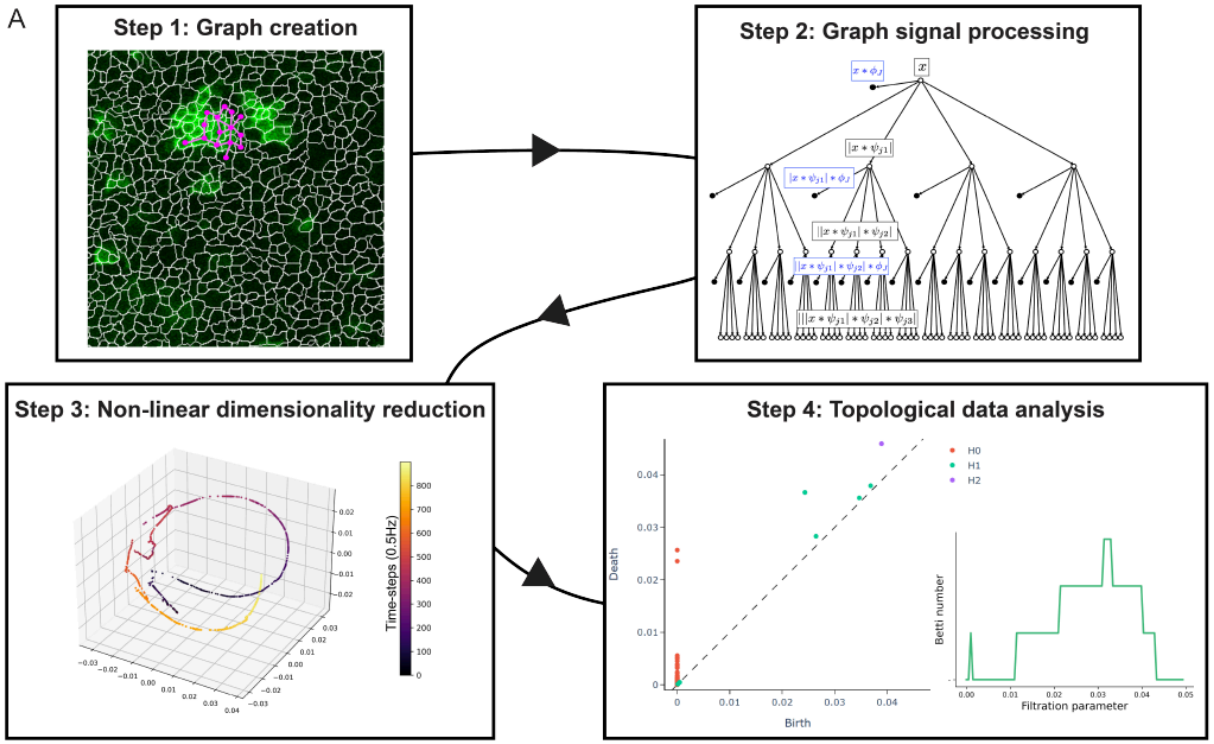

Dhananjay Bhaskar
Jess Moore
Feng Gao
Valentina Greco

Graph signal-based descriptors for signaling dynamics and regime analysis

Geometric Scattering

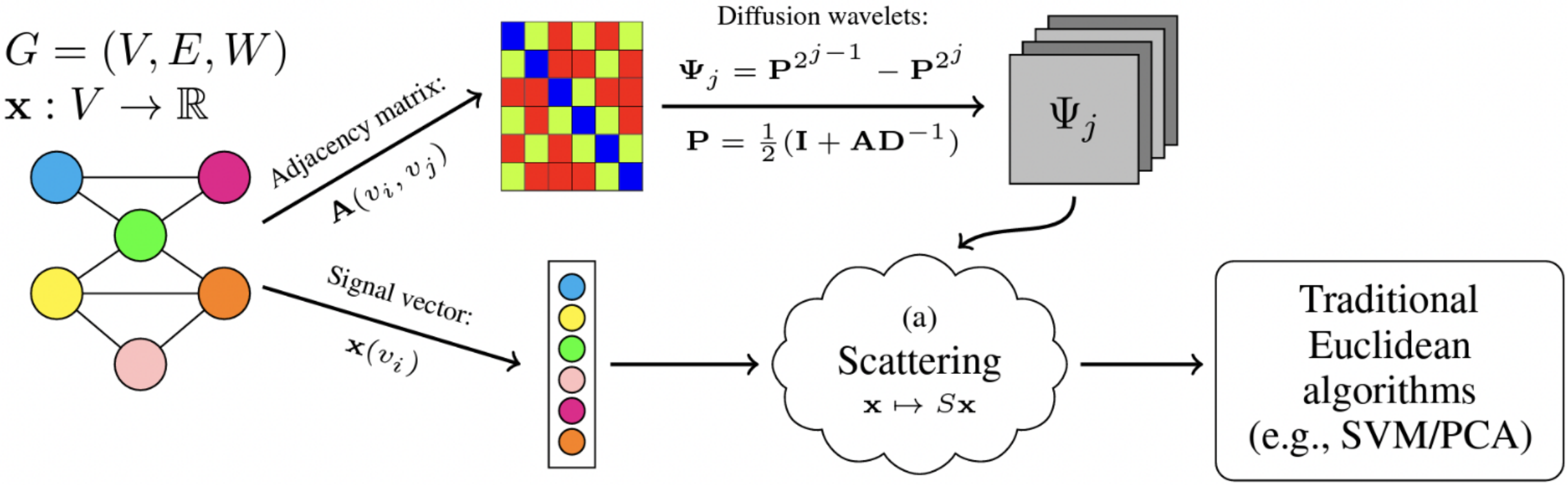

Gao et al., *PMLR*, 2019

Geometric Scattering

- Given a graph **G(V, E)** define the left stochastic diffusion matrix:

$$\boldsymbol{P} := \tfrac{1}{2}\left(\boldsymbol{I}_n + \boldsymbol{W}\boldsymbol{D}^{-1}\right) \qquad \boldsymbol{W}[v_i, v_j] := \begin{cases} w(v_i, v_j) & \text{if } \{v_i, v_j\} \in E, \\ 0 & \text{otherwise,} \end{cases}$$

- Define wavelet matrix at scale 2^j:

$$\boldsymbol{\Psi}_j = \mathbf{P}^{2^{j-1}} - \mathbf{P}^{2^j} = \mathbf{P}^{2^{j-1}}(\mathbf{I} - \mathbf{P}^{2^{j-1}})$$

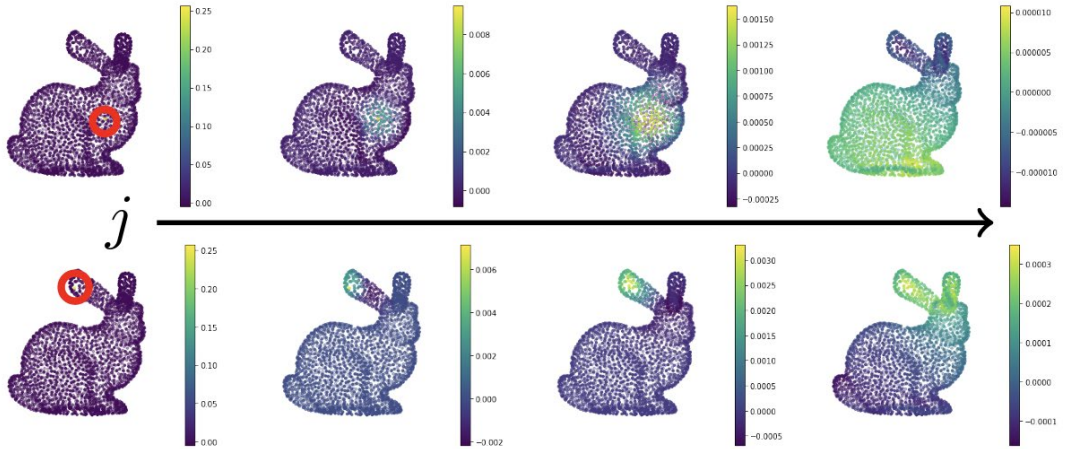

Geometric Scattering

- Construct a filter bank:

$$\mathcal{W}_J := \{\boldsymbol{\Psi}_j, \boldsymbol{\Phi}_J\}_{0 \le j \le J}$$

$$\boldsymbol{\Psi}_0 := \boldsymbol{I}_n - \boldsymbol{P},$$
$$\boldsymbol{\Psi}_j := \boldsymbol{P}^{2^{j-1}} - \boldsymbol{P}^{2^j} = \boldsymbol{P}^{2^{j-1}}\left(\boldsymbol{I}_n - \boldsymbol{P}^{2^{j-1}}\right), \quad j \ge 1$$
$$\boldsymbol{\Phi}_J := \boldsymbol{P}^{2^J}$$

- Compute wavelet coefficients:

$$\boldsymbol{\Psi}^{(J)}\mathbf{x}(v_\ell) = [\boldsymbol{\Psi}_j \mathbf{x}(v_\ell) : 1 \le j \le J]$$

(captures frequencies of input signal **x** within neighborhood radius 2^j)

GSTH Methodology

"Geometric Scattering Trajectory Homology"

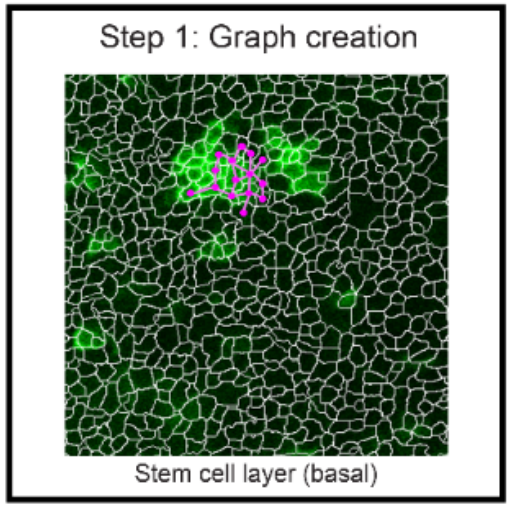

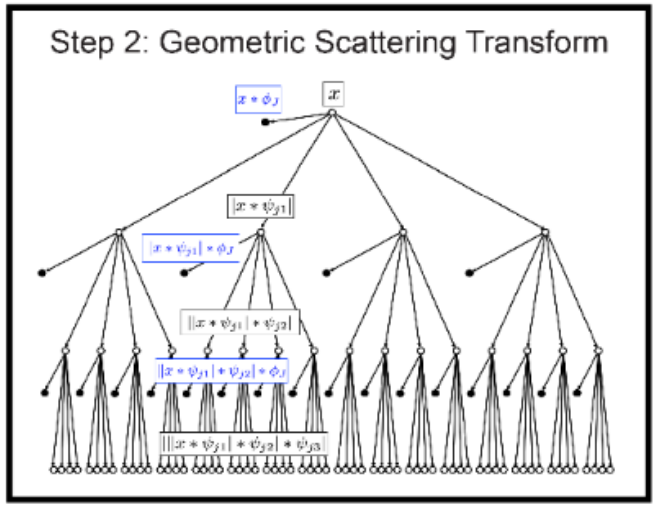

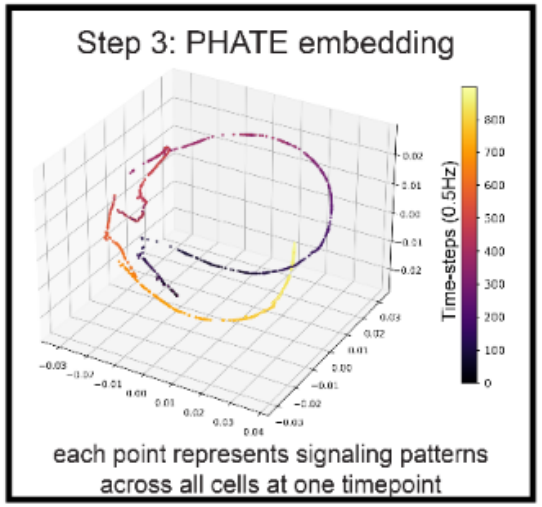

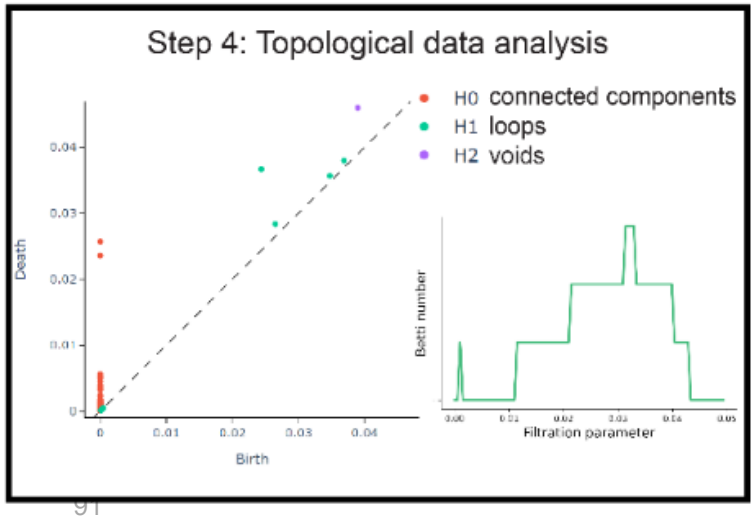

Moore et al., *JCB* (to appear)

Epithelial vs Neuronal Cells

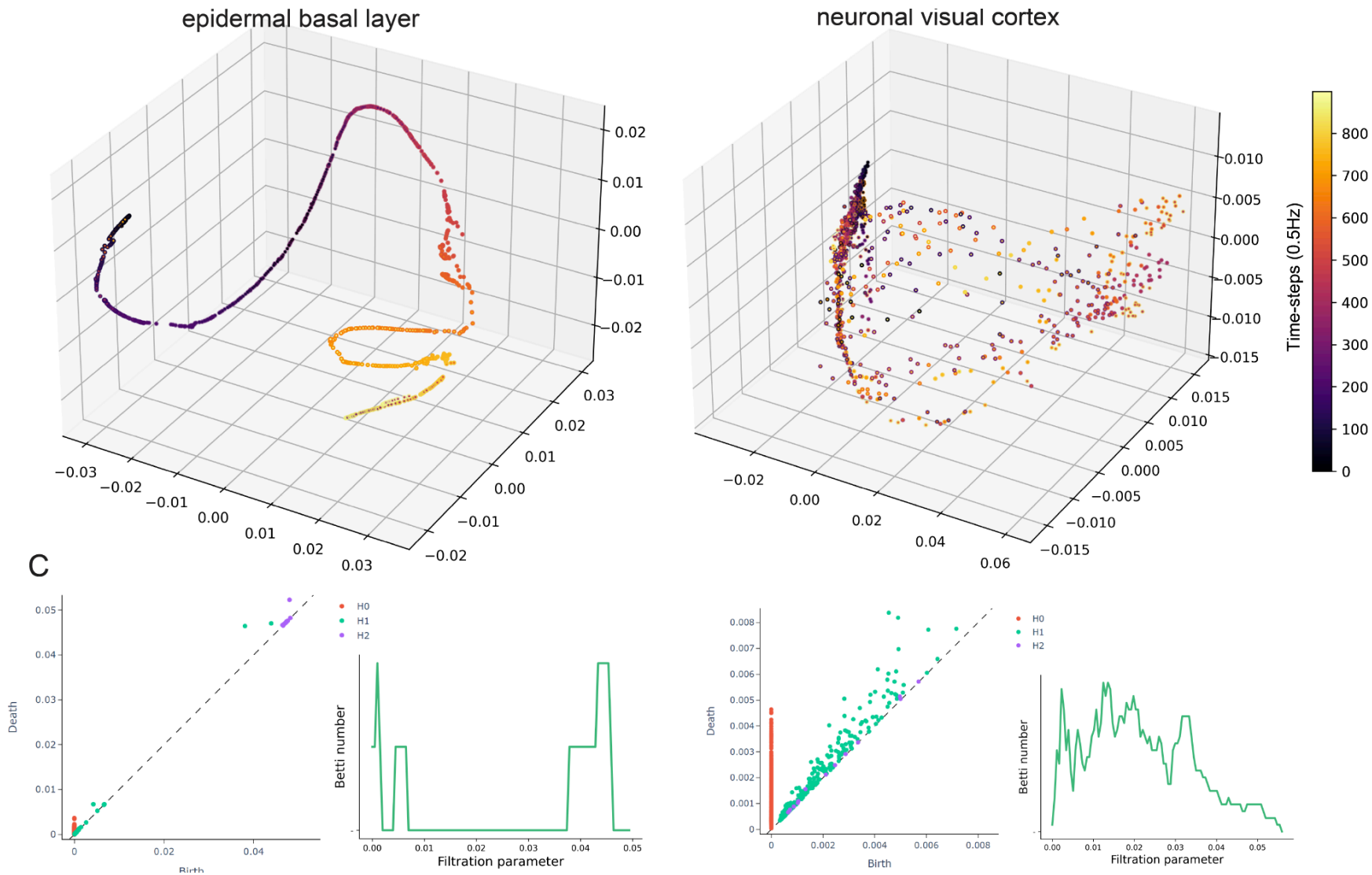

G2 stem cells are essential for homeostatic Ca^{2+} signaling

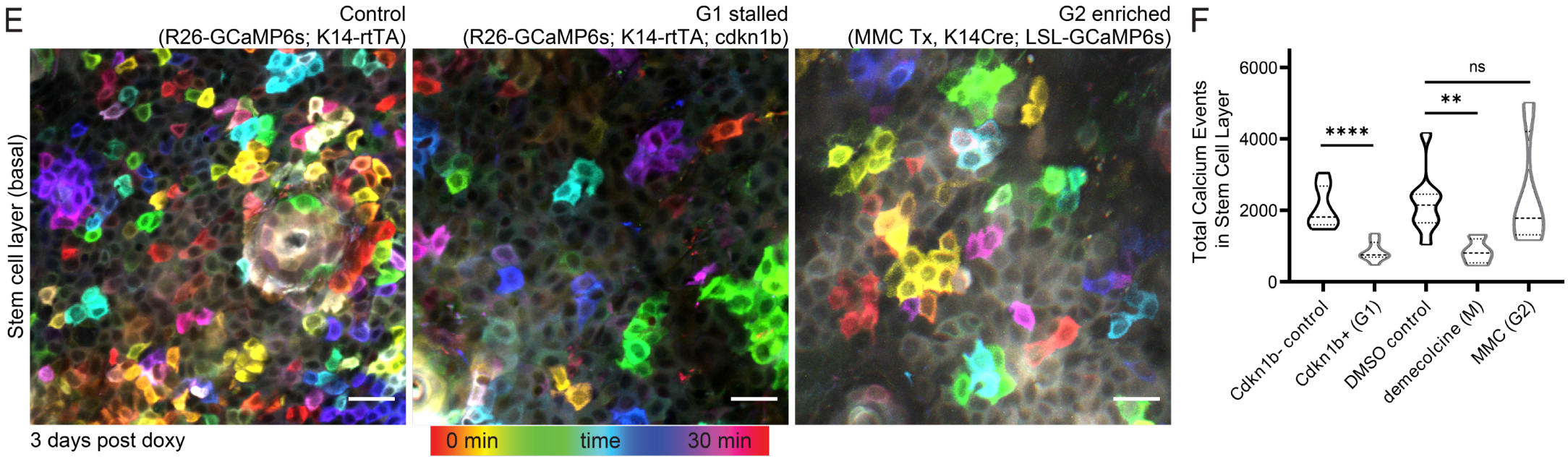

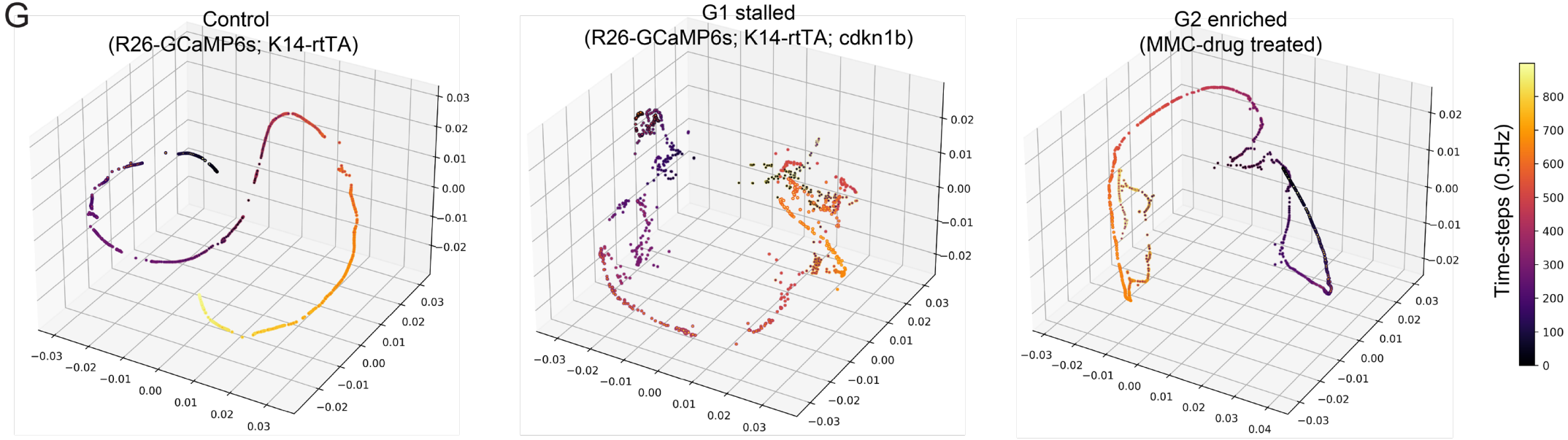

Ca^{2+} signaling in the mouse epidermis

DMSO

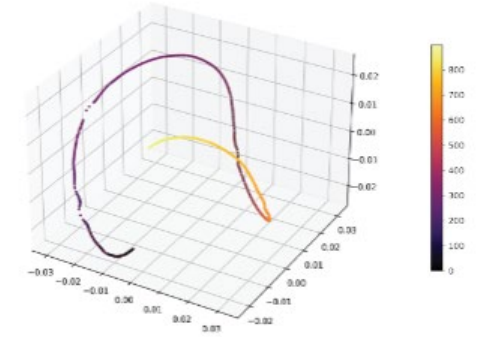

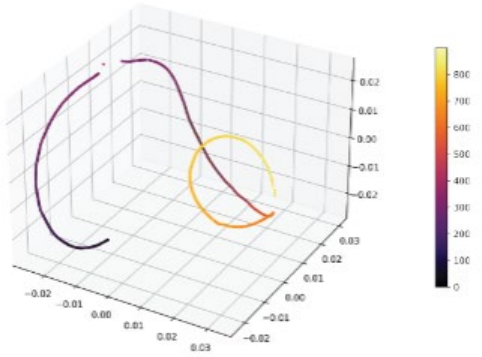

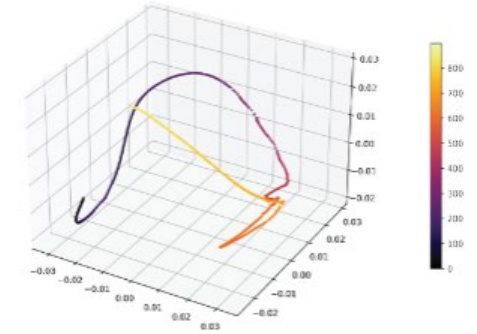

thapsigargin

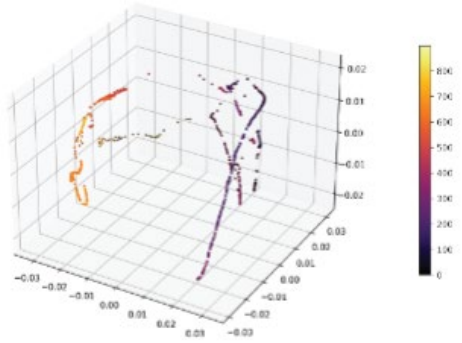

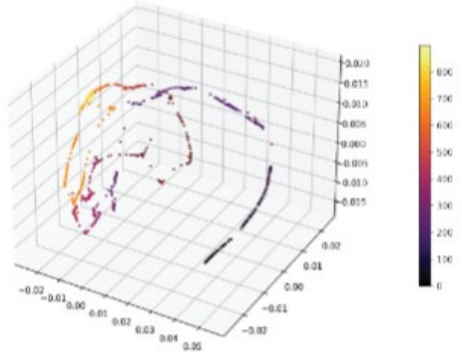

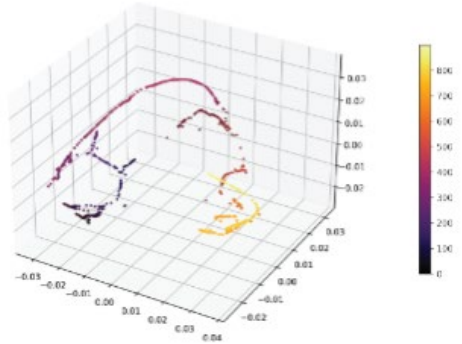

2-APB

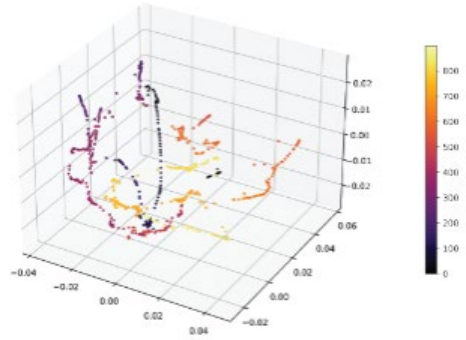

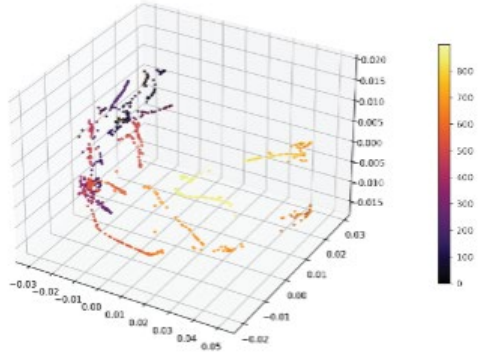

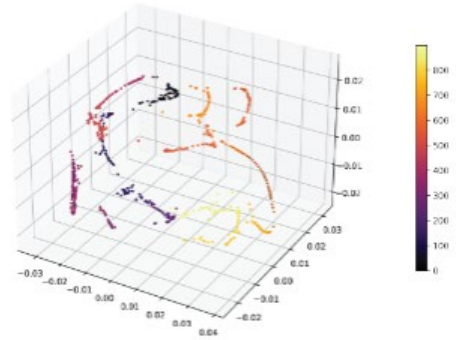

Recovery of model parameters with GSTH

Table 3 Performance of GSTH model ablations on model parameter recovery (MSE) and classification of experimental conditions.

		Mathematical Model[1]				Experimental Data[2]		
		Kuramoto	Intercellular Ca^{2+} Waves					
Model	Ablation	R	K_{SERCA}	V_{SERCA}	$\tau_{\max}$	Epidermal Signaling	ERK Signaling	PVC Signaling
GSTH	None	0.0063	0.0372	0.0646	24.81	0.89	0.65	0.44
GST	PH	**0.0016**	**0.0189**	**0.0232**	**9.74**	**0.95**	0.73	**0.62**
GST-RNN	PH	0.0058	0.0417	0.0722	26.94	0.86	0.58	0.37
GST-κ	PH	0.0347	N/A	0.1953	N/A	N/A	N/A	N/A
GS-PCA-H	PHATE	0.0125	0.0506	0.1103	51.63	0.77	0.57	0.44
GS-tSNE-H	PHATE	0.0118	0.0438	0.1078	38.29	0.81	0.73	0.51
Graph PH	GST	0.0124	0.0397	0.0859	11.32	0.91	**0.76**	

[1]Mean squared error (MSE) for regression, lower is better.

[2]Classification accuracy, higher is better.

MAGAN: Manifold-Aligning GAN

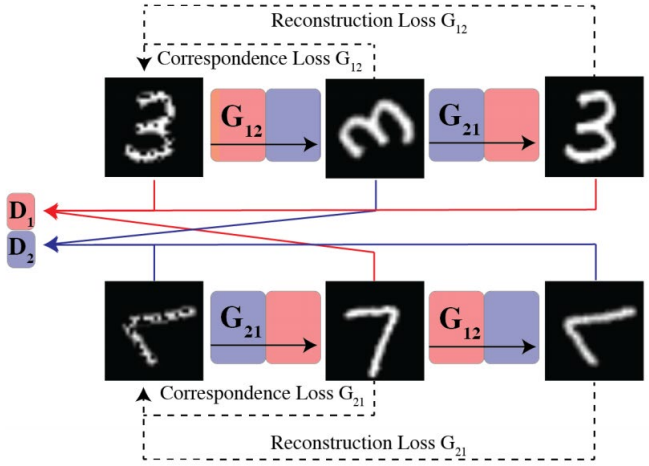

Amodio, Krishnaswamy ICML 2018

Archetypal Analysis Network

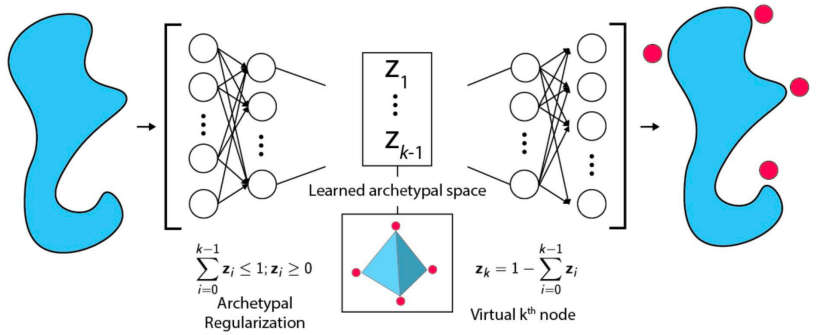

van Dijk, Burkhardt et al., IEEE Big Data 2019

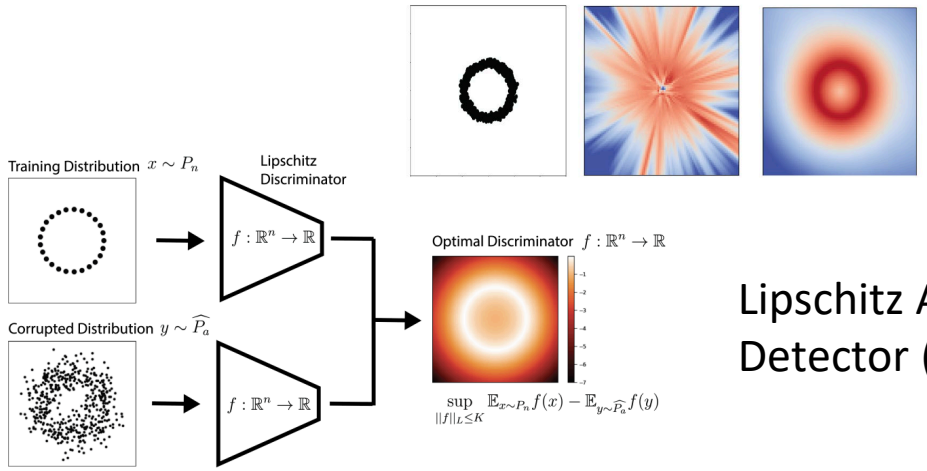

Lipschitz Anomaly Detector (LAD)

Tong, Wolf, Krishnaswamy, MLSP 2020
(Best Student Paper Winner)

SAUCIE

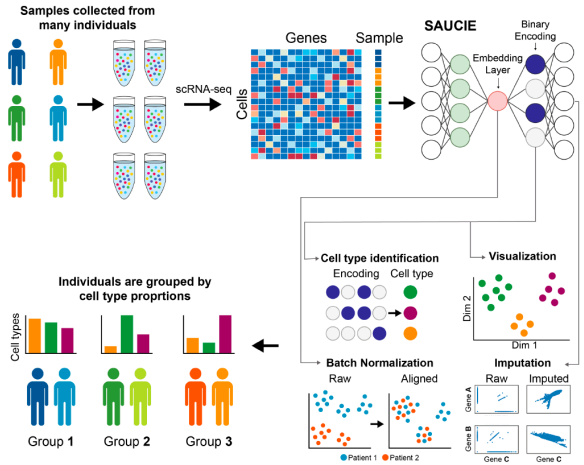

Amodio et al., Nature Methods 2019

Krishnaswamy Lab Resources

Website

https://www.krishnaswamylab.org

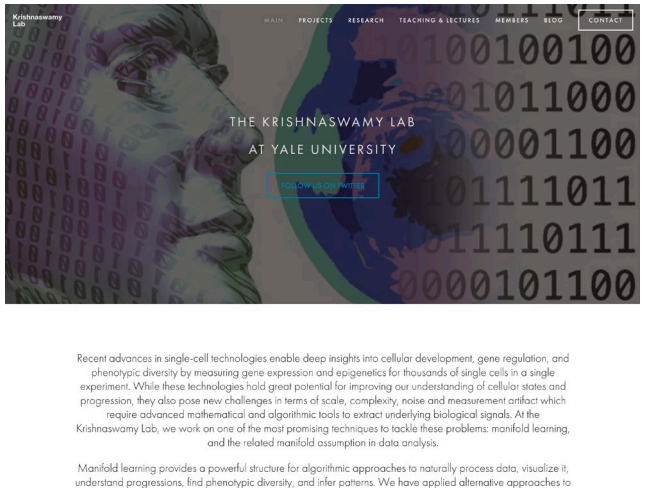

GitHub

github.com/KrishnaswamyLab

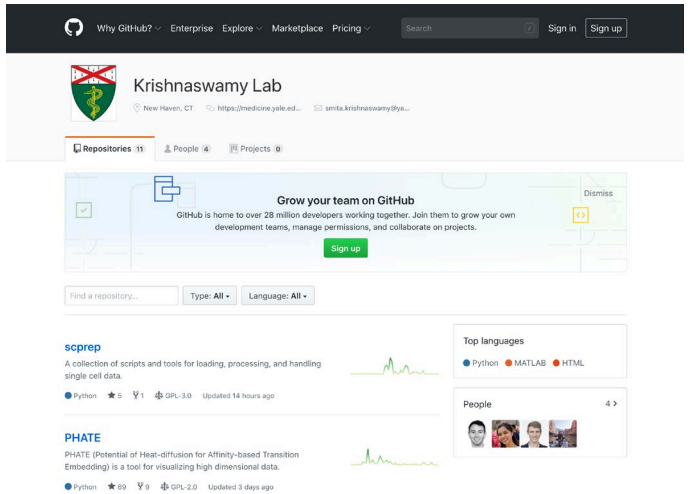

Twitter

@krishnaswamylab